Battery-less RFID-Based Wireless Sensor Architectures for 5G IoT Applications

by

Nabil Khalid

A thesis submitted in partial fulfillment of the requirements for the degree of

Doctor of Philosophy

in

Electromagnetics and Microwaves

Department of Electrical & Computer Eng

University of Alberta

Abstract

In this thesis, novel battery-less wireless sensor architectures and sensing elements are proposed and demonstrated. The proposed passive wireless sensor architectures integrate a UHF RFID chip, and a UHF sensing element to enable the reading of environmental conditions wirelessly, without increasing the complexity of a typical RFID chip and substantial loss of read range of the chip. The architectures are designed so that the sensor only changes the phase of the reflected RFID signal, with minimal affects to the incoming interrogator signal to ensure optimal range. The phase change is detected by the reader using a non-coherent IQ demodulator. Since the sensing elements must be responsive at UHF, novel sensing elements are designed and reported.

Along with hardware development, in-depth analysis and modeling of the proposed architectures and sensing elements are presented. Furthermore, to address the challenges of phase ambiguity while operating at different distances, signal processing techniques are formulated. The proposed architectures can easily integrate any type of sensing element such as temperature, humidity, and water level. A flood sensor, a temperature sensor, and a voltage sensor, operating wirelessly without a battery are demonstrated in a home and office environment.

Preface

Parts of this thesis are already published or are in the process of publication. Chapter 1, chapter 2, and chapter 3 have been extracted from a paper that was published as, N. Khalid, R. Mirzavand, A. K. Iyer, A Survey on Battery-Less RFID-Based Wireless Sensors, *MDPI Micromachines.* 2021; 12(7):819. I was responsible for the literature survey, data collection, data analysis, and manuscript composition. Following that, chapter 4 has been published as, N. Khalid, R. Mirzavand, H. Saghlatoon, M. M. Honari and P. Mousavi, "A Three-Port Zero-Power RFID Sensor Architecture for IoT Applications," in *IEEE Access*, vol. 8, pp. 66888-66897, 2020. I was responsible for architecture designing, data collection, mathematical modeling, and manuscript composition. Chapter 5 has been published as, N. Khalid, R. Mirzavand, H. Saghlatoon, M. M. Honari, A. K. Iyer and P. Mousavi, "A Batteryless RFID Sensor Architecture With Distance Ambiguity Resolution for Smart Home IoT Applications," in *IEEE Internet of Things Journal*, vol. 9, no. 4, pp. 2960-2972, 2022. I was responsible for architecture designing, data collection, mathematical modeling, signal processing, and manuscript composition. Following that, chapter 6 has been published as, N. Khalid, A. K. Iyer and R. Mirzavand, "A Battery-Less Six-Port RFID-Based Wireless Sensor Architecture for IoT Applications," in *IEEE Internet of Things Journal*, 2022. I was responsible for architecture designing, data collection, mathematical modeling, and manuscript composition. Finally, chapter 7 is being prepared for publication.

To my lovely mother, Farzana Khalid, for all the sacrifices she made in her life to educate me and make me a stronger man.

There's Plenty of Room at the Bottom.

– Richard Feynman, Caltech, 1959.

Acknowledgements

I would like to express my gratitude and sincere thanks to my advisors, Dr. Ashwin K. Iyer, Dr. Pedram Mousavi (late), and Dr. Rashid Mirzavand who led me into this exciting area of battery-less wireless sensors. Being a part of their research groups, I learned a lot. My cordial thanks also extend to Dr. Kambiz Moez, Dr. Masum Hossain, and Dr. Mohtada Sadrzadeh for taking part in my thesis committee, for critical reading of this thesis, and their valuable comments and suggestions.

I would like to express my gratitude to the members of the research group for their contributions to my personal and academic life in terms of friendship, advice, and collaboration. I would like to express my sincere thanks to Dr. Mahdi Honari, and Dr. Hossein Saghlatoon, for helping me carry out this research work and for sharing their valuable suggestions. I would also like to thank Dr. Stuart Barth, Dr. Asad Bukhari, Dr. Faheem Khan, and Dr. Moussa Waleed (late), for their help, advice, knowledge sharing, or support in any form while carrying out this research work.

I also gratefully acknowledge the support of Alberta Innovates, Natural Sciences and Engineering Research Council of Canada (NSERC), and Mitacs for their financial support in carrying out this research.

Lastly, I am very grateful to my family for their unconditional support throughout. If it were not for their support and dedication to my education, I would never have made it as far as I have.

Table of Contents

List of Tables

List of Figures

Glossary

analog-to-digital converter (ADC)

Electronic Article Surveillance (EAS)

in-phase (I)

integrated circuit (IC)

Internet of Things (IoT)

low-noise amplifier (LNA)

PathWave Advanced Design System (ADS)

phase-locked loop (PLL)

quadrature (Q)

radar cross-section (RCS)

radio frequency (RF)

Radio Frequency Identification (RFID)

ultra-high frequency (UHF)

Symbols

ϵ Permittivity

ϵ_r Relative permittivity

Γ_{in} Input Reflection coefficient

Γ_{RFID} Reflection coefficient of RFID chip

Γ_{sensor} Reflection coefficient of sensing element

θ_{RFID} Phase delay of RFID chip

θ_{sensor} Phase delay of sensing element

Chapter 1

Introduction

1.1 Background of Battery-less Wireless Sensors

Wireless sensors are becoming increasingly popular in the home and industrial sectors and are used for a range of applications, from temperature or humidity monitoring to food quality inspection of products being sold in a market. One of the main reasons for using wireless technology is that it affords non-contact, non-invasive sensing. This ability not only eliminates the need for long cables required for information transfer, but also reduces the spread of germs, and brings comfort to the users. To fully exploit the capabilities of wireless sensors and automate processes, the future generation of wireless communication, 5G, Internet of Things (IoT), and the evolving Industry 4.0 aims to incorporate them on a massive scale, due to which research on wireless sensors is on a dramatic rise [1–3].

For the past two decades, RFID has been widely used for object identification and tracking purposes [4]. It took many years for this technology to become affordable and reliable in a variety of applications. The technology was initially focused on replacing bar codes and Electronic Article Surveillance (EAS) for preventing theft. Later on, the application horizon of RFID got wider and it was introduced in several applications such as tracking inventory at a warehouse for supply management purposes, automated toll collection without the need for stopping, and automatic unlocking of doors when entering parking structures or buildings premises [5, 6].

As time passes the applications of RFID are rapidly expanding, and RFID-based sensors are one of its most interesting applications. Initially, RFID technology was merely introduced for object identification. By the year 2004, the technology started incorporating sensing capabilities [7]. Although extending the chip's capability from identification to sensing is straightforward, the design must ensure that the extension does not affect the performance of an RFID tag. Hence such an addition should collect sufficient power to run the RFID chip and the sensing element without having any significant impact on the read range of the RFID tag [8, 9].

RFID tags are generally classified into three categories: active, semi-passive, and passive, as shown in Fig. 1.1. An active RFID tag has its own power supply and a transmitter for communication, whereas a semi-passive RFID has its own power source but does not have any transmitter, and instead uses a backscattering technique for establishing communication. On the other hand, a passive RFID chip, which is often the cheapest variety, has no internal power source and no transmitter, and thus uses the power of the electromagnetic field transmitted by the reader to power-up its circuitry and backscatter the received signal [10–12].

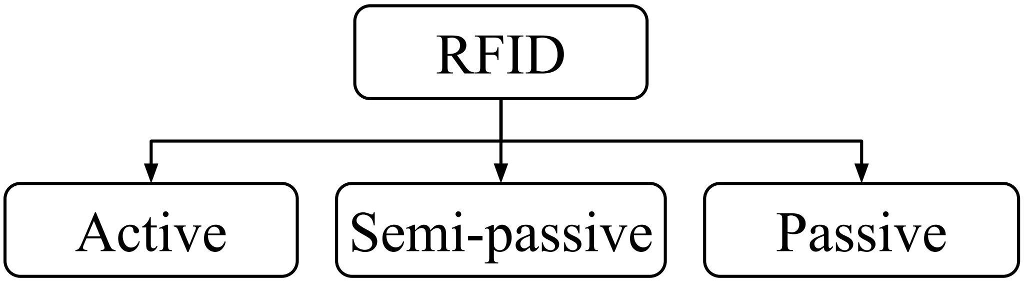

Figure 1.1: Taxonomy of RFID tags available in the market.

A sensing element may be incorporated in any of the aforementioned categories to design an RFID sensor. Using active or semi-passive technology requires a power source, which makes the wireless sensor bulky and expensive, whereas passive technology is much cheaper but incorporating sensing elements in it is quite challenging due to the limited available power and flexibility. Hence, passive technology must be carefully engineered to address these challenges [3, 11, 13–20].

RFID is now a widely used technology for tracking and inventory management services, and as such, is governed by several design standards [21]. However, wireless sensors, especially RFID-based sensors, are still an emerging technology, and therefore might be referenced using different names in the community. Particularly, passive wireless sensors are sometimes also termed as battery-less, self-powered, or even zero-power [8, 11, 22–29].

1.2 Research Motivation

Battery-less RFID-based wireless sensors have gained a lot of interest because they are lightweight, cheap, and long-lasting. In particular, the ones operating at UHF are of greater interest as they offer a good compromise between size and read range. An illustration showing the operation of battery-less wireless sensors is shown in Fig. 1.2. There are several different designs proposed in the past that can be generally categorized into chip-less sensors, chip-based antenna resonance modifying sensors, multi-port chip-based sensors, digitally integrated sensors, and chip-based ambient energy harvesting sensors. In the following sections, we will discuss these categories in detail and observe the benefits and drawbacks of each [8, 30–50].

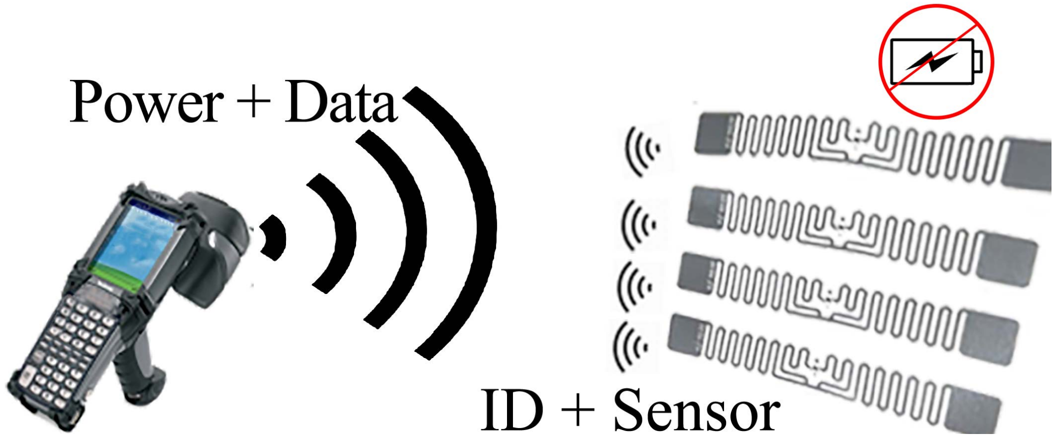

Figure 1.2: Battery-less wireless sensors get energy from the reader and respond by backscattering the incident power signal.

1.3 Research Objectives

The current research, therefore, aims to develop novel passive wireless sensor architecture designs that address the aforementioned challenges. The designs comprise a UHF RFID chip, an antenna, UHF sensing elements, and multi-port circuits. These components are arranged such that a significant part of the reader signal is sent to the RFID chip to store or harvest energy, while the backscattered signal is passively combined with the signal from the sensing element. The UHF sensing element only introduces some phase change to the backscattered signal that is returning back to the reader. Since these architectures keep the sensing element and the antenna separate, the radiation characteristics of the antenna are not altered by the changes in the response of the sensing element, as it does in some previously published wireless sensors [51–53].

The proposed design can be used in several different applications, and is especially suited to smart home IoT. A smart home generally requires several sensors such as humidity, temperature, or flood sensors, as shown in Fig. 1.3. These sensors are required to be densely deployed in a closed vicinity. Therefore, chip-based RFID technology is an ideal candidate as it supports spatial multiplexing in such an environment. Moreover, the eradication of batteries from the sensors is of key interest for home users. This is because batteries require periodic maintenance and pose a hazard of missing an alarm in the event of a battery run out. A fully passive system will significantly reduce any such hazards. Lastly, a longer read-range (greater than 5 m for smart homes) will reduce the number of readers required in a given room. These readers may easily connect to WiFi to upload data to servers for processing and also to keep users informed.

The goals of this research are five-fold:

- propose a wireless sensor design for mid-range applications (2 to 10 meters) without needing any battery;
- provide an in-depth analysis and modeling of the proposed design on

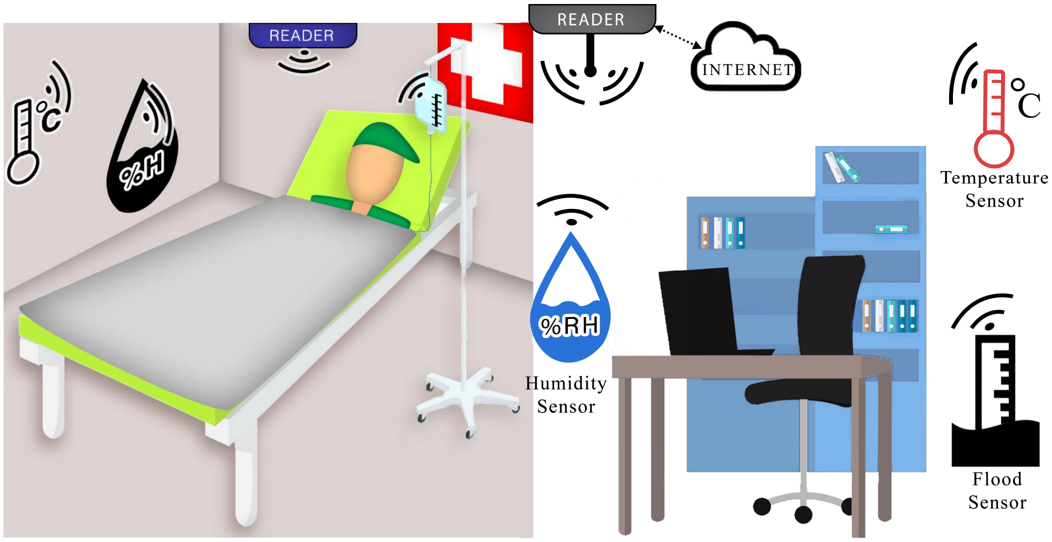

(a) (b)

Figure 1.3: Potential applications of zero-power wireless sensor network from determining environmental condition (a) in healthcare monitoring (b) in a smart home or office environment.

how the phase delay information of the reflected signal can be used to passively determine the sensed value;

- provide signal processing techniques to remove phase ambiguity at different distances;
- propose novel sensing element designs operating at UHF;
- demonstrate performance of the proposed sensor in a home-office environment.

1.4 Thesis outline

The remainder of this thesis is organized as follows. In chapter 2, we discuss the fundamentals of an RFID-based wireless sensors to develop a basic understanding of how the individual components of the system may be engineered to meet the requirements, e.g. complexity, cost, size, read range, and accuracy of a given application. In chapter 3, state-of-the-art system topologies of battery-less RFID-based wireless sensors are discussed in the context of their complexity, cost, size, read range, and accuracy. Chapter 4 shows a novel

RFID battery-less wireless sensor architecture based on a circulator. Distance ambiguity is resolved using the architecture proposed in chapter 5. Following that, a six-port-based wireless sensor architecture is proposed in chapter 6. A novel non-hybrid six-port-based wireless sensor architecture is proposed in chapter 7. Finally, chapter 8 concludes the thesis.

Chapter 2

Fundamental Principals of RFID Based Wireless Sensor Systems

An RFID-based wireless sensor consists of several components. A block diagram of all the key components is shown in Fig. 2.1 and details of each component are discussed below.

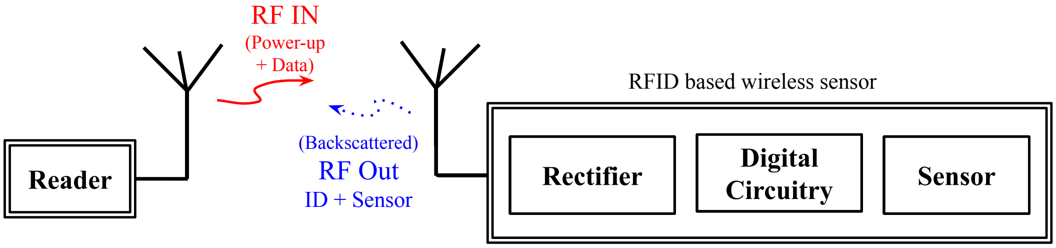

Figure 2.1: Components of an RFID-based wireless sensor system.

2.1 Antenna

An antenna is a transducer that converts free space electromagnetic energy to guided electromagnetic energy and vice versa to enable wireless communication in an RFID system. Although any radiating structure can be termed as an antenna, the efficiency with which it can transform electromagnetic energy plays a major role in determining its amenability for use in sensor communication [30].

To design antennas, certain characteristics are of key importance. These characteristics are the resonant frequency, bandwidth, impedance, gain, radiation pattern, and polarization. Any design is a trade-off of these characteristics and must be optimized based on the application of interest. In an RFID-based sensor, usually small size, planar, and high gain antennas are desired to ensure longer read range and lower fabrication cost [54, 55].

To achieve small size, different miniaturization techniques are used. Amongst them, meander line antennas are of great interest due to their simplistic design [56–63]. In these antennas, the antenna arms are folded to reduce the size and produce distributed capacitive and inductive reactance that produces a global effect on the antenna impedance. Operating an antenna well below its natural resonance frequency to satisfy space constraints implies that the antenna becomes more difficult to match, and impedance matching directly impacts the RFID read range. Therefore, the reactance must be properly engineered to effectively reduce the size of the antenna [64, 65].

Although a significantly smaller size can be achieved with meander line dipole antennas, they are prone to degradation due to nearby objects and cannot be placed directly on metallic surfaces. Therefore, for applications where a wireless sensor is required to be placed on a metallic object, different classes of antennas may be considered. Normally patch antennas have a ground plane attached at one side, and can thus be used for this purpose. However, due to their large size at UHF frequencies, modified versions such as fractal and meandered patch antennas are preferred for RFID tags [55, 66–69].

2.2 Rectifier

A rectifier in an RFID tag is the main circuit that converts the incident electromagnetic energy received by the antenna into a DC supply voltage. This voltage is required to operate all the internal circuitry of the tag, which includes the analog circuitry, base-band DSP circuitry, and memory of the tag [70–75].

The power efficiency and stability of the rectifier are determining factors for the range of the RFID tag. Generally, Schottky diodes are used in AC/DC rectifiers, however, for RFID tags they are avoided. This is because they can not be co-fabricated with CMOS technology, which is required for DSP and memory design, whereas, a separate fabrication of both would result in inconsistencies that degrade the performance of the chip. Therefore, diode-connected MOS FETs are preferred when designing RFID rectifiers as they can be accurately co-fabricated with other components [76–78]. A detailed model incorporating the fabrication process yields rectifiers with optimum performance [79–82].

If standard threshold voltage CMOS devices are used, the rectifier cannot be turned on when the voltages at its terminals are lower than its turn-on voltage, which affects the read range of the RFID tag. Solutions using near differential-drive rectifiers, photovoltaic-assisted rectifiers, and zero threshold-based technologies such as Silicon-on-Sapphire, and Hetero-junction Tunnel FET provide a significant improvement to read range [45, 83–91].

2.3 Digital Circuitry

Generally, an RFID tag consists of digital circuitry that is used to transmit the identity data of the chip. This circuitry obtains data from the memory of the tag and modulates it over the backscattered signal. To integrate a sensing element into an RFID tag, additional digital circuitry that can utilize off-the-shelf sensing elements may be added. This addition allows the recording of sensed data directly inside the tag and sending it back to the reader using digital modulation techniques along with the identification data. The major benefit of this technique is that the accuracy of the sensor can be very high [23]. However, a clear drawback is that this digital circuity will require additional power. For passive RFID tags, the power is limited, and these additional circuits can only operate at the expense of read range reduction.

On-chip digitally integrated sensors are comprised of three major blocks — a digital control circuit, an off-the-shelf sensing element, and an analog-to-digital converter (ADC). The digital control circuitry drives the sensing element by providing the required current or voltages. The element generates an analog voltage based on the physical parameter being measured. This voltage is converted into a digital format using the ADC and transmitted back to the reader using the aforementioned RFID circuitry. Using this technique, different sensing elements such as temperature, gas, and food-quality can be easily connected [23, 35, 92, 93].

2.4 Sensing Element

The sensing element is the heart of the wireless sensor. It is the component that is actually sensitive to the parameter of interest. From a point of view, there are two types of sensing elements: resistive and reactive [94–97]. Resistive sensing elements are the ones for which the resistance across the terminals changes with variations in the physical parameter being measured. Similarly, reactive sensing elements are usually capacitive or inductive in nature whose reactance varies. Resistive sensing elements are usually lossy as power must be dissipated to read their value. On the other hand, reactive sensing elements, especially the capacitive variety, can be very energy-efficient as very little current is drawn to operate them. A simple structure of resistive and capacitive type humidity sensing element is shown in Fig. 2.2 [98].

Based on the layout or packaging design, sensing elements can exhibit certain parasitics. As a result, not all sensing elements can be used at high frequencies, such as those employed in RFID. If on-tag digital circuitry for the tag exists, generally off-the-shelf sensing elements may be used. However, if the topology being used drives the sensing element using the high-frequency incident signal, then the sensing element must be responsive and sensitive at the frequency being used. In this case, a reader must be able to understand the received information and separate it from the regular RFID's identity information. Elements operating at high frequency are not easily available in the market. As a result, different types of sensing elements for RFID sensors are currently being explored by researchers to increase their frequency of operation while simultaneously reducing their power consumption [35, 36, 99–105].

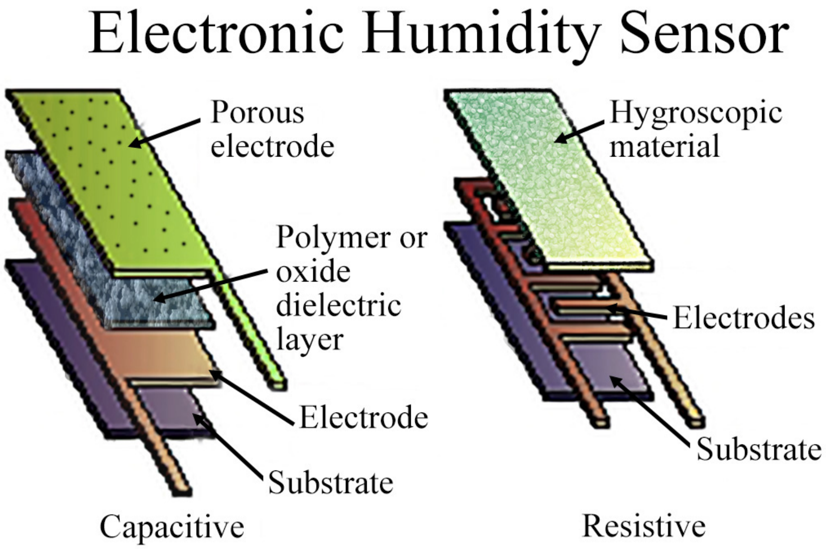

Figure 2.2: Design comparison of resistive and capacitive type humidity sensing element.

2.5 Reader

In an RFID system, a reader, also known as an interrogator, is the device that communicates with an RFID tag [106]. Moreover, in passive RFID tags, the reader is the device that also provides energy to the tag for its operation. The same is true for the case of battery-less wireless sensors.

The sensing information in an RFID-based wireless sensor may be transmitted using either digital or analog communication. Therefore, a reader must be able to understand the received information and separate it from the regular RFID's identity information. In the case of analog communication, received signal strength at different frequencies and/or phase delay in the backscattered signal are of key interest. Hence, it is necessary to ensure that the chosen reader can provide the required information. Readers based on IQ demodulators are often able to extract the phase and amplitude of the backscattered signal and are hence preferred for such applications.

Typically, reader ICs are available in the market that covers the entire RFID UHF frequency range of 860 MHz to 960 MHz and supports EPCglobal Class-1 Generation-2, ISO-18000-6A(61), ISO-18000-6B(62), and ISO-18000-6C(63) standards. These ICs can normally provide an output power of up to

+10 dBm, which can be further increased to +30 dBm by using an external power amplifier. Sensitivity levels of -90 dBm are easily available that allow the reading of chips at fairly long distances of up to ~30 m [107, 108].

Chapter 3

Literature Survey

Different arrangements and utilization of the RFID tag's components can result in different topologies. There are currently four principal topologies being used, each offering different levels of complexity, cost, read range, and accuracy. Here, the details of each topology will be discussed to analyze their pros and cons.

3.1 Chip-less RFID Sensor Topology

The simplest form of RFID sensor requires no integrated circuit (IC) and communicates sensed data by simply varying the radar cross-section (RCS) of the tag at a certain frequency [8, 30–33]. This is achieved by attaching a sensing element, having an input impedance of Z_S, with an antenna, having an input impedance of Z_A, through a matching network. A block diagram is shown along with an example of a strain sensor in Fig. 3.1 and Fig. 3.2, respectively. RCS is a combination of structural-mode reflection and antenna-mode scattering. An incoming electromagnetic wave is partly absorbed and partly reflected from the surface of the antenna. The signal reflected from the surface is known as structural-mode reflection, whereas any part of the absorbed signal that is reflected due to impedance mismatches is known as antenna-mode scattering [109–112]. The sensing element, which could be designed for sensing temperature, humidity, or gas, transforms any change in the physical quantity into a variation in its electrical properties such as resistance or reactance. As a result, the resonance frequency or the quality of the matching network is altered. Hence, this causes a change in the RCS of the antenna at a given frequency.

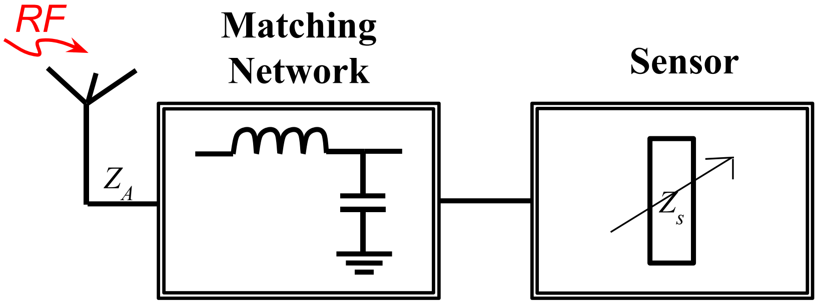

Figure 3.1: Block diagram of a chip-less RFID-based wireless sensor.

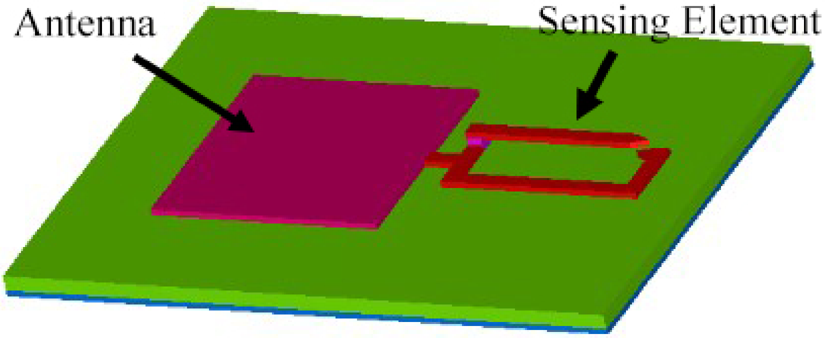

Figure 3.2: A chip-less RFID-based wireless strain sensor design [31].

To read data from a chip-less RFID sensor, a reader transmits a frequency sweep signal of a specific bandwidth and analyzes the backscattered signals that it receives. These backscattered signals are affected by the physical location of the sensor and its RCS. If the physical location and distance between the sensor and the reader are fixed, then the effect of the physical location can be easily factored out to determine the RCS, specifically of the sensor.

When the antenna impedance Z_A is matched to the sensing element's impedance Z_S, the reflection goes to zero and the RCS drops to a minimum. As the mismatch increases with a change in the impedance of the sensing element, which is affected by the physical condition being sensed, the mismatch between the antenna and the sensing element increases. This eventually increases the RCS of the sensor. As a result, the amplitude of the backscattered signal increases. This increase is directly related to the sensing element and can be easily translated to the change in the physical quantity by using predetermined calibration coefficients.

Another perspective to understanding this type of sensor is that when the sensing element mismatches, the resonance frequency of the circuit will shift, and thus the sensor will be matched to another neighboring frequency. The reader can easily search this resonance by measuring the backscattered signal at different frequencies and matching it with the predetermined calibration data to determine the sensed value and the corresponding physical quantity [113–116].

Although the aforementioned is by far the most cost-effective method of RFID sensing, it requires a higher frequency bandwidth and is also prone to multi-path and environmental effects. Moreover, areas having multiple sensors in close proximity are not supported. Therefore, this method is mostly preferred in uncluttered areas such as farms or fields. There are techniques where multiple resonators are used so that data in multiple frequency bands could be analyzed to reduce the effect of multi-path and environmental noise [102]. Besides, diode frequency doubling is sometimes used in the sensor so that reception at the higher harmonic is free of environmental backscatter, which is high at the actual frequency of transmission [117–119]. Another technique is to use a direct conversion six-port network in which information is divided into in-phase and quadrature components. The reference signal for calibration purposes is sent as an in-phase component while the sensing element signal is sent as the quadrature component so that they could be analyzed together to determine the sensed value [120, 121]. Nevertheless, these techniques increase the cost and reduce the read range of chip-less wireless sensors. The read range demonstrated by these sensors ranges from 2 m to 30 m [8, 30, 102, 113–116, 120, 121]. Moreover, due to multi-path and analog communication, the accuracy of these sensors is low.

3.2 Chip-based RFID Sensor Topology

To address the challenge of multi-path propagation and support multiple sensors in close proximity, wireless sensors must incorporate digital communication techniques. This is achieved in chip-based RFID tags, where the backscattering is digitally controlled and acts as a digitally modulated signal. This enables assigning a unique identifier to multiple tags in a vicinity, employing anti-collision protocols, and providing error reduction methods. All these techniques are built into the RFID EPC-Gen2 protocol. Chip-based RFID tags based on this protocol can be modified in several ways to integrate sensing elements inside them. These modifications generally include an antenna-resonance shifting-based sensor, a multi-port architecture to remove the sensing element from the incoming signal path, a digitally integrated sensor using digital circuitry, and an ambient energy harvesting block to get additional power from the surroundings.

Chip-based Antenna Resonance Topology

One of the simplest topologies of chip-based RFID sensors operates on principles that are very similar to chip-less RFID sensors. Generally, the RFID tag is connected to an antenna using some kind of matching network. The matching network will have its resonance at a particular frequency. Any change in the reactive or resistive component of the matching network will shift its resonance frequency or alter the loss of the network. As a result, the RCS of the RFID tag will vary [34–39].

To read data from wireless sensors working on the chip-based antenna resonance topology, a reader first sends an interrogation signal. This signal energizes the rectifier circuitry, and when the charging reaches a threshold level, the IC wakes up. The IC backscatters the interrogation signal by shorting and matching its terminal to send binary signals. As a result, the backscattered signal amplitude increases or decreases and the reader determines the high and the low signal. This information is used to demodulate the data being sent by the RFID tag. Since the sensing element influences the matching network of the RFID tag, the backscattered signal will be different at different frequencies. The reader can simply sweep the frequency of its interrogation signal to determine the tag's RCS at different frequencies. By utilizing the digital signal and the amplitude of the backscattered signal at different frequencies, the reader identifies the tag and determines the sensed value, respectively. A block diagram of this topology is shown in Fig. 3.3 and an example of such a sensor is shown in Fig. 3.4.

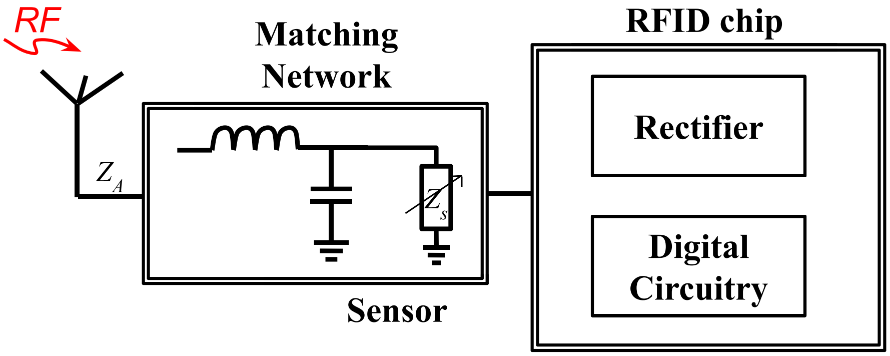

Figure 3.3: Block diagram of a chip-based antenna resonance wireless sensor.

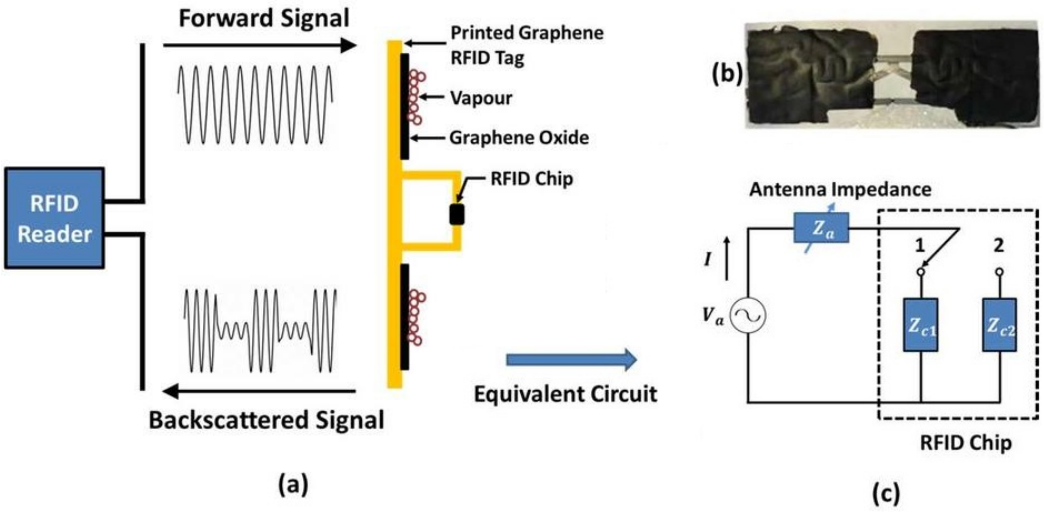

Figure 3.4: (a) Operating principle of the chip-based antenna resonance RFID sensor. (b) Printed with a 15 μm thick layer of graphene oxide on top. (c) The equivalent circuit of the sensor [122].

In practice, the modifications in the matching network due to the changes in the sensing element also affect the quality of the matching network. Therefore, the shifted resonance may not provide maximum power transfer to the RFID tag. As a result, based on the sensor's dynamic range, the read range, which is directly dependent on the strength of the interrogation signal received by the rectifier circuit, might be lower at some states of the sensing element. This will eventually determine the actual read range of the RFID sensor. Moreover, since the sensor information is delivered through analog communication, only moderate accuracy is obtained. Furthermore, the shift in resonance requires a higher bandwidth for the sensor to operate. On the other hand, the design is low cost as the sensing element is passively integrated into the matching network. Chip-based RFID antenna resonance wireless sensors have been proposed that operate within the read range of 3 to 5 m [34–38].

Chip-based Digitally Integrated Topology

Another chip-based RFID topology is one in which the sensing element is attached to digital circuitry, which reads its value and sends the data digitally back to the reader [123]. To accomplish this, the incoming interrogation signal first energizes the rectifier circuit. After the required threshold level is achieved, the added digital circuitry in the IC uses a portion of this power to determine the sensed value.

One of the methods to design the digital circuitry is to have a phase-locked loop (PLL) based sensor interface that compares the phase of two oscillators, where one of the oscillators is connected to a reference capacitor and the other is attached to the capacitive sensing element. Any change in the element introduces a phase difference between the two oscillators. This change is determined through the error port of the PLL. The amplitude of the error signal is directly related to the difference between the capacitance value of the reference capacitor and the element. The error signal is read by an on-chip ADC, which is then digitally concatenated to the tag's identity data and sent back to the reader through the backscattered signal [44]. A simple block diagram and a chip-level block diagram of the digitally integrated sensor are shown in Fig. 3.5 and Fig. 3.6, respectively. The chip level block diagram includes details of a digitally integrated temperature sensor, which shows what components are required to design the sensor.

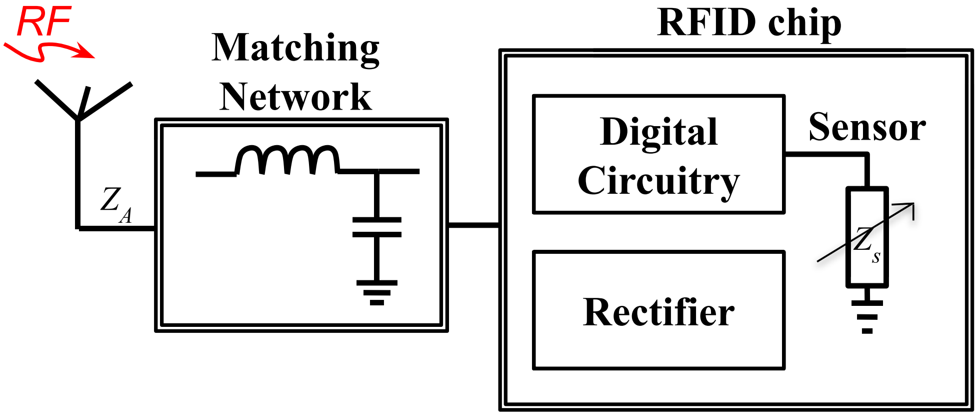

Figure 3.5: A simple block diagram of a chip-based digitally interfaced sensor.

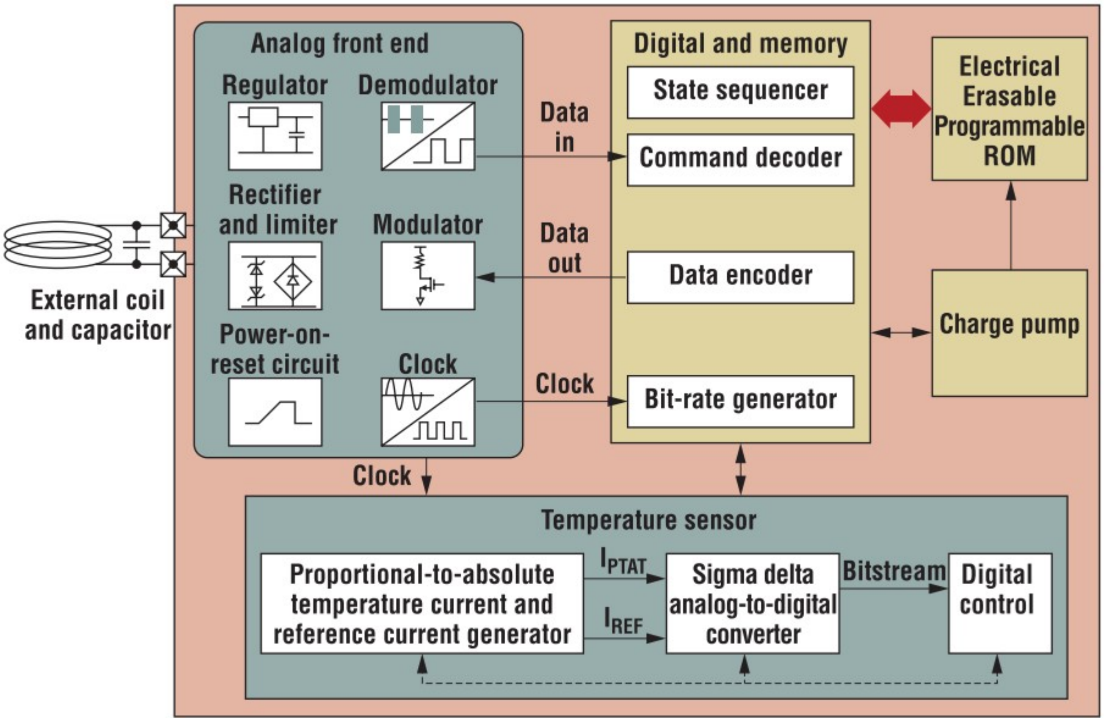

Figure 3.6: A chip-level block diagram of a chip-based digitally interfaced RFID sensor [23].

The main challenge in a chip-based digitally integrated sensor is to have digital circuitry that operates at very low voltage and uses a minimum amount of power to read the sensed value with suitable accuracy. This added circuitry can significantly reduce the read range of an RFID chip and slightly increase its cost. Currently, sensors utilizing this topology have been demonstrated with read ranges of around 0.7 – 2.2 m [43, 44]. It should be noted that, since the sensed information is communicated digitally, the accuracy is high and the bandwidth is the same as a regular RFID chip.

Chip-based Ambient Energy Harvesting Topology

To improve the read range of chip-based RFID sensors without adding a battery, harvesting the energy from the ambient can be of help. There are multiple power sources in the ambient — solar power and indoor lights or RF signals from radio and TV stations, WiFi networks, and cellphone towers [45–48]. By attaching a small solar cell and/or using a wide-band receiver that is capable of receiving RF signals from the ambient, the overall energy received by an RFID-based wireless sensor can be tremendously increased. Therefore, without adding any battery, the read range of the sensor can be improved. A block diagram and a prototype of such a sensor tag are shown in Fig. 3.7 and Fig. 3.8, respectively.

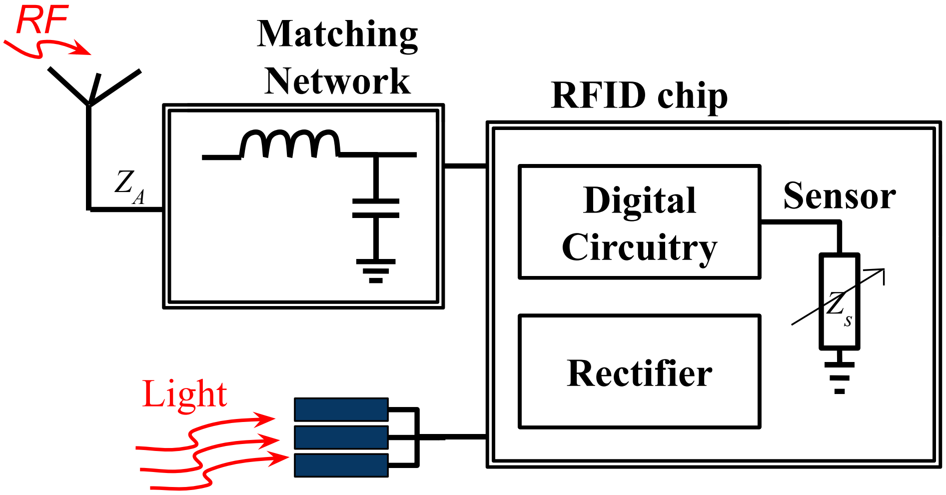

Figure 3.7: Block diagram of a chip-based ambient (light) energy harvesting wireless sensor.

If the RFID chip operates on the principles of backscattering the transmitted signal, the limiting factor, in this case, will be the reader's sensitivity as

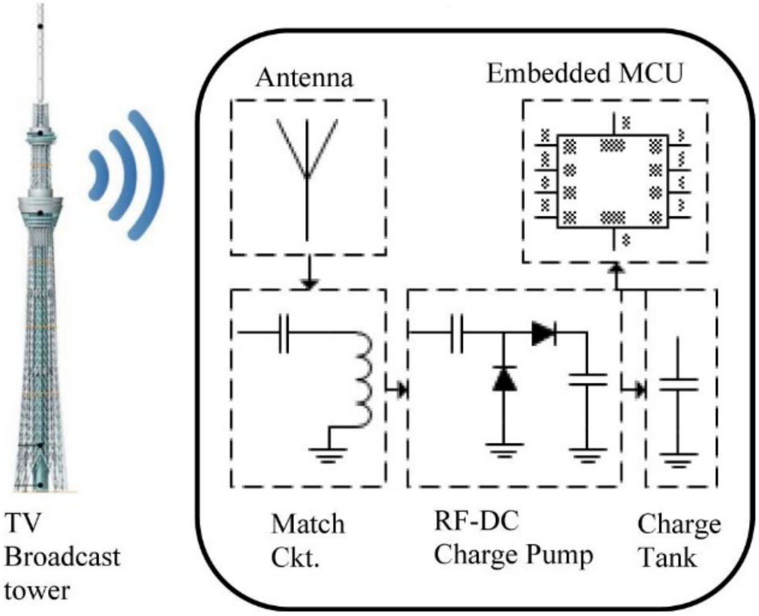

Figure 3.8: Prototype of a chip-based ambient (RF) energy harvesting wireless sensor [46].

follows. In RFID communication, a power-up signal faces two-way path-loss and any losses inside the RFID tag, which can be antenna mismatch, sensing element loss, and RFID's backscattering switch loss. In an ideal case where there is no power lost inside the tag and considering the maximum allowed EIRP of 36 dBm, with the receiver sensitivity of -90 dBm and the tag's antenna gain of 3 dB, the two-way path-loss at 915 MHz allows for 66 dB path-loss in one direction. This corresponds to around 52 m of the distance between the reader and the tag. Here we have considered that the RFID tag is getting enough energy from the ambient to fully power-up its internal circuitry and the digital circuitry of the sensor. Wireless sensors utilizing this topology and only incorporating solar cells have shown a read range of around 15 m [20]. Since the sensor information is sent digitally, the accuracy is high. Furthermore, the bandwidth is the same as a regular RFID chip, whereas, the cost increase due to the added solar panels.

In the following chapters, chip-based multiport topology is introduced and 4 novel wireless sensor architectures are proposed. In a chip-based multiport topology, sensing element is separated from the forward signal path flowing towards the RFID. It only contributes to the backscattered signal path flowing back to the reader.

Chapter 4

A Three-Port battery-less RFID Sensor Architecture for IoT Applications

A novel battery-less wireless sensor architecture is proposed and demonstrated in this chapter. The proposed wireless sensor, which is a passive sensor, combines UHF RFID and a capacitive sensing element to enable the reading of physical and chemical parameters wirelessly, without compromising much on the read-range, and complexity of conventional RFID tags. The sensor alters the phase of the backscattered RFID signal, which is detected at the receiver using a non-coherent in-phase (I)quadrature (Q) demodulator. Due to the universal nature of this architecture, any type of sensors, such as temperature, humidity, and water level sensor, can be realized. For the sake of simplicity, a varactor diode was initially used to get a thorough understanding of the system. Following that, a flood sensing element was used to evaluate the performance of the battery-less wireless sensor in a real-world application.

4.1 Introduction

At a very fundamental level, a wireless sensor is simply expected to identify a node and send a sensed parameter wirelessly to a base station. Thus, there are three major components of its operation: communication, identification, and parameter sensing [124]. To perform these operations, energy is required by a sensor. Whatever technique is used to provide this energy directly influences the cost, life-span, wireless operable range, and circuit complexity [37, 38, 97, 120].

One method to provide energy to a sensor node is adding a battery to it, which could be utilized to perform all the required operations. Although the wireless range of a battery-assisted sensor is very long, usually in tens of meters, the battery is actually a hurdle in a wireless sensor: it increases the cost of the system, it needs to be replaced every few months and it makes the sensor bulky [125]. Passive wireless sensors, on the other hand, harvest energy, which is sent by a reading device, and perform all the required operations. However, their range of operation is usually lower, up to a few meters [126]. Therefore, it is very important to engineer the hardware of battery-less wireless sensors in order to increase their working range.

battery-less RFID tag-based sensors, especially the ones operating in the UHF band, are gaining a lot of interest [97, 105, 114, 115]. Several designs have been proposed in the past such as chipless-based RFID sensors [127–131] chip-based tags [51–53, 132–134], and digitization circuitry based [43, 135–139]. To the best of the author's knowledge, there is no RFID-based sensor design that integrates a sensing element passively without affecting the read range of the RFID. The range in the previous designs was affected mostly because the integration techniques involved sensors in the forward path, which attenuates the signal reaching the RFID chip and eventually reduce the read range.

In this chapter, a novel wireless sensor architecture that successfully solves the challenges faced by wireless sensors is proposed. The proposed sensor architecture consists of a circulator, an antenna, an RFID chip, and a capacitive sensing element. These components are connected in a sequence that the interrogation signal, which is being sent by a reader, is fed to the RFID to harvest energy. When the RFID responds, the reflected signal is directed to the sensing element before being returned by the antenna. This sequencing is accomplished by using a circulator. The proposed sensing element is capacitive in nature and thus it adds phase delay to the reflected signal, based on the sensed value. The signal is reflected by the element and reaches back to the reader after being radiated back by the antenna. It should be noted here

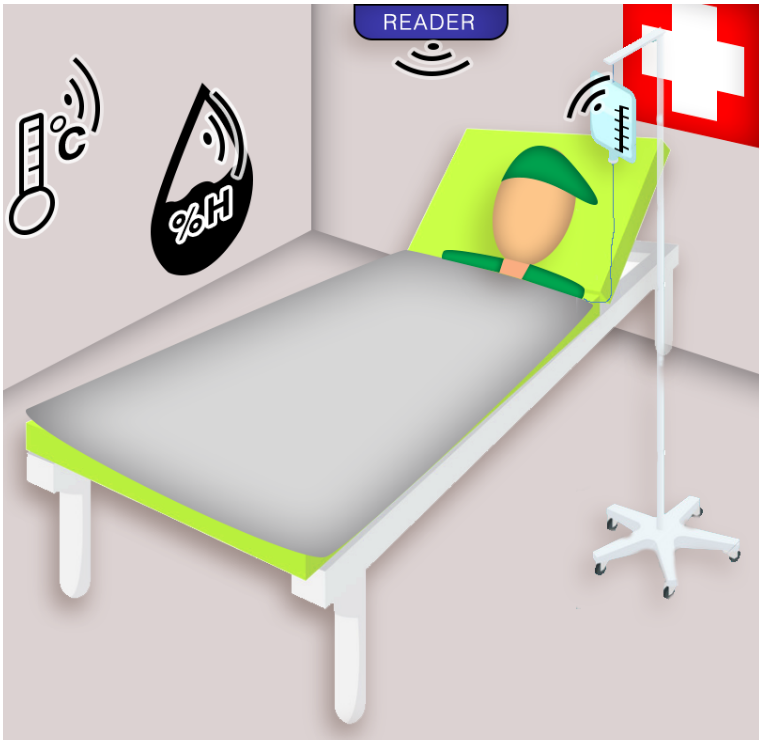

Figure 4.1: Potential applications of battery-less wireless sensor network from determining the environmental condition to healthcare monitoring.

that, since the element is physically separated in our architecture, unlike other previously discussed works on RFID-based sensors, the radiation characteristics of the antenna and the performance of RFID such as read-range are not compromised by the changes in the parameter being sensed [51–53].

At the reader, the phase delay due to the changes in physical or chemical parameters experienced by the sensing element can be easily determined by using a non-coherent IQ demodulator. These demodulators are widely available in commercial RFID readers. Therefore, by using this technique, the cost of the sensors can be significantly reduced without compromising much on the working range and complexity. This new design can open the door for several new applications ranging from personal use to industrial ones. An illustration in Fig. 4.1 shows a humidity sensor and a temperature sensor being used in a medical room to observe the environment and a liquid level detector is used to monitor the amount of dose given to the patient.

The goals addressed in this chapter are threefold:

- propose an architecture for wireless sensors that provides a longer range without requiring a battery at the node;
- using the phase of the backscattered signal for passively determining the sensed parameter;
- demonstrate its operation in a real-world scenario.

The remainder of this chapter is organized as follows. In Section 4.2, we discuss the working principle of the sensor node. In Section 4.3, the details of the proposed design are discussed. Section 4.4 is dedicated to the discussion of the results. Finally, the chapter is concluded in Section 4.5.

4.2 Working Principle

UHF RFID setup generally consists of two components: an interrogator, which reads information of an RFID tag; a tag, which keeps the tag ID and responds to an interrogator. The interrogator, sometimes also referred to as a reader, transmits an RF signal for a small duration of time. This signal serves three purposes. The first is to energize the tag by transmitting an unmodulated RF signal. This energy is used to wakeup the tag. Following that, an interrogation signal is sent to request the tag to respond. Finally, the tag responds by sending its ID.

Along with the tag ID, some other useful sensing information such as temperature, humidity, water level, moisture, flood, etc. can also be included. This inclusion allows making a simple RFID a wireless sensor node. To send the information, the system requires some modifications based on preference. The sensed information can either be sent back in the digital or in analog domain. Digital transmission is generally more immune to noise however it also requires more power. Analog communication, on the other hand, is more power efficient. In a scenario where nodes are powerless, the power efficiency of the system is paramount. Therefore, analog communication is selected in our case.

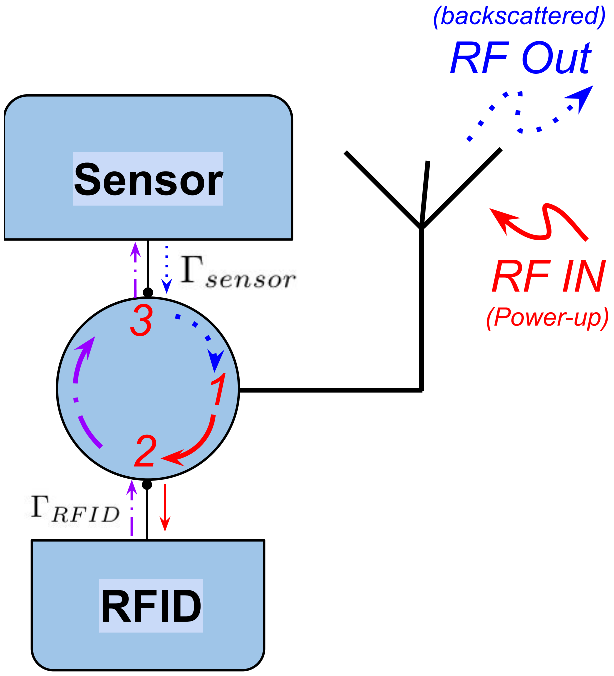

Figure 4.2: Block diagram of the proposed battery-less wireless sensor.

To realize the system, the power being reflected by the tag is sent through a capacitive sensing element on its way back to the reader. The block diagram is shown in Fig. 4.2. As a result, the element adds some extra phase delay, depending on the condition of the element, which allows reading the sensed value at the reader, without compromising any power. Thus, the addition of an element to the system doesn't theoretically reduce the read-range of the RFID tag.

Reading the phase at the reader is accomplished by a non-coherent IQ demodulator, which is in-built in almost every commercially available reader. The reader mixes an in-phase and a quadrature version of the transmitted signal with the received one and determines the amplitude of the output. These amplitudes are eventually used in determining the phase of the received signal.

To achieve the required specifications, a three-port system was developed, for which the details are provided in the following section.

4.3 System Design

The proposed system is an integration of an RFID and a sensing element in a three-port structure. To understand the system, we will first discuss the three-port structure and then the whole system.

4.3.1 Three-port Structure

A three-port RFID structure uses a non-reciprocal device to send the backscattered signal from the RFID to a different port, which is connected to a sensing element. The signal after entering the element is reflected from it with a phase change, based on the sensed value. It should be noted here that, since the element is capacitive, the loss of signal power is minimal. This attribute is highly desirable for a battery-less sensor.

The required characteristics of a three-port structure are obtained in a circulator. A circulator is a nonreciprocal device that allows power flow between ports in a certain direction only. The direction of power flow depends on its construction and can be either clockwise or counterclockwise. For a typical circulator offering clockwise circulation, with every port matched, the scattering matrix is given by [140],

$$\mathbf{S_{circulator}} = \begin{bmatrix} 0 & 0 & 1 \\ 1 & 0 & 0 \\ 0 & 1 & 0 \end{bmatrix}. \tag{4.1}$$

During the power up state, when RFID is storing energy, all the power is sent to the RFID, which acts as a matched load. Thus the scattering matrix of the three-port structure is considered as (4.1). However, in the case when the RFID chip is reflecting the signal for communication, the scattering matrix is no more the same. A signal flow graph, shown in Fig. 4.3 can be used to determine the characteristics of the system.

The signal that is reflected by the sensor is formulated as follows:

$$\Gamma_{in} = \frac{b_1}{a_1} = S_{11} + \frac{S_{13}S_{32}S_{21}\Gamma_{RFID}\Gamma_{sensor}}{(1 - S_{33}\Gamma_{sensor})(1 - S_{22}\Gamma_{RFID})}, \tag{4.2}$$

where S_{ij} are the scattering parameters of the circulator, Γ_{RFID} and Γ_{sensor} are the reflection coefficient of the RFID chip and sensing element, respectively.

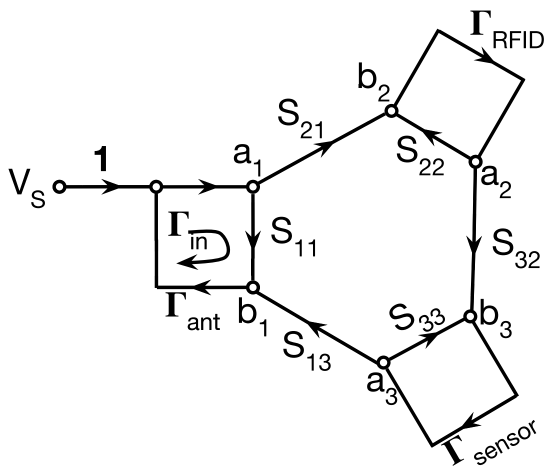

Figure 4.3: Signal flow graph of the sensor when RFID is backscattering.

For the case when $S_{11} = S_{22} = S_{33} = \Gamma_{ant} = 0$ and $S_{13} = S_{32} = S_{21} = 1$, then the input reflection coefficient is given by

$$\Gamma_{in} = \frac{b_1}{a_1} = \Gamma_{RFID}\Gamma_{sensor}. \tag{4.3}$$

Considering the RFID and the sensing element to be perfectly reflective (lossless), we get

$$\Gamma_{in} = e^{j(\theta_{RFID}+\theta_{sensor})}, \tag{4.4}$$

where, θ_{RFID} and θ_{sensor} are the phase delay caused by the RFID and the sensing element, respectively. Here, θ_{RFID} depends on the distance between the RFID and the reader and is a known parameter, whereas, θ_{sensor} is the phase delay caused due to the capacitance of the sensing element. This capacitance depends on the physical parameters that the sensing element is reading. The resulting phase delay can be easily read by the reader, which is explained later.

A circulator can be physically realized in different ways, such as a Ferrite core, directional coupler with a mismatched port, etc. For simplicity, we have used a low-cost ferrite-core clockwise circulator, SKYFR-001400 from Skyworks, that offers very low insertion-loss, less than 0.5 dB [141].

4.3.2 Capacitive Sensing Element

The sensing element could be designed to be either resistive, in which resistance changes with the change in the physical parameter, or reactive, in which reactance changes with the change in the physical parameter. The former ones are usually lossy and not preferred when energy efficiency is a concern. In the latter ones, since only the reactance of the sensing element changes ($Z = \pm jX$), they are more energy efficient. In capacitive sensing elements, usually change in the parameter of interest causes permittivity variation that results in a change in the capacitance ($C = \epsilon \frac{d}{a}$). Therefore, they are a good candidate for a battery-less wireless sensor.

Capacitive sensing elements are widely available in the market. However, their operating frequency range is low, usually in the order of tens of kilohertz. Therefore, for a sensing element to operate in the proposed system, new sensing elements with simple configurations were designed.

For a thorough understanding of the system, first, a varactor diode circuit was utilized to mimic a capacitive sensing element. These diodes have a wide tuning range from 1 pF to 53 pF at 915 MHz. They provide important information regarding the behavior of the system such as the amount of phase change per picofarad. The circuit design consists of a simple biasing network and a DC-blocking capacitor. An illustration is shown in Fig. 4.4 (a).

Another sensing element was designed to determine flooding in a given region. In the flood sensing element, a design with two closely-spaced electrodes is used to form a capacitor. As the water level rises, the average permittivity of the capacitor changes, which in turn changes the capacitance of the sensing element. The reason for using such a sensor was the ease in its manufacturability compared to other designs based on interdigitated capacitors.

Finally, this change is superimposed on the RFID signal by altering the phase of the backscattered signal from the tag and can be easily read by the reader. An illustration of the sensor is shown in Fig. 4.4 (b).

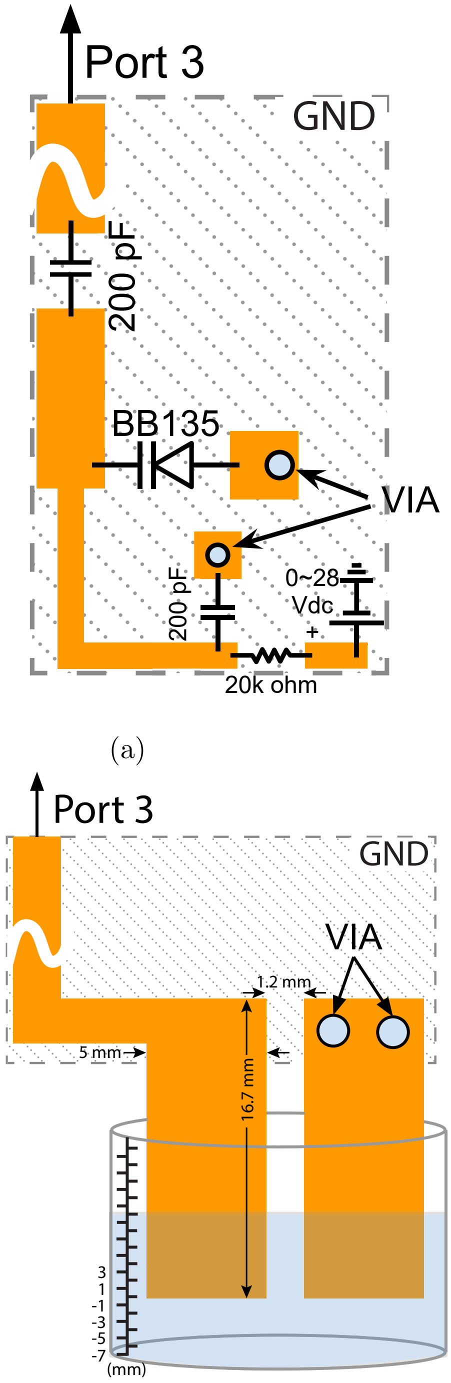

(a)

(b)

Figure 4.4: Sensor topologies: (a) varactor (b) flood.

4.3.3 RFID Matching Network

The RFID tag used for proving our concept was Higgs-4 by Alien in SOT 323 packaging [142]. It is a highly integrated single-chip IC that operates at

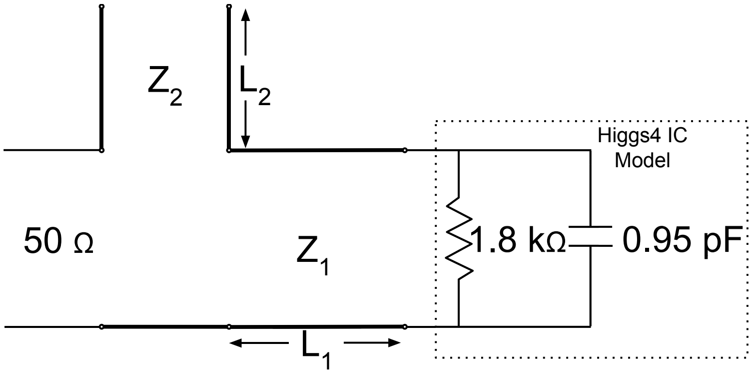

Figure 4.5: Schematic of the single-stub design used to match the RFID to 50-ohms.

UHF frequencies. The IC is designed to meet the standards of EPC Gen 2. The minimum required power to wakeup this IC is -18.5 dBm. The operating frequency of the IC spans from 840 MHz to 960 MHz with an equivalent parallel RC circuit at its input. The resistance and the capacitance of the IC are 1.8 kΩ and 0.95 pF, respectively.

In order to connect the IC to the system, a matching network is required to transform the tag impedance to 50 Ω to match it to the impedance of the circulator. A differential or non-differential matching network may be designed. A differential matching network provides out-of-phase signals at the input of the IC and thus develops higher voltage difference at the input pins but at the expense of complexity. For simplicity, we used a non-differential matching network in which one port of the IC was grounded and the other was attached to a matching network, which was designed to match the tag's input impedance, from $Z_{in} = 18 - j181\ \Omega$ at 915 MHz to 50 Ω. A single-stub matching network with an open-circuited series stub was used for the matching [32]. The network was initially designed using a Smith chart for 50 Ω transmission lines with a distance from the load to stub as 83.716°, while the open-circuited stub was calculated to be 80.737°. A schematic is shown in Fig. 4.5.

To realize the circuit, the stubs were first meandered and then optimized to cover the whole bandwidth from 902 MHz to 928 MHz using Keysight's Advanced Design System, version 2019. The optimizer was set to vary the

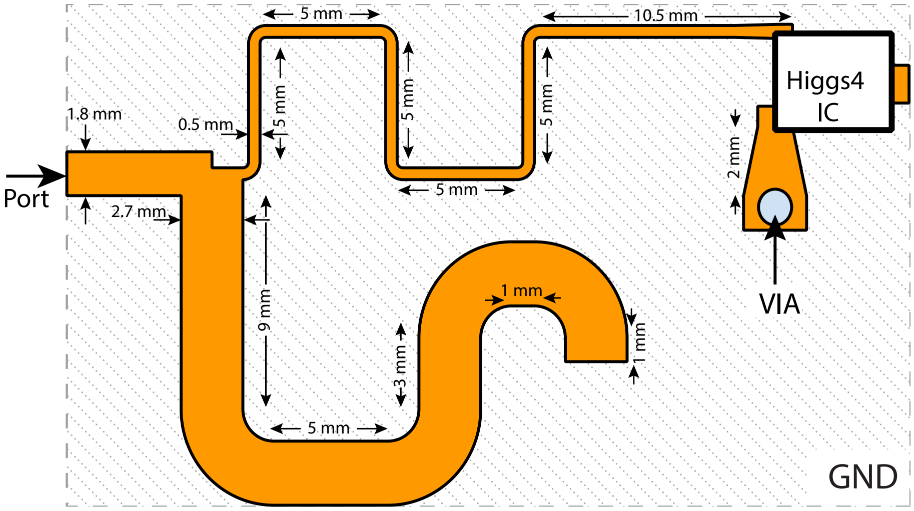

Figure 4.6: Final miniaturized and optimized version of the matching circuit of the Higgs 4 IC that utilizes microstrip technology to match the IC to 50 ohm impedance.

stubs' widths and lengths using the Least Pth algorithm until the reflection coefficient of less than -10 dB for the whole bandwidth was achieved. The final optimized circuit was fabricated on an RO4003C substrate with relative permittivity (ϵ_r) of 3.38, a thickness of 0.81 mm, and a loss tangent ($tan\delta$) of 0.0027. The final miniaturized circuit, with all the physical dimensions, is shown in Fig. 4.6.

4.3.4 System integration

For a clockwise ferrite core circulator, each component must be connected in a proper sequence to have optimum performance. An antenna may be connected to port 1 of the circulator. If so, the RFID tag with its matching network must be connected to the following port, in the clockwise direction, i.e. port 2. Finally, the sensing element is connected to the last remaining port, as shown in Fig. 4.2. The final integrated system is shown in Fig. 4.7.

The reason for connecting the sensing element after the RFID is as follows. Normally, a capacitive sensing element is considered lossless, however, practically, it may have some losses. If the signal from the reader is sent to the sensing element before it is sent to the RFID tag, it will be attenuated. As a result, the signal reaching the RFID terminals will be smaller in amplitude.

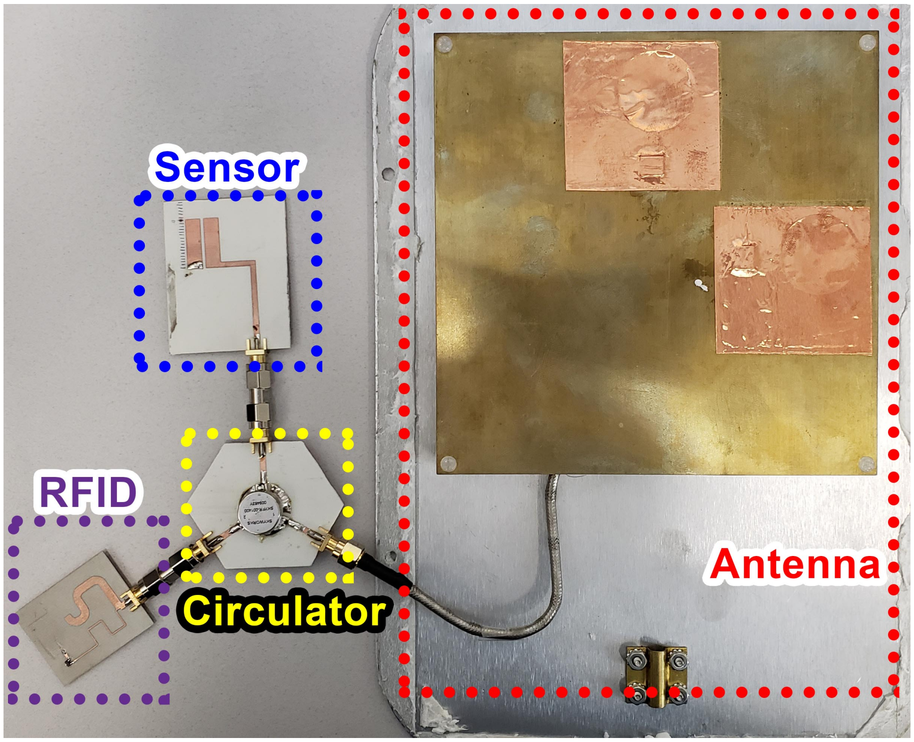

Figure 4.7: Final fabricated design of the battery-less wireless sensor.

Thus, the RFID will store less energy.

On the other hand, if the sensing element is connected after the RFID, in the circulator, the RFID wakes up with a stronger signal resulting in a higher read-range. In this case, the only loss a power-up signal faces is the circulator's insertion loss, which is only 0.5 dB. On the other hand, losses in the backscattered signal will include imperfect reflection from the tag; the circulator's insertion loss from the tag to the sensing element; the sensing element loss and the circulator's insertion loss from the sensor to the antenna. As the sensitivity level of a typical reader can be as low as -90 dBm, the backscattered signal being attenuated can be tolerated. Therefore, this observation confirms that charging the RFID tag is a limiting factor and advice that the capacitive sensing element should be connected after the RFID to avoid any loss in the signal being received by the tag for power-up purposes.

The overall power-up signal loss in this configuration can be determined as follows. Keeping in mind that the insertion loss of the circulator is 0.5 dB, to receive -18.5 dBm at the RFID tag, we need to make sure that the node receives a signal power of -18 dBm (0.5 dB higher than the tag). Using the Path loss formula, we can find that a 0.5 dB of path loss is incurred for a distance of 27.6 mm. Therefore, the reduction in the distance of the RFID in the proposed configuration is simply 0.027 meters, which is negligible in our case.

4.3.5 Reader

The reader used in our experiments was the AS3993 Fermi evaluation kit that included all the components and was able to provide up to 22 dBm of output power (extendable to 30 dBm for a longer range) [143]. It includes a combination of a directional coupler and a low-pass filter to separate the transmitted signal from the received one. The received signal is fed to a non-coherent I and Q, IQ, mixer and sampled by an ADC to determine the strength of the IQ components of the signal independently. By applying simple trigonometry, $\tan^{-1}(\frac{Q}{I})$, the phase of the received signal is determined.

Finally, the phase delay caused due to the setup and distance between the RFID reader and the tag, which is θ_{RFID}, is nullified by calibrating the system using a known capacitance value attached to the RFID. Following that, the extracted phase value is transformed into the respective parameter, such as voltage in the case of varactor or water level in the case of flood sensor, to determine the state of the physical parameter of interest.

4.4 Results

4.4.1 Individual components

In this subsection, the performance of individual components is discussed and a comparison between the simulated and the measured results are shown.

As a first step, the performance of the designed RFID matching circuit was determined by measuring its scattering parameters. Although the simulated circuit was designed to be matched at 915 MHz, the measured response of the fabricated circuit was found to be shifted to 895 MHz. This shift did not have severe effects on the performance of the system when operating at 915 MHz.

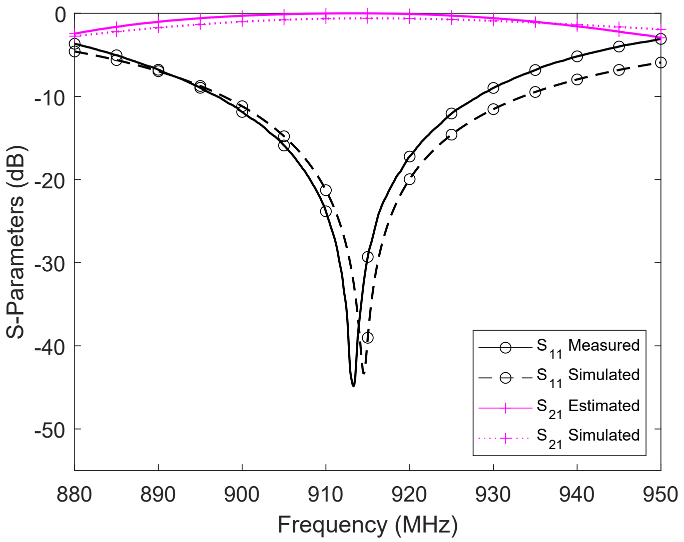

Figure 4.8: Frequency response of the RFID matching circuit.

The scattering parameters are shown in Fig. 4.8. Here, the input is marked as port 1, and the resistance of the RFID is marked as port 2. As port 2 does not exist in reality, an estimated response, S_{21} Estimated, was calculated using the S_{11} Measured. This helps in determining the power transfer to the RFID at different frequencies.

Since the performance of the proposed sensing structure is aimed to be demonstrated by the change in the capacitive load (varactor diode), the characterization of the varactor diode is required. Figure 4.9 shows the simulated and measured results of the impedance response of the NXP BB135 varactor diode [144]. The discrepancies between the simulated and measured results can be attributed to the fact that a high-frequency model of the varactor diode was not used. However, the deviation is small at lower voltages, i.e. from 0 to 10 volts.

Using the above results, a mathematical model between the phase of the reflected signal and voltage was developed using the process of curve fitting and reported by the following equation,

$$C = 3.314 \times 10^{-11} e^{-1.218V} + 1.978 \times 10^{-11} e^{-0.1748V}, \tag{4.5}$$

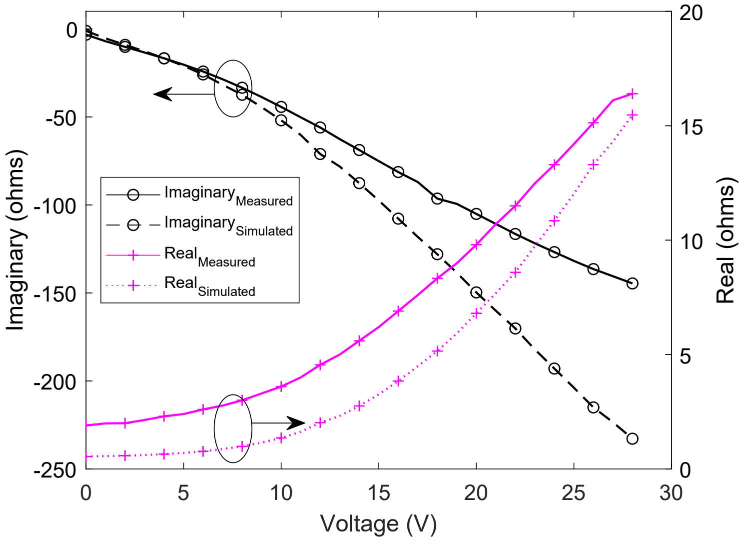

Figure 4.9: Impedance response of the varactor at 915 MHz.

and for a perfectly reflective capacitor,

$$\angle\Gamma = \tan^{-1}\frac{-2\omega C Z_o}{1-(\omega C Z_o)^2}, \tag{4.6}$$

where, $Z_o = 50\Omega$, $\omega = 2\pi f$, V is the voltage applied across the varactor and C is the capacitance of the varactor. These equations are useful in predicting the change in the phase of the reflected signal for voltages ranging from 0 to 10 volts.

The flood sensing element was also fabricated on the same substrate. The impedance response of the sensing element for increasing water levels was recorded and the results are presented in Fig. 4.10. The measured results are compared with the simulated results that were obtained by performing a full 3D EM simulation. The sensing element was designed to have a 7 mm space below the electrodes. Thus the actual electrodes were 7 mm above the base of the container. As the water level increases, a change in the reactance of the sensing element can be seen. The change is significant as the water reaches closer to the electrodes at $h = 0$ mm. It can also be seen that the resistance of the sensing element also starts increasing as the level of the water increases. This, in turn, may result in the reduction of the range and, therefore, its use should be avoided in this region if the long range is a concern.

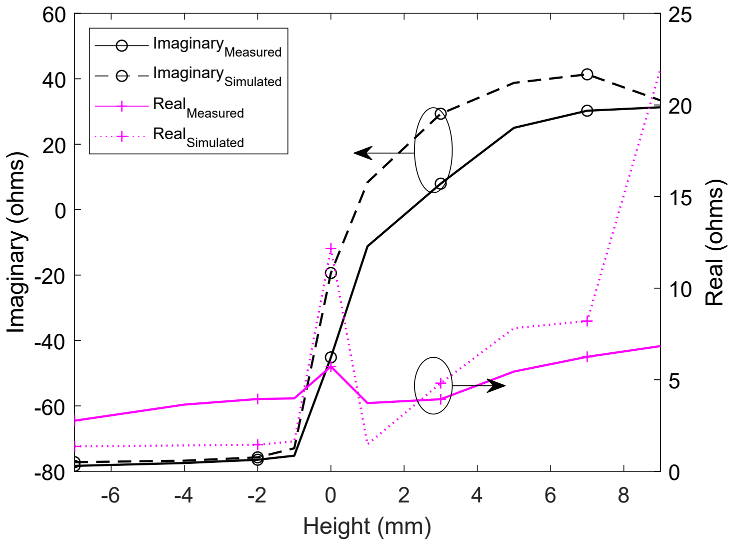

Figure 4.10: Impedance response of the flood sensing element at 915 MHz as the level of the water changes while keeping the electrodes 7 mm above the base of the container.

A mathematical relation between the phase of the reflected signal and voltage was found by developing the following exponential curve,

$$\boldsymbol{X_c} = \begin{cases} 0.483h - 75.17 & -\infty < h < -1 \\ -75.06e^{-0.3893h} + 34.4 & -1 \leq h < 9. \end{cases} \tag{4.7}$$

Using the relation $C = 1/\omega X_c$, we can again use (4.6) to predict the phase change for the change in the height of the water.

4.4.2 Full RFID system

We will now show the full battery-less wireless sensor setup and its performance. The setup consists of a reader, that measures the phase change and the proposed battery-less wireless sensor. For initial testing, the varactor diode was attached and the response of the system was observed. The setup is shown in Fig. 7.13 and the results are shown in Fig. 4.12. A clear one-to-one relationship can be seen in the results. Small variations in the results are expected since, to mimic a realistic scenario, the experiments were performed on a metallic table without the use of RF absorbers.

In the initial test, a triangular voltage was applied across the varactor diode to change its capacitance from 53 pF to 3 pF at 915 MHz. The corresponding

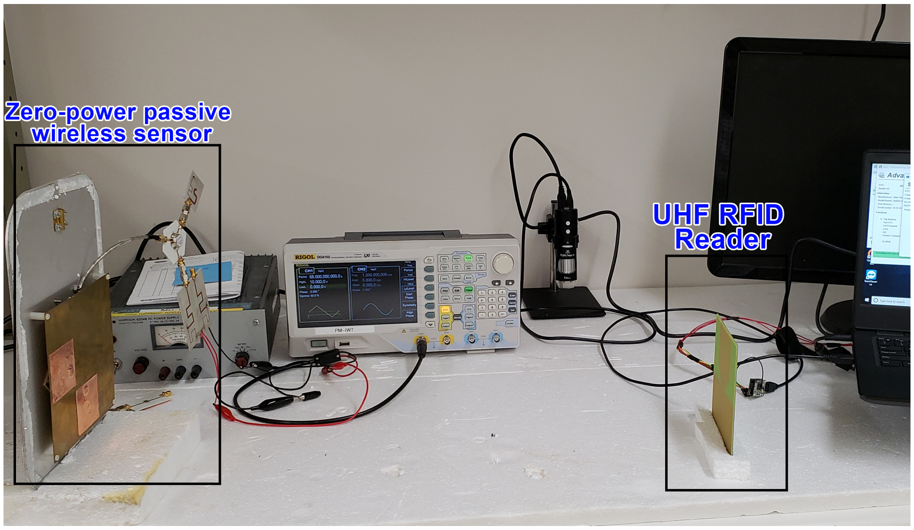

Figure 4.11: battery-less wireless RFID sensor with varactor attached at the sensing element port.

voltages were between 0 and 10 volts. It can be observed from Fig. 4.12 that the phase at the reader changes as the voltage across the varactor diode is varied. Initially, when the time is 0 sec, the voltage is at 5 volts and the phase is 49°. Next, when the voltage reaches its maximum value of 10 volts, the phase also reaches its maximum value of 75°. Similarly, when the voltage across varactor reaches 0 volts, the phase at the reader is read as 23°. The multiple sweeps show how repeatable the values are. An estimated phase, that was calculated using (4.6) and (4.5), is also shown in Fig. 4.12 to compare the simulated and measured results. The discrepancy between the measured and simulated phase at the edges (below and above 20 and 70 degrees, respectively) is higher is because the reader provides unstable measurements in these regions. There are other readers in the market, such as ThingMagic M6e, that may produce better results.

The proposed sensor was found to be working up to 7 meters. This was also verified through simple calculations. We need -18.5 dBm to power-up the tag. Therefore, the maximum acceptable path loss can be calculated using the following relation: -18.5 dBm = 22 dBm (reader power) + 2.1 dBi (reader antenna gain) - PL + 6.5 dBi (tag antenna gain) - 0.5 dB (circulator insertion loss) which leads to PL = -48.6 dB. At 915 MHz, this path loss is incurred for

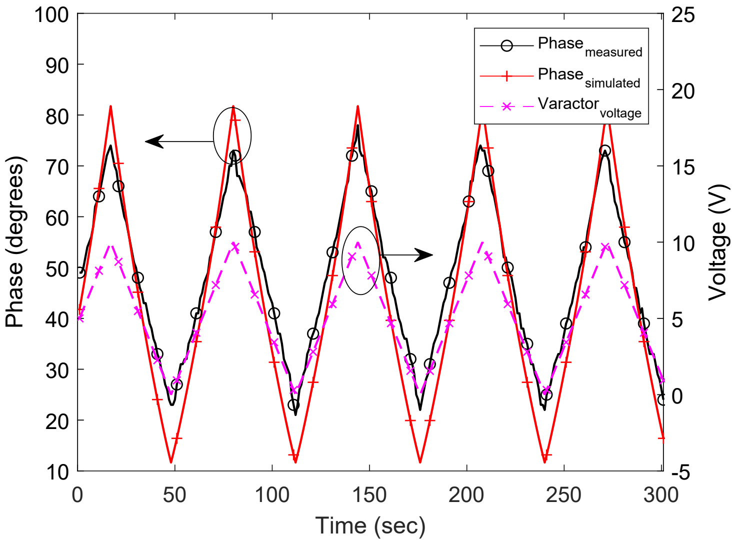

Figure 4.12: Measured phase change at the receiver as the voltage across the varactor is changed with time.

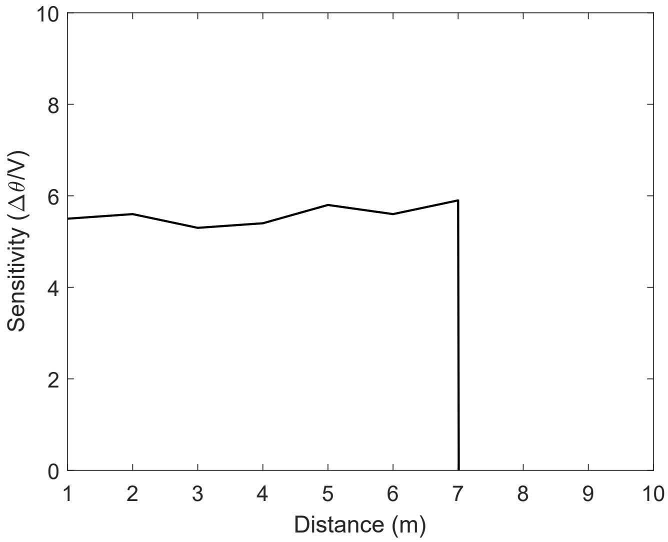

Figure 4.13: Sensitivity of the sensor at various distances.

a distance of 7 meters.

The experiments were repeated at different distances, ranging from 1–7 meters, to find out the sensitivity of the sensor, while the Tx power level was set to 22 dBm. As shown in Fig. 4.13, no noticeable change in the results was observed. The reason that the sensitivity remains unchanged is attributed to the fact that the charging of the tag is currently the limiting factor and it does not allow the reading of the sensor node at distances where the reflected signal would reach close to the sensitivity level of the reader.

This behavior could be further explained by considering the following situation. The RFID tag in the sensor node must operate until it receives the minimum required, power-up signal, of -18.5 dBm. Considering the worst-case scenario of the tag being at a distance of 7 meters, the backscattered signal received at the receiver can be calculated using the following relation: P_{rec}= -18.5 dBm (minimum required power of the power-up signal) - 1 dB (loss due to imperfect reflection from the tag [145]) - 0.5 dB (circulator's insertion loss) - 1.5 dB (loss in the sensing element) - 0.5 dB (circulator's insertion loss) + 6.5 dBi (tag antenna gain) - 48.6 dB (Path loss for 7 meters) + 2.1 dBi (reader's antenna gain). Therefore, the signal strength of the backscattered signal is calculated as -62 dBm. Nevertheless, the backscattered signal of -62 dBm, is still much higher than the sensitivity of the reader, which is -90 dBm. Therefore, the sensitivity of the sensor node remains unchanged for its distance of operation of 7 meters, and hence it can be said that the sensitivity of the proposed sensor is dependent on the receiver's sensitivity.

Finally, the performance of the battery-less wireless sensors in a real-life application was observed. In this test, the flood sensor was used to determine the level of water in a beaker. The setup is shown in Fig. 4.14 and the results are shown in Fig. 4.15. Initially, there is no water in the beaker and the phase is calibrated to around 0°. As soon as the water is injected into the beaker, the phase delay increases as shown in Fig. 4.15. When the water level reaches the electrodes (h=0 mm), the value reaches to around 65°. For comparison, the phase calculated using (4.6) and (4.7) is shown in Fig. 4.15. The measured results are in good agreement with the simulated ones.

To evaluate the performance of the sensor, the beaker was filled four times and the maximum value of all four peaks was observed to be slightly different. This indicates that the sensor may not be used to accurately measure water levels, however, in the case of flood sensing, a threshold value of 10° is always observed to be crossed, thus reliable flood sensing is possible.

All the above experiments were performed at a fixed distance from the

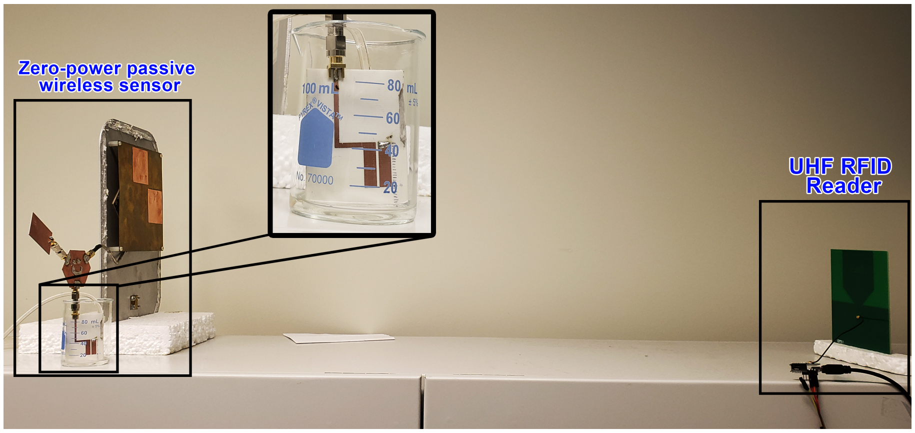

Figure 4.14: battery-less wireless RFID sensor with flood sensor attached at the sensor port.

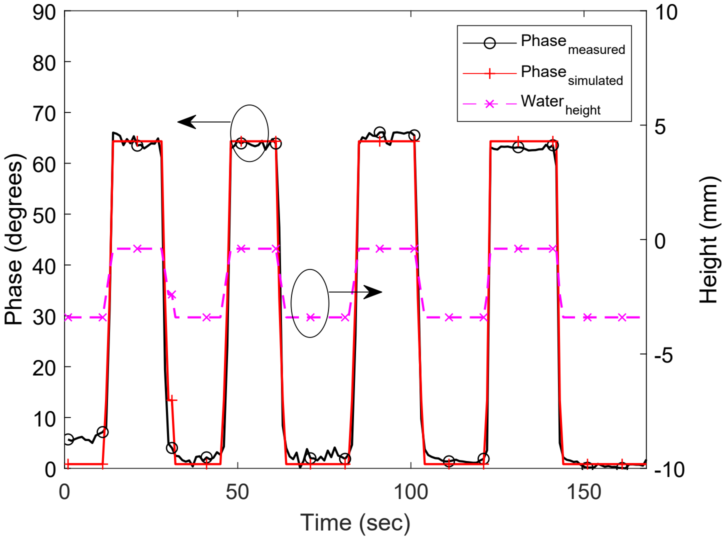

Figure 4.15: Performance of flood sensor shown by adding and removing water repeatedly.

reader. As the phase difference is dependent on the distance between the reader and the tag, the phase is expected to be different for different distances and is thus ambiguous for all the distances. To remove the ambiguity, the phase difference between three frequencies, two closely spaced and one further, can be used to determine the exact distance. Then the phase change due to distance can be adjusted to find the exact value of the sensor. Another method is to use a separate reference tag that is not affected by the environment. The phase difference between the reference tag and the sensor can be used to remove the

Table 4.1: Comparison of the proposed three-port wireless sensor with prior passive wireless sensor designs.

Parameter	**This work**	**Chipless [127–129] [130, 131]**	**Chip-based [51–53] [132–134]**
Battery	No	No	No
Complexity	low	low	Medium
Sensing	Any	Any	Any
Multiple nodes	Yes	No	Yes
Anti-collision	Yes	No	Yes
Bandwidth required	∼KHz	∼MHz	∼MHz
Range (m)	7	30	3–5

phase ambiguity.

A comparison of the proposed battery-less wireless sensor with the other state-of-the-art wireless sensors is done in Table 4.1. It can be seen that the proposed sensor offers low complexity, and allows multiple nodes to operate simultaneously along with a good operating range of 7 meters. Moreover, it requires less bandwidth as it can operate in any single channel of the RFID UHF band, which is typically 500 kHz. Since the proposed architecture modifies the phase of the backscattered signal, the changes in the parameter being sensed should be stationary compared to the modulation rate of the communication signal, which is usually in milliseconds.

4.5 Conclusion

In this chapter, a novel battery-less wireless sensor is proposed that works without a battery. The proposed architecture integrates an RFID tag with a sensing element and antenna using a circulator. The sensing elements, which are designed to be capacitive, add phase delay to the signal transmitted by the UHF RFID tag based on the parameter that is being sensed by the sensing element. A general system consisting of a varactor diode and a real system with a flood sensor is demonstrated. Results show that the architecture can be used to sense different parameters such as water level, flood, and moisture. It was also discussed how this architecture provides a longer range compared to other sensors available, without the use of batteries, and thus can be used in several different applications ranging from healthcare, and industrial to smart home monitoring.

Chapter 5

A Battery-Less RFID Sensor Architecture with Distance Ambiguity Resolution for Smart Home IoT Applications

In this chapter, a novel battery-less wireless sensor design is proposed and demonstrated. The proposed passive wireless sensor node integrates a UHF RFID chip, a filter, and a reactive sensing element to enable the reading of environmental conditions wirelessly, without increasing the complexity of a typical RFID chip and substantial loss of read-range. The sensing element changes the phase of the reflected RFID signal based on the sensed parameter, whereas, the filter helps in resolving any phase ambiguity that may arise due to the placement of the node at different distances. The phase change is detected at the reader using a non-coherent IQ demodulator. The design can easily integrate any type of sensing element such as temperature, humidity, and water level sensor. A flood sensor and a temperature sensor were used to demonstrate the performance of the proposed design in a home and office environment.

The design in the previous chapter could not be operated at variable distances as it required phase calibration. To the best of the authors' knowledge, there is no wireless sensor design based on RFID technology that passively integrates a sensing element without reducing the read-range of the RFID chip and can operate at any distance without requiring phase re-calibration, simultaneously.

In this chapter, we propose a novel passive wireless sensor design that addresses the aforementioned challenges of wireless sensors. The design comprises a UHF RFID chip, a filter, a UHF capacitive sensing element, an antenna, and a circulator. These components are arranged such that the reader signal is first sent to the RFID chip to store or harvest energy, while the backscattered signal is diverted to the sensing element, which is connected through a filter. The UHF sensing element, which must be capacitive or inductive in nature, only introduces some extra phase delay to the backscattered signal that is returning to the reader. The filter, in series, allows some frequencies to pass and reflects some frequencies. The frequencies that are reflected from the filter, without entering the sensing element, are used to estimate the reference phase of a frequency in the passband. This reference phase is subtracted from the actual phase measured at the passband frequency to compensate for phase delays due to distance and determine the phase delay only due to the sensing element. Since this architecture keeps the sensing element and the antenna separate, the radiation characteristics of the antenna are not altered by the changes in the sensing element, as it does in some previously published wireless sensors [51–53].

The proposed design can be used in several different applications and is especially suited to smart home IoT. A smart home generally requires several sensors such as humidity, temperature, or flood sensors, as shown in Fig. 5.1. These sensors are required to be densely deployed in a closed vicinity. Therefore, chip-based RFID technology is an ideal candidate as it supports spatial multiplexing in such an environment. Moreover, the eradication of batteries from the sensors is of key interest for home users. This is because batteries require periodic maintenance and pose a hazard of missing an alarm in the event of a battery run out. A fully passive system will significantly reduce any such hazards. Lastly, a longer read-range (greater than 5 m for smart homes) will reduce the number of readers required in a given room. These readers may easily connect to WiFi to upload data to servers for processing and also to keep users informed.

The goals addressed in this chapter are four-fold:

- propose a wireless sensor design for mid-range applications (5 to 10 meters) without needing any battery;
- use the phase delay information of the reflected signal to passively determine the sensor value;
- build in the ability to factor out changes in distance between the wireless sensor and the reader;
- demonstrate its performance in a home-office environment.

The remainder of this chapter is organized as follows. In Section 5.1, the working principle of the proposed battery-less wireless sensor is discussed. The details of the sensor design are provided in Section 5.2. Before concluding the chapter in Section 5.4, the results are presented and discussed in Section 5.3.

5.1 Working Principle

A typical RFID setup usually consists of two main components: a reader, which is capable of reading RFID chips in its vicinity, and a chip, where the information is saved. For operation, the reader transmits an RF signal that serves two purposes. The first is to power-up the chip while the second is to communicate wirelessly. For energizing, a simple RF signal is sent for a short duration, long enough to wake up the chip. For communication, digital modulation techniques are normally used. They are more immune to noise and allow multiple chips to be read simultaneously. For the chip to respond back, the incident signal of the reader is backscattered by changing the chips' antenna impedance from matched to short circuit. The backscattered signal is detected by the reader and demodulated to extract the ID of the chip.

Besides the chip ID, some extra useful information required in smart homes, for example, water level, humidity, and temperature may also be included. This information may be added in either digital or analog domains, depending

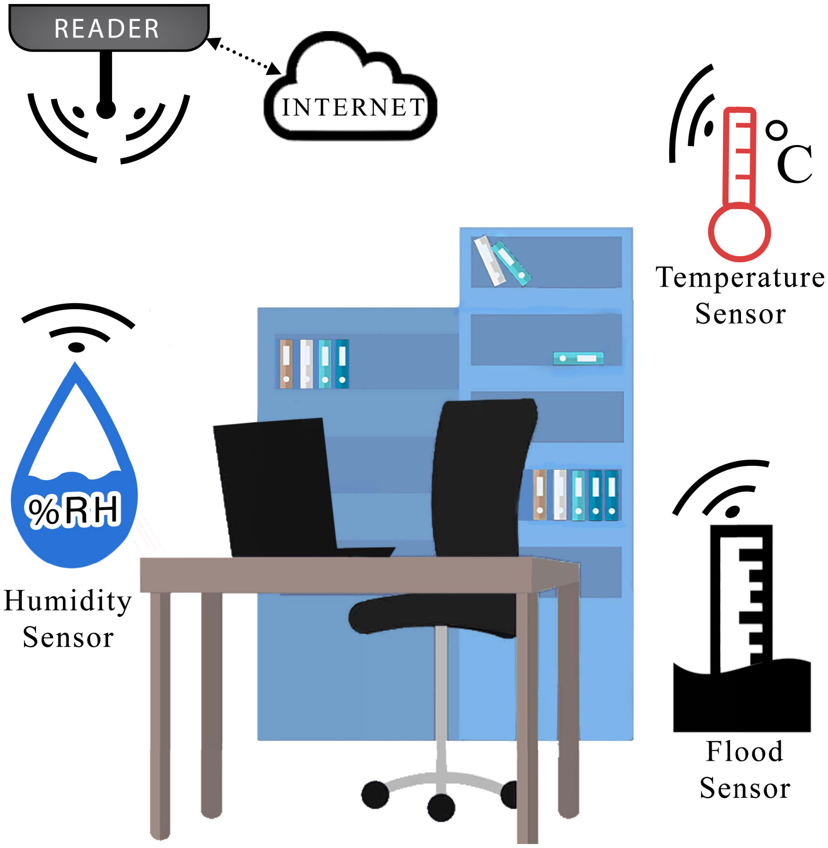

Figure 5.1: Concept art of battery-less wireless sensors communicating with an internet-connected reader in a smart home or office environment.

on the user's requirements. If high accuracy is a concern, then digital techniques are a better option. On the other hand, if a longer distance is desired, analog modulation is preferred due to its higher energy efficiency. Analog communication is prone to noise and hence the accuracy may be slightly reduced [146]. However, for smart home applications, this may not be a concern.

The proposed system concept is a hybrid of analog and digital communication. chip IDs are communicated through digital communication while the sensing data is sent through analog communication. To achieve the hybrid implication, the digitally modulated backscattered signal from the chip is passed through a reactive sensing element for additional analog modulation. The block diagram is shown in Fig. 5.2. The analog modulation is in the form of an additional phase delay versus the sensor condition. As reactive sensing elements do not dissipate any power, theoretically, the read-range of an RFID

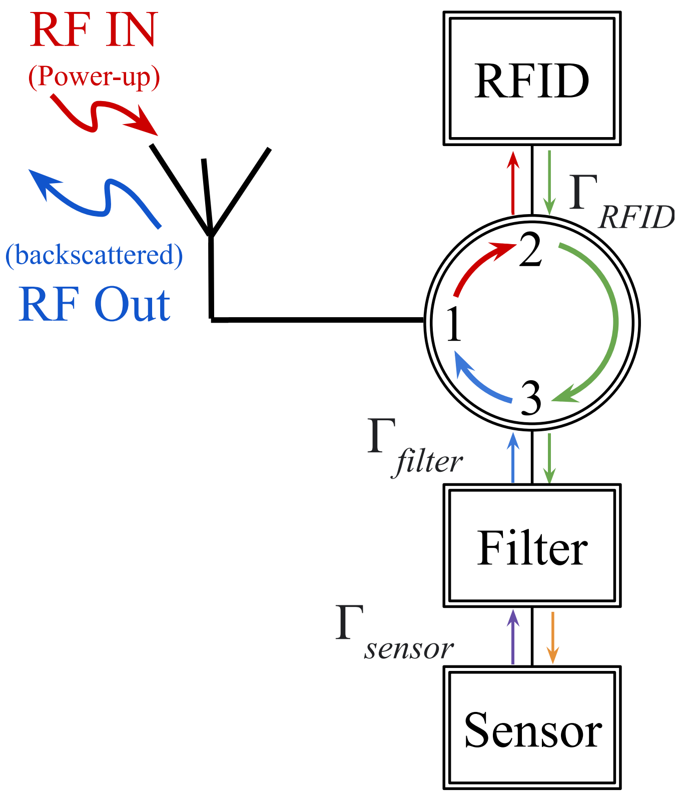

Figure 5.2: Block diagram of the proposed novel battery-less wireless sensor with distance ambiguity resolution.

chip is not affected by this additional circuitry.

The additional phase delay contributed by the sensing element is read out at the reading device by a built-in non-coherent IQ demodulator. The reader determines the amplitude of the in-phase and the quadrature version of the received signal and uses them to calculate the phase delay of the backscattered signal. This eventually provides sensing of the physical parameter of interest, based on the sensor type. A WiFi enabled reader can easily upload these data to the internet for data processing or to update the home occupants through a mobile application.

5.2 System Design

The system proposed in this chapter is obtained by integrating an RFID chip with a sensing element and a filter in a three-port structure. First, we will elaborate on the model of the proposed system, then we will discuss how an RFID chip establishes communication, how the sensing element alters the phase of the backscattered signal of the RFID chip, and how the filter helps in resolving the distance ambiguity in the phase of the backscattered signal.

5.2.1 Model

In a three-port RFID-based structure, a circulator is used to direct the reflected (backscattered) signal from the RFID chip to another port, which is connected to a reactive sensing element [147]. This signal, after passing through the sensing element, is reflected from it with an additional phase change, which is directly proportional to the sensed value.

Ideally, in a three-port wireless sensor, the phase should alter only due to the physical change in the sensing element. However, the wireless sensor node architecture proposed in [147] would experience phase change not only due to the sensing element but also the distance. Although the additional phase change due to the distance may be resolved through some kind of calibration, this can work only for a fixed distance and this technique will restrict any further changing in the distance. However, the ability to change distance is a much desirable property in wireless sensors. Therefore, a method to resolve this issue must be devised.

A method to resolve the distance ambiguity is to determine the phase delay of the setup with the sensing element excluded. This phase delay can act as a reference phase. In order to determine this reference phase, a controlled mechanism in the node is required that has the capability to direct an RFID signal to the sensing element, when required, or reflect it back before entering the sensing element.

The required behavior could be achieved by adding a filter in series with the sensing element. A filter is a fully passive device that passes signals within its passband while reflecting any out-of-band frequencies. Hence, an out-of-band frequency signal can be used to determine the reference phase, as it is reflected prior to entering the sensing element. This reference phase can be used to remove the effects of distance ambiguity and environmental variations from the actual phase delay, determined by a signal in the passband of the filter. A detailed mathematical model is presented in the following paragraphs.

Generally, a circulator is a device that forces the power between certain ports to flow in one direction only. This direction is totally dependent on its construction and can be either counterclockwise or clockwise [140]. Its scattering matrix is given by,

$$\mathbf{S_{circ.}} = \begin{bmatrix} S_{11} & S_{12} & S_{13} \\ S_{21} & S_{22} & S_{23} \\ S_{31} & S_{32} & S_{33} \end{bmatrix}. \tag{5.1}$$

For a typical circulator designed to operate in a clockwise mode, with all of its ports matched, the scattering matrix is given by,

$$\mathbf{S_{circ.}} = \begin{bmatrix} 0 & 0 & 1 \\ 1 & 0 & 0 \\ 0 & 1 & 0 \end{bmatrix}. \tag{5.2}$$

However, in our case, the RFID chip alternates between a matched load and an unmatched load. Moreover, the sensing element also acts as an unmatched load. In this case, the isolation of a circulator is dominated by the mismatch at the other port. Therefore, a thorough model is required to understand the operation of the sensor. A detailed end-to-end signal flow graph, shown in Fig. 5.3, provides deeper insight, which helps in understanding the proposed system.

The backscattered signal of the sensor node, incorporating reflections, insertion loss, and imperfect isolation of the circulator due to mismatch, is formulated as follows:

$$\begin{aligned} \Gamma_{in} = \frac{b_1}{a_1} = S_{11} + \Bigg[& \frac{S_{21}\Gamma_{RFID}S_{32}S_{13}}{(1 - S_{22}\Gamma_{RFID})(1 - S_{33}\Gamma_{RFID})} \quad , \\ & \times \left(S_{f11} + \frac{S_{f12}S_{f21}\Gamma_{sensor}}{1 - S_{f22}\Gamma_{sensor}} \right) \Bigg] \end{aligned} \tag{5.3}$$

where S_{ij} ($\forall\, i, j = 1, 2, 3$) is the scattering parameter of the circulator, S_{fij} ($\forall\, i, j = 1, 2$) is the scattering parameter of the filter, and Γ_{sensor} and Γ_{RFID} are the reflection coefficient of the sensor and the RFID chip, respectively.

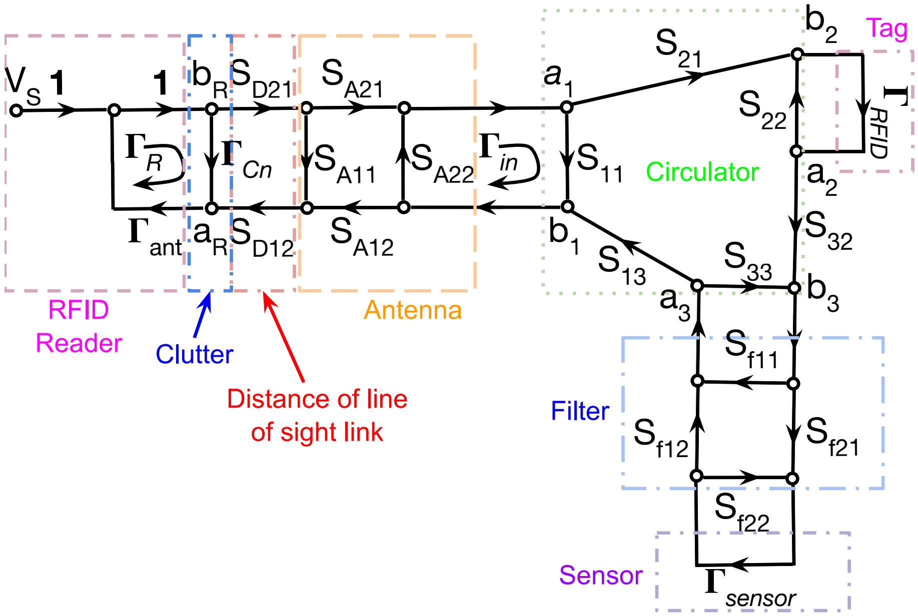

Figure 5.3: Signal flow graph of the sensor node and the path for the instant when the RFID chip is in the reflecting state. Where, R, D, A, and f represent the reader, thedistance of the chip from the reader, antenna, and filter, respectively.

On the other hand, the backscattered signal to the reader is formulated as:

$$\Gamma_R = \frac{b_R}{a_R} = \Gamma_{C_n} + S_{A11}S_{D21}S_{D12}+ \frac{S_{D21}S_{D12}S_{A21}S_{A12}\Gamma_{in}}{1 - S_{A22}\Gamma_{in}}, \quad (5.4)$$

where S_{D21} and S_{D12} are path-loss for the power-up signal and the backscattered signal respectively. Moreover, S_{Aij} $(\forall\, i, j = 1, 2)$ is the scattering parameter of the RFID chip antenna. In addition, Γ_{C_n} represents all sources of clutter and hence can be written as $\Gamma_{C_n} = \sum_{n=1}^{O} S_{D_{n21}} S_{D_{n12}} \Gamma_n$. Here $S_{D_{n21}} S_{D_{n12}}$ represents two-way path-loss, Γ_n represents the RCS of the object and O represents the total number of objects under consideration. This may incorporate any structural mode reflections of the antennas attached to the circulator. Since these are all unnecessary signals and considered noise by a reader, to reduce the noise floor, readers typically incorporate a mechanism to cancel out these signals [148].

For the case when the RFID chip is harvesting energy, the chip acts as a matched load, i.e. $\Gamma_{RFID} \approx 0$. The majority of power contributing to the backscattered signal can be formulated by considering $S_{11} = S_{22} = S_{33} = 0$ and $S_{13} = S_{32} = S_{21} = 1$. The reflection coefficient at the reader (Γ_R) for the matched case is given by

$$\Gamma_R = \frac{b_R}{a_R} = S_{A11}S_{D21}S_{D12}. \tag{5.5}$$

When the RFID chip reflects the power to establish communication, Γ_{RFID} is close to 1. This is because the chip acts as a mismatched load, resulting in the reflection of any incident power. The majority of the power contributing to the backscattered signal can be formulated by considering $S_{11} = S_{22} = S_{33} = S_{A11} = S_{A22} = 0$ and $S_{13} = S_{32} = S_{21} = 1$, the reflection coefficient at the reader (Γ_R) is given by

$$\begin{aligned}\Gamma_R = \frac{b_R}{a_R} = S_{D21}S_{D12}S_{A21}S_{A12}\Bigg[&\frac{S_{f11}\Gamma_{RFID}}{1 - S_{f22}\Gamma_{sensor}} \\ &+ \frac{-S_{f11}S_{f22}\Gamma_{sensor}\Gamma_{RFID} + S_{f21}S_{f12}\Gamma_{sensor}\Gamma_{RFID}}{1 - S_{f22}\Gamma_{sensor}}\Bigg]\end{aligned} \tag{5.6}$$

It should be kept in mind that the assumption for infinite port-to-port isolation may not hold valid when operating at extremely high frequencies. At those frequencies, more robust models may be required.

For a reciprocal channel and antenna, the backscattered signal at a frequency, f, in the passband of the filter is formulated as:

$$\Gamma_{R\_pass}(f) = |\Gamma_R(f)|e^{j(2\theta_D(f)+2\theta_A(f)+2\theta_{filter}(f)+\theta_{RFID}(f)+\theta_{sensor}(f))}, \tag{5.7}$$

whereas the signal at a frequency, f, in the stopband of the filter is formulated as:

$$\Gamma_{R\_stop}(f) = |\Gamma_R|e^{j(2\theta_D(f)+2\theta_A(f)+\theta_{filter\_stop}(f)+\theta_{RFID}(f))}, \tag{5.8}$$

where $\theta_D(f)$, $\theta_A(f)$, $\theta_{filter}(f)$, $\theta_{RFID}(f)$, $\theta_{sensor}(f)$, and $\theta_{filter\_stop}(f)$ are the phase delays at f caused, respectively, due to sensor-to-reader distance, antenna, filter in the passband, RFID chip circuitry, sensing element, and filter in the stopband, respectively.

When comparing (5.7) and (5.8), it can be seen that (5.8) excludes the effects of the sensing element and it may be used to remove the phase delay due to distance in (5.7). However, practically, (5.8) cannot be measured directly at the frequency being used to measure (5.7). In order to measure it, either the filter must be modified (which is an impractical solution) or Γ_{R_stop} must be estimated using some frequencies that are in the stop band of the actual filter. Once estimated, it may be divided by (5.7) to remove the effect of the distance.

The estimated phase can be easily determined by measuring two frequencies in the stopband and then using a two-point formula to estimate it for the frequency in the passband as,

$$\theta_{R_{stop\_est}}(f) = \frac{\theta_R(f_{stop2}) - \theta_R(f_{stop1})}{f_{stop2} - f_{stop1}}(f - f_{stop2}) + \theta_R(f_{stop2}). \tag{5.9}$$

Using (5.9), we can find the following relation,

$$\angle\Gamma_{R\_stop\_est}(f) \approx \angle\Gamma_{R\_stop}(f). \tag{5.10}$$

The approximation may be invalidated if any of the selected frequencies undergo multipath reflections while others don't, and vice versa.

Now, the phase of the backscattered signal that contains the sensed information, which is unaffected by the change in distance, can be determined using the following relationship:

$$\Gamma_{R\_sensor}(f) = \frac{\Gamma_{R\_pass}(f)}{\Gamma_{R\_stop\_est}(f)}. \tag{5.11}$$

This relationship is mathematically evaluated using (5.10) to check if the desired outcome is achieved. Since the required information is found in the phase of the backscattered signals, the outcome is evaluated as,

$$\begin{aligned}\angle\Gamma_{R\_sensor}(f) = {} & (2\theta_D(f) + 2\theta_A(f) + 2\theta_{filter}(f) + \theta_{RFID}(f) + \theta_{sensor}(f)) \\ & - (2\theta_D(f) + 2\theta_A(f) + \theta_{filter\_stop}(f) + \theta_{RFID}(f)),\end{aligned}$$

$$\angle\Gamma_{R\_sensor}(f) = \theta_{sensor}(f) + \theta_{difference}(f), \tag{5.12}$$

where $\theta_{difference}(f) = 2\theta_{filter}(f) - \theta_{filter\_stop}(f)$. It can be seen that a small difference is incurred in this technique. Regardless, this difference can be easily measured during the calibration process and remains constant regardless of the distance of the sensor.

In practice, once the reference phase is determined using (5.9) along with $\theta_{difference}(f)$, it may be subtracted from $\theta_{R\_pass}(f)$ to determine the relative phase of the sensor, as:

$$\angle\Gamma_{R\_sensor\_relative}(f) = \theta_{R\_pass}(f) - \theta_{R_{stop\_est}}(f) - \theta_{difference}(f), \tag{5.13}$$

$$\angle\Gamma_{R\_sensor\_relative}(f) = \theta_{sensor}(f), \tag{5.14}$$

where $\theta_{sensor}(f)$ is the phase delay caused by the capacitive nature of the sensing element. This delay is directly proportional to the physical input being sensed by the sensor. It can be easily read at the reading device to eventually determine the physical state of the object under observation.

5.2.2 Physical Realization of the Components

Circulator

There are several ways to make a circulator such as using a ferrite core, transistor [149], or a directional coupler with an unmatched load at a port. In this work, an SMD-based low-cost clockwise circulator with ferrite-core, SKYFR-001400 from Skyworks [141], with insertion loss less than 0.5 dB, is used.

Capacitive Sensing Element

In a capacitance-based sensing element, a change in reactance ($Z = \pm jX$) helps to determine any change in the object under observation. To achieve this, some sensing elements are designed so that changes in the object under observation cause changes in the permittivity (ϵ) of the capacitor, which in turn changes its capacitance ($C = \epsilon\frac{A}{d}$, where A and d are the area of the capacitor and distance between them, respectively). Since the resistive part of the capacitance-based sensing element is minimal, such elements are more energy-efficient. Hence, they are considered a good option for a battery-less wireless sensor platform.

To demonstrate the performance of the proposed sensor, we have shown the operation with a flood/moisture detector and a temperature sensing element.

These elements, due to their reactive nature, cause a phase change in the backscattered signal of the RFID chip and can be easily determined at the reading device.

The flood/moisture sensing element was designed to determine the presence of liquids in a given region. In this sensing element, two electrodes with a small gap are designed to form a planar capacitor. As the volume of fluid changes in the surroundings, the average permittivity of our designed capacitor varies; as a result, the capacitance of the sensing element changes. A model of the proposed sensing element is depicted in Fig. 5.4(a). The reason behind using such a sensor was the ease in its manufacturability compared to other designs based on interdigitated capacitors.

Similarly, a temperature sensing element was designed to determine variations of temperature in the environment. A combination of thermistors and capacitors was used to design a sensing element for which the capacitance changes with the temperature change. The thermistor used possessed a negative temperature coefficient of around 56 Ω at room temperature. To improve reflections at the input of the sensing element, multiple parallel branches were introduced until enough sensitivity was achieved over a wide range of temperature values. Multiple parallel branches reduce the resistance of the sensing element and ensure that the response remains reactive, which is required to operate in the proposed architecture.

The impedance responses of both the flood and the temperature sensing elements were simulated and measured. The impedance response of the proposed flood sensing element for increasing water levels and the impedance response of the proposed temperature sensing element for increasing temperatures are shown in Figs. 5.5 and 5.6, respectively.

The electrodes of the flood sensing element were designed to keep 7 mm of empty space at the bottom. As the water level (h) rises, a shift in the reactive part of the sensing element is observed. The shift is abrupt when the liquid approaches the electrodes, which are at $h = 0$ mm. A rise in resistance of the sensing element can be seen as the water level rises. This can be explained by the fact that the water is lossier than the air at the frequency

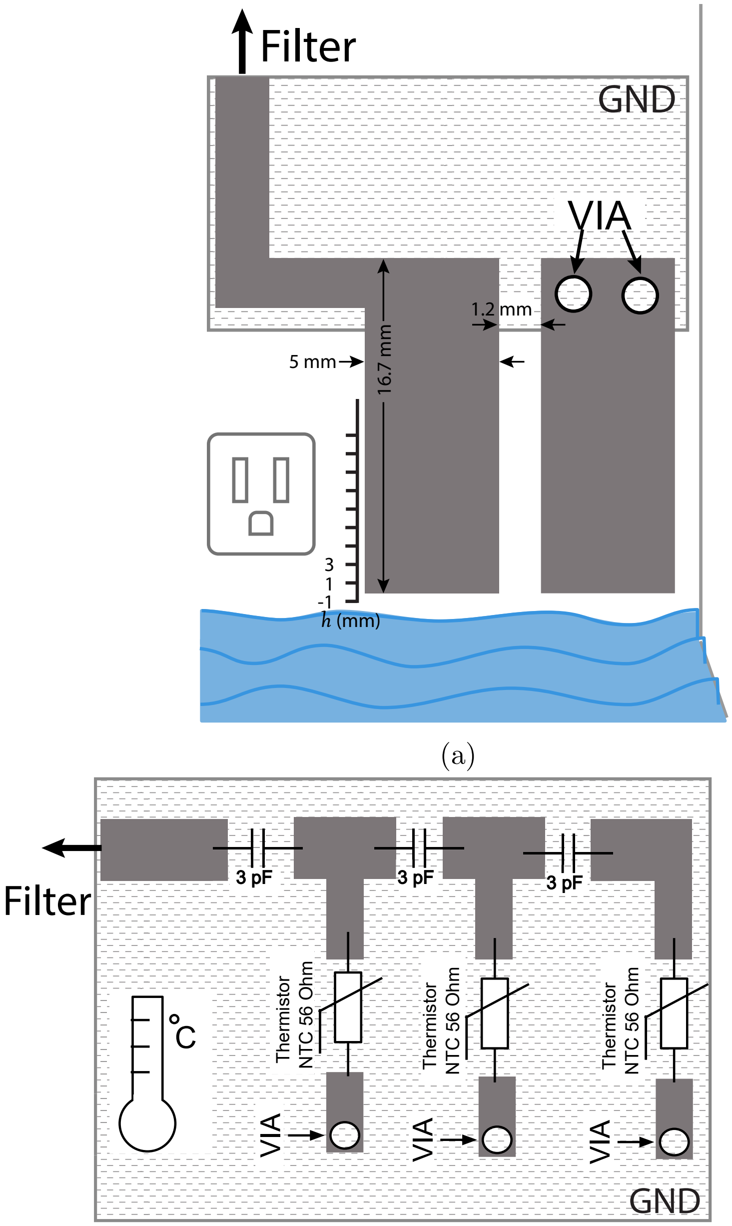

(a)

(b)

Figure 5.4: UHF Sensor topologies: (a) flood/moisture (b) temperature.

of operation. Regardless, it shouldn't be a concern as a certain amount of loss in the backscattered signal can be tolerated.

RFID Chip

The RFID chip used in this design was Higgs-4 by Alien [142] with a minimum wake-up power of -18.5 dBm. In order to connect this chip to the node, a

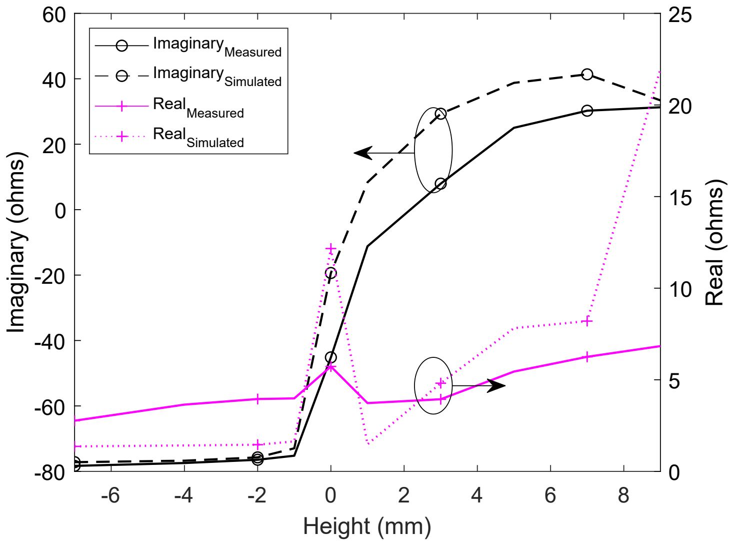

Figure 5.5: Impedance response of the proposed flood sensing element at a fixed frequency of 915 MHz with varying water levels in a container.

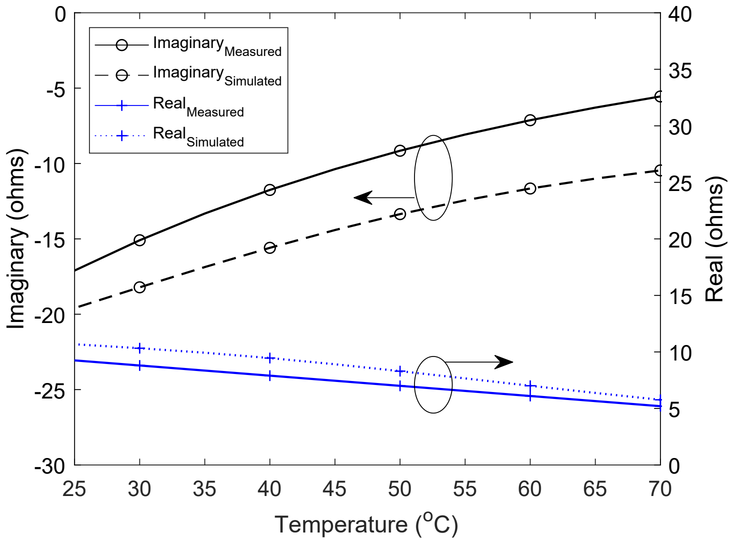

Figure 5.6: Impedance response of the temperature sensing element at 915 MHz at temperatures varying from 25 ^{o}C to 70 ^{o}C.

matching network was designed to transform the chip impedance of $Z_{in} = 18 - j181\ \Omega$ to 50 Ω. To design the network, a single-section open-circuited series stub was utilized. The stubs were then tuned to achieve an operational bandwidth from 902 MHz to 928 MHz. The schematic and frequency response of the designed matching network are shown in Figs. 5.8 and 5.7, respectively.

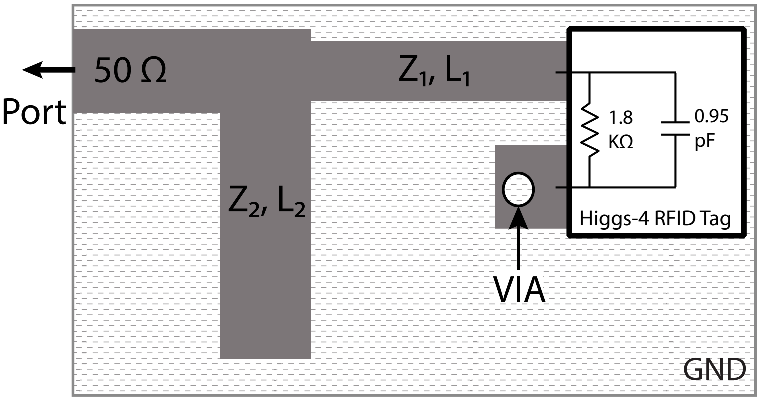

Figure 5.7: RFID chip matching network using open-circuited single-stub. Optimized values for a wider bandwidth: Z_1=96.5 Ω, L_1=70.19°, Z_2=39 Ω, and L_2=69.1°.

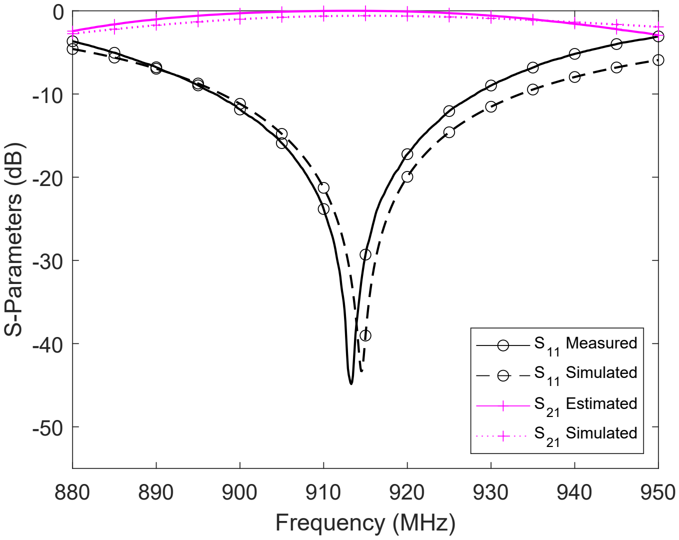

Figure 5.8: The frequency response of the proposed matching network for the integration of RFID chip in the node, which was measured at -18.5 dBm input power.

Here, port 2 corresponds to the 1.8 kΩ resistor inside the RFID chip, which was kept as a termination in our simulations.

Filter

A proper selection of the filter is necessary in this design. Therefore, a few considerations are required. The first is that the filter needs to have a high Q (>50) and a small shape factor (∼1, i.e. extremely high roll-off factor) [150].

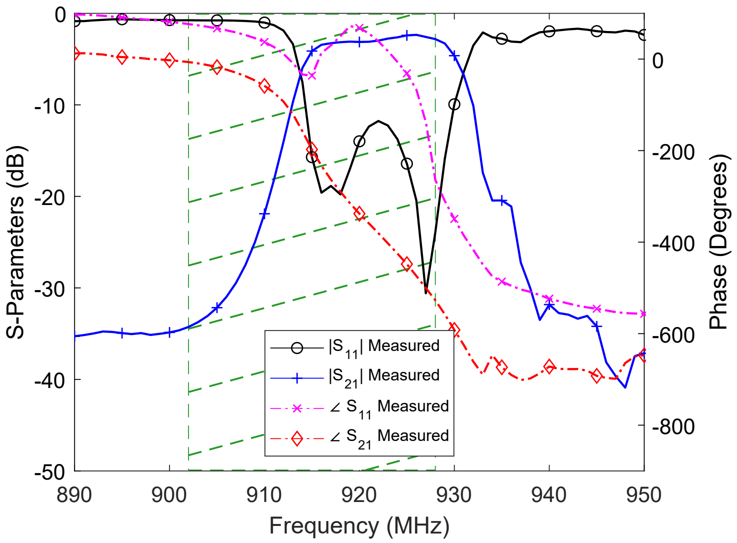

Figure 5.9: The frequency response of the narrowband SAW filter used to resolve the phase ambiguity arising due to changes in the distance.

The frequency band assigned for the UHF RFID in North America is from 902 MHz to 928 MHz. Since we are using different frequencies to resolve the distance ambiguity, we must ensure that both the passband and the stopband of the filter lie within this frequency band. Since at least 2 frequencies would be required in the stopband, it would be useful to have at least two 500 kHz-channels of the UHF RFID band in the stopband of the filter. However, for a higher accuracy and to combat multipath issues, having the flexibility of a larger frequency spacing by leaving multiple channels in the stopband would be necessary.

Given the requirements, a narrowband SAW filter can be a good candidate as it provides a high Q and a small shape factor. In our case, we used SF2294E, which is a surface mount RF SAW filter, by Murata. The center frequency of this filter is 922.5 Mhz, while the 3 dB bandwidth is 16.2 MHz and 30 dB bandwidth is 44.9 MHz. Therefore, the quality of this filter is calculated as 56.94 and the shape factor is approximately 2.7. The measured frequency response is shown in Fig. 5.9.

The filter has a rejection of at least 30 dB at frequencies below 906 MHz. Therefore, frequencies below 906 MHz may be used to determine the reference

]

signal. For sensory signals, any frequency in the passband, 915 MHz up to 928 MHz, may be used. The insertion loss of this filter in the passband is up to 3.1 dB.

Antenna

Since the sensors are expected to be installed on walls or non-metallic cabinets, the preferred antenna radiation pattern for this purpose would be one that is directional. Additionally, the antenna in the sensing chip should be as compact as possible and have good radiation performance. Furthermore, it needs to have good coverage with a reasonable antenna gain working over the UHF band. Although conventional dipole antennas can provide good coverage, their relatively large size and lower gain make them undesirable in this application. The patch antennas also do not seem to be a good fit for this type of sensor due to their broadside radiation.

One antenna type that can provide a unidirectional radiation pattern with low-profile and low fabrication cost is a monopole antenna. Compared to a dipole antenna, a monopole has a higher gain and higher front-to-back ratio due to the ground plane that makes the radiation pattern unidirectional [151]. Moreover, the meandered or folded structures can be used to shrink the antenna size [152]. Therefore, the folded monopole antenna has been selected and designed to cover the desired frequency band, as shown in Fig. 5.10. It consists of a folded strip and a ground plane. The length of the strip (Ls) adjusts the resonant frequency and the ground plane behind it increases the front-to-back ratio and antenna gain. The proper values of width of the strip (Ws), the interval between two folded branches (s), and its distance from the ground plane (d) would match the antenna at a desired frequency. In case of flood sensor, a space at the corner of the ground plane is reserved for the sensing structure to isolate it from the antenna, as shown in Fig. 5.10. As the temperature sensing element and antenna have no coupling effects on each other, the isolated space was not required. The optimum parameters of the antenna to work over the desired UHF RFID band are: Ls= 80 mm, Ws= 0.5 mm, d= s= 6.25 mm. The reflection coefficient and radiation gain of the simulated antenna are plotted

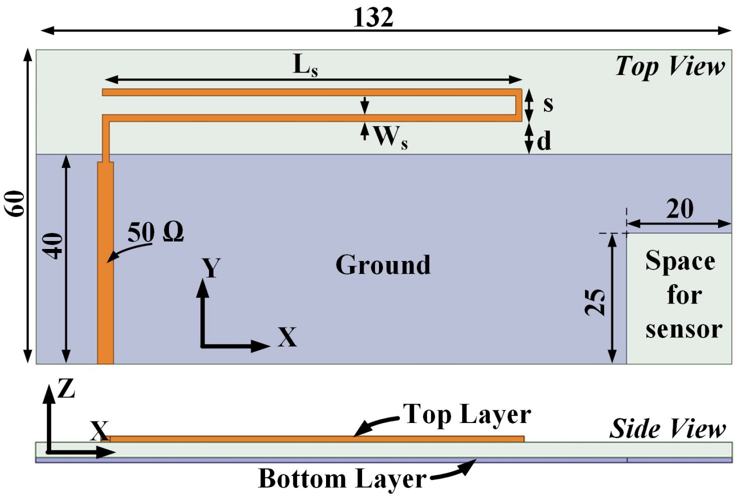

Figure 5.10: Top and side views of the monopole antenna designed for the proposed sensor (units are in mm).

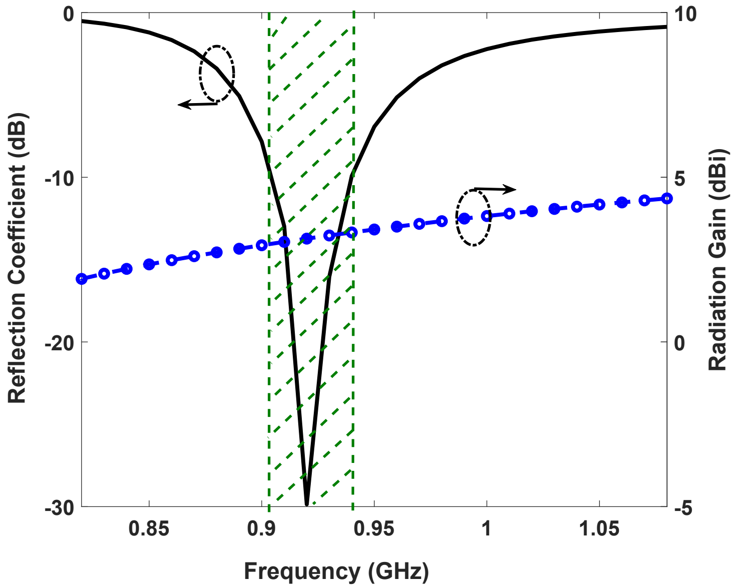

Figure 5.11: Reflection coefficient and radiation gain of the proposed antenna with Ls= 80 mm, Ws= 0.5 mm, d= s= 6.25 mm.

in Fig. 5.11. As shown, the antenna has a reflection coefficient lower than -10 dB and a radiation gain of higher than 3.1 dBi, over the whole frequency band of 902-940 MHz.

5.2.3 Reader

The reader used for experimentation purposes was AS3993 Fermi. It can provide with an output power of up to 22 dBm and can be extended to 30 dBm [143]. This reader was selected as it generates IQ signals from the backscattered signal using a mixer that can be used to determine the signal phase. A circularly polarized antenna, with 6.5 dBi gain in each polarization, was attached to the reader.

The reader is programmed to determine delay at different frequencies, as devised above in Sec. 5.2.1. The frequencies in the stopband of the filter are used to nullify the phase delays added due to any components of the setup, the distance between the chip and the RFID reader, and the RFID chip. Finally, the extracted phase value is mapped onto the respective physical parameter — for example, the water level for the flood sensor or temperature in case of the temperature sensor — to eventually find out the state of the physical parameter being sensed.

5.2.4 Components Integration

The integration of all the components is very crucial to the performance of the system. This is because the RFID chip must receive a minimum power of -18.5 dBm to respond back. Therefore, the power-up signal must reach the RFID chip with minimum losses incurred on its way. To cater for this, the RFID chip must be attached to the 2nd port of the circulator, in the clockwise direction, while the filter and sensing element circuit is attached to the 3rd port, as also depicted in Fig. 5.2. The final fabricated flood and temperature sensing elements are shown in Figs. 5.12(a) and 5.12(b), respectively. These circuits were fabricated on a 0.81 mm thick RO4003C substrate provided by Rogers corporation. The relative permittivity (ϵ_r) of this substrate was 3.38, and the loss tangent ($tan\delta$) was 0.0027. The size of our proposed sensor is comparable to a commercial RFID tag. The length and width of our proposed design are 132 mm and 60 mm, respectively, whereas, for commercial UHF RFID tags [153], the length and width are typically in the range of 96 mm and

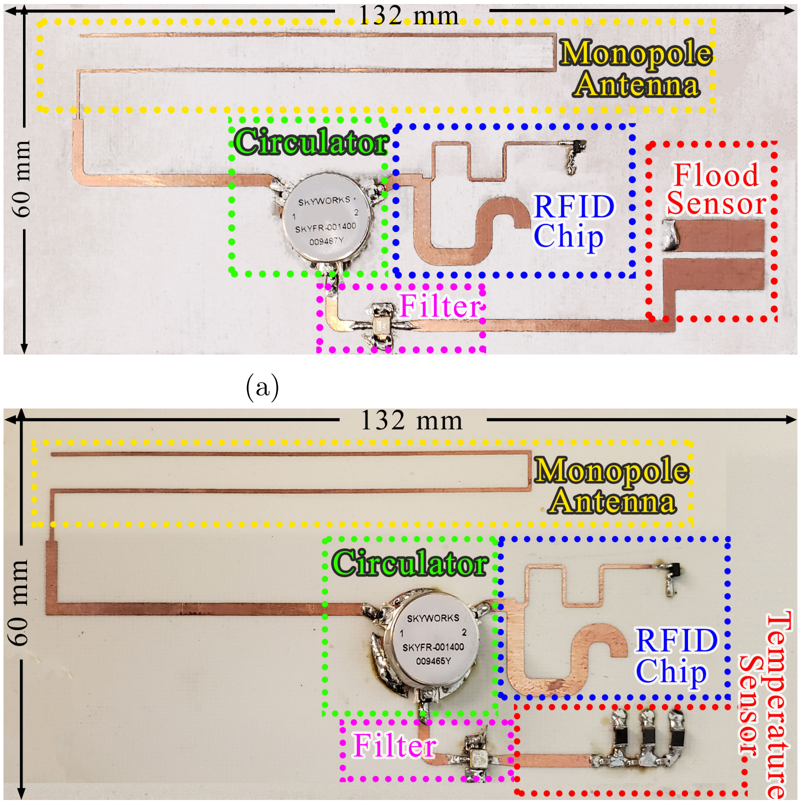

(a)

(b)

Figure 5.12: Final fabricated sensors: (a) flood (b) temperature.

20 mm, respectively.

To consider the effect of other circuit components such as the circulator, matching circuit, and sensing part on the performance of the antenna, the entire structure was full-wave simulated in Ansys HFSS, as shown in Fig. 5.14. To excite the antenna, a port was placed close to the circulator. As shown in Fig. 5.13, the 3D radiation pattern of the antenna is unidirectional. Fig. 5.14(a) confirms that the reflection coefficient of the antenna with/without other parts of the system does not differ significantly over the frequency band of interest. The antenna impedance bandwidth with the presence of other elements is 4.1%, spanning over the entire 902-940 MHz, which was as desired. The co- and cross-polarization patterns of the antenna in XOY and ZOY planes, respectively, at 915 MHz are depicted in Fig. 5.14(b). The high co- to cross-polarization separation shows that the antenna is linearly polarized, as expected. Also, as shown in Fig. 5.13 and 5.14(b), the 3 dB beamwidth

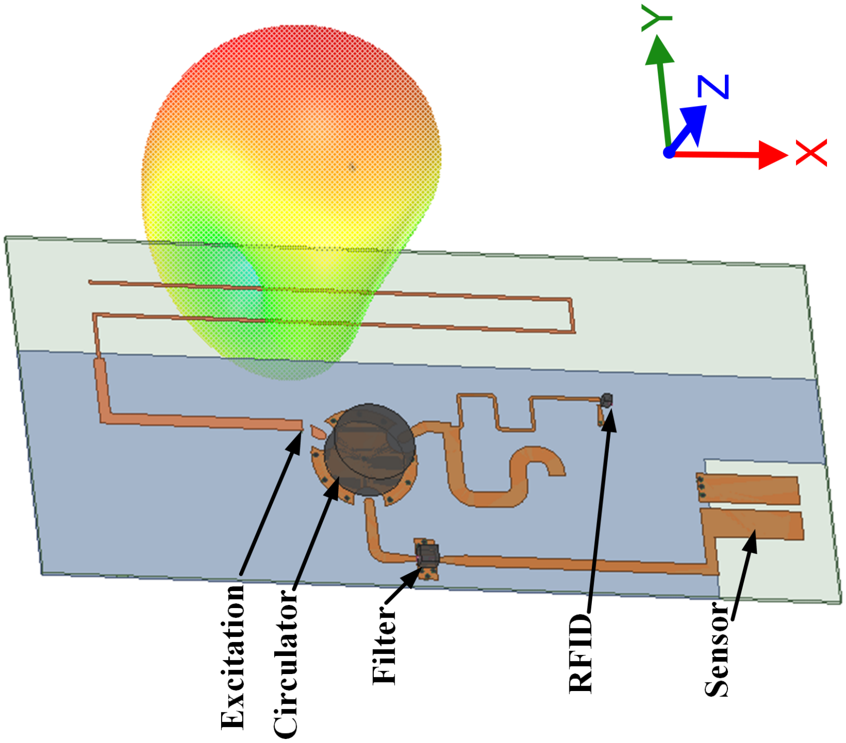

Figure 5.13: Antenna 3D radiation pattern with the presence of entire chip's elements

of the antenna in the ZOY plane is very large (around 160°), which demonstrates very good coverage of the proposed antenna. Therefore, the read-range of the sensing system is expected not to change much with the position of the reader.

If the sequencing of the components is followed as proposed, the maximum theoretical distance can be determined using the following simple relation: -18.5 dBm (minimum required RFID chip power-up signal) = 22 dBm (maximum power of the reader) + 6.5 dBi (antenna gain of the reader) - PL dB (maximum allowed path loss for the given power-up) + 3.1 dBi (antenna gain of the sensor node) - 0.5 dB (insertion loss of the circulator). This gives maximum allowed path loss, PL = 49.6 dB. At our frequency of operation of around 915 MHz, this path loss is seen at a distance of 7.9 m.

In order to determine the maximum distance a backscattered signal can be detected, the following relation can be used: -90 dBm (RFID reader sensitivity) = -18.5 dBm (minimum required RFID chip power-up signal) - 1 dB (imperfect

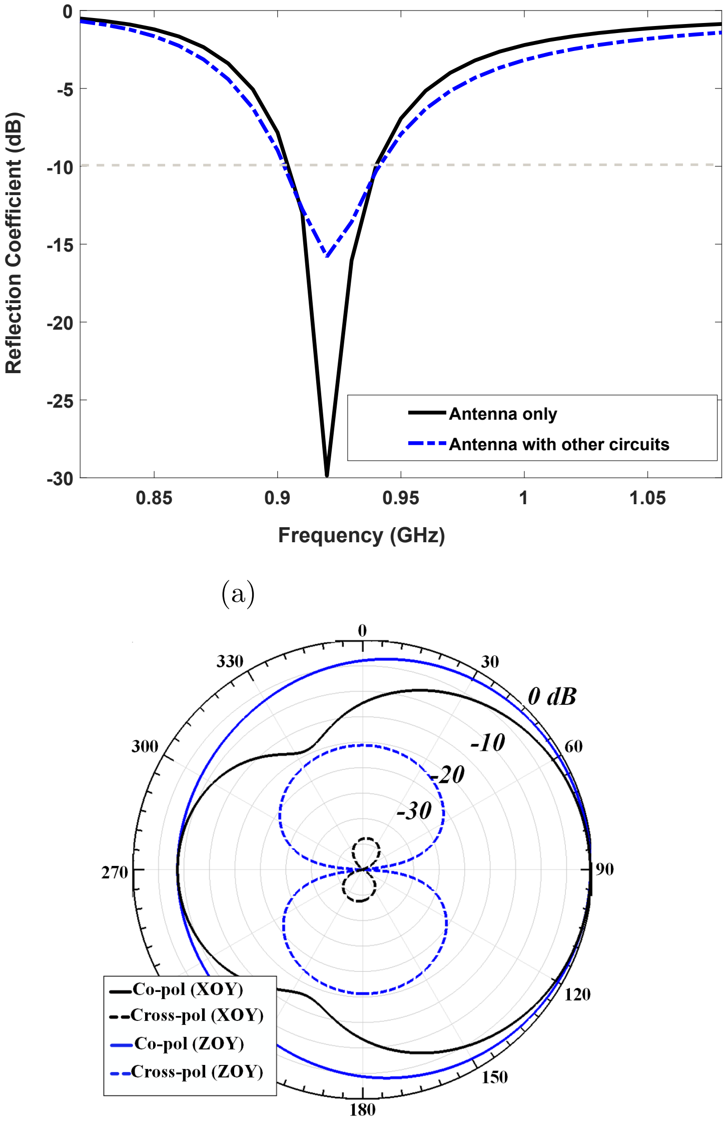

(a)

(b)

Figure 5.14: Antenna performance with the presence of entire chip's elements, (a) reflection coefficient, and (b) normalized co- and cross-polarization in both XOY and ZOY planes at 915 MHz.

reflection loss of the chip [145]) - 0.5 dB (insertion loss of the circulator) - 3.1 dB (insertion loss of the filter) -1.5 dB (sensing element's losses) - 3.1 dB (filter's insertion loss) - 0.5 dB (insertion loss of the circulator) + 3.1 dBi (antenna gain of the sensor node) - PL dB (maximum path loss for backscattered) + 6.5 dBi (reader's antenna gain), which gives maximum path loss for backscattered, PL = 71.4 dB. At our frequency of operation, 915 MHz, this path loss is observed

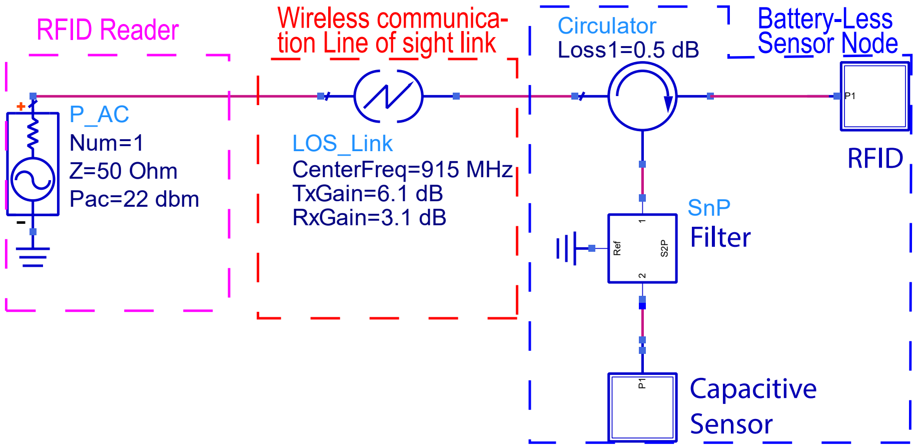

Figure 5.15: ADS schematic of the battery-less wireless sensor design.

at a distance of 97 m.

The above calculations confirm that the limiting factor for the reader-chip distance is the chip's power-up condition and by increasing the reader power, this distance can be increased. However, since the RFID standards allow up to 36 dBm EIRP transmitter power, the maximum improvement will be 7.5 dB (36 dBm - 22 dBm - 6.5 dBi) over the reader power of 22 dBm. If added, this will provide a larger path loss of 57.1 dB which, for 915 MHz, is incurred at a distance of 19 meters. Therefore, 19 meters is the maximum distance that can be achieved in our proposed design while adhering to the RFID standard.

5.3 Results

First, simulations were performed to confirm if the devised model operates properly at different distances. The model was implemented in PathWave Advanced Design System (ADS) 2019, as shown in Fig. 5.15.

For this specific case, the passband frequency was set to 927 MHz and the first stopband frequency was set to 902 MHz while the second stopband frequency was set to be 905 MHz in (5.9) to (5.14).

The results in Fig. 5.16 show that by using (5.14) and the methodology described in 5.2.1, the phase delay due to a change in distance can be nullified. It can be seen that the phase delay for different values of capacitance does not change with the change in distance.

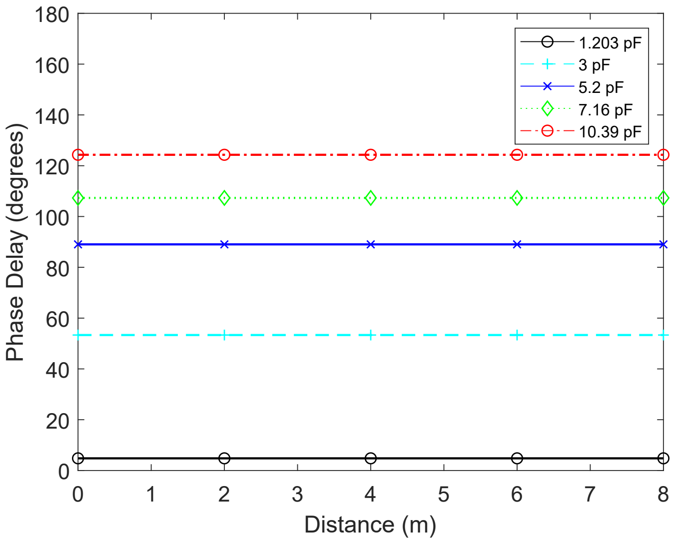

Figure 5.16: ADS simulation results showing the phase of the backscattered signal for different capacitance values becomes independent of distance after using the proposed setup.

After the distance ambiguity was resolved, the performance of the proposed wireless sensors were tested. The setup used to test the performance of our sensor comprises a reader, which measures the phase of the backscattered signal and the proposed battery-less wireless sensor. Both wireless temperature and flood sensors were placed closely and tested concurrently in real-test scenarios that mimic a smart home environment. The setup and result in a long enough period of testing are shown in Fig. 5.17 and 5.18, respectively.

To test the flood sensor, a beaker containing the sensing element was filled and emptied several times and the phase delay was recorded. When the beaker was emptied, the phase delay was almost 0°. As soon as the water started filling in the beaker, the phase delay also started to increase, as shown in Fig. 5.18. Finally, when the water reached the level of electrodes ($h = 0$ mm, as shown in Fig. 5.4(a)), the observed phase delay reached around 65°.

To evaluate the sensor's performance in the long run, the tests were repeated multiple times. Because the reactance of flood sensing element is not in a linear relationship with the height of the water, as shown in Fig. 5.5, phase delay was also found not to be linear. Therefore, as the height of the water reaches 0 mm, i.e. close to the electrodes, the phase changes abruptly

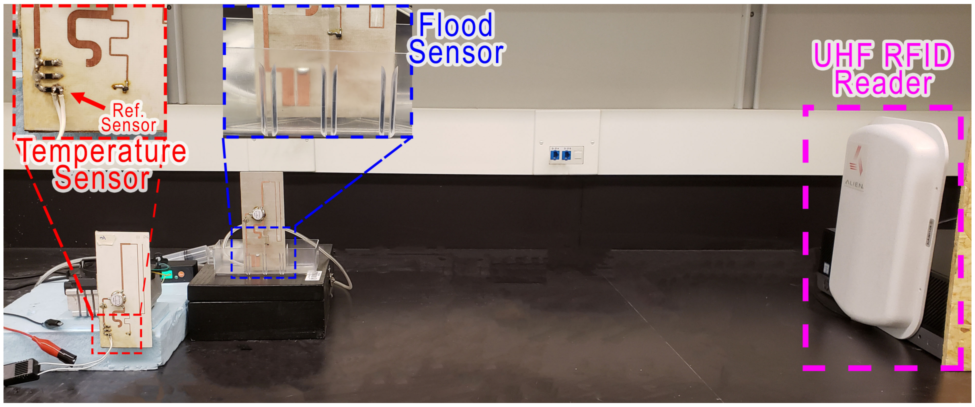

Figure 5.17: Test setup for battery-less RFID-based flood and temperature sensor.

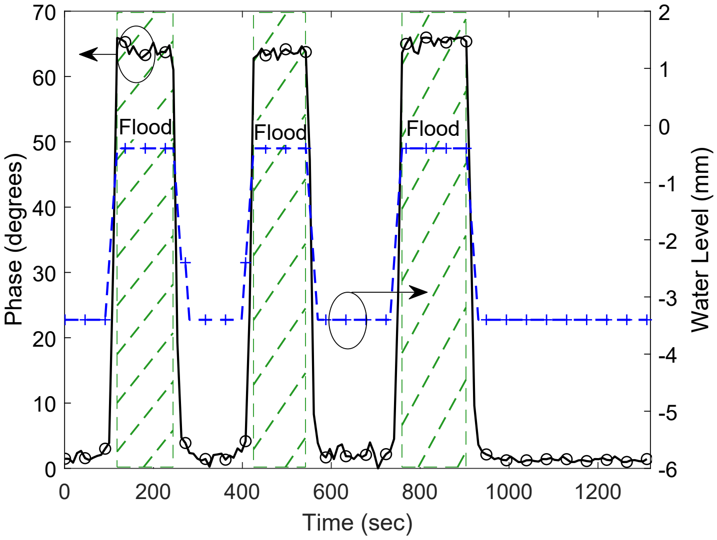

Figure 5.18: Performance of the proposed water level sensor shown by repeatedly removing and adding water in a beaker.

and reaches around 65°.

To test the temperature sensor, a Peltier heater/cooler, CM23-1.9-08AC by Marlow, was attached to the ground plane of the sensing element [154]. The other side of the Peltier device was attached to a heatsink. By varying the voltage between the terminals of the device, the sensor was cooled down to 17°C and heated up to 51°C, as shown in Fig. 5.19. A reference temperature sensor was soldered to the ground via of a thermistor to observe the applied temperature, as shown in Fig. 5.17. A delay of approximately 8 secs was found in our sensor design. This delay is attributed to the substrate that is

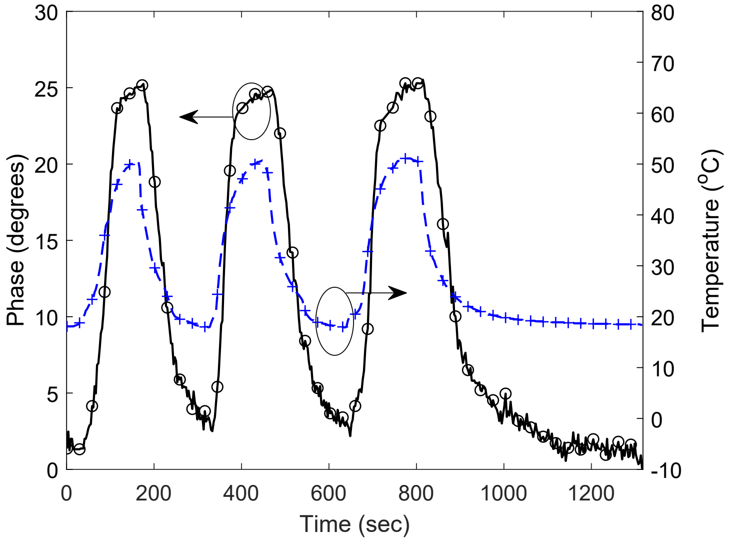

Figure 5.19: Performance of the proposed temperature sensor for different values of temperature.

Table 5.1: Performance comparison of the three-port battery-less wireless sensor with other passive wireless sensors.

Parameter	**This work**	**Antenna Resonance-based sensors [51, 52] [53, 132] [133, 134]**	**Digitally integrated sensors [135, 136] [137, 138] [43, 139]**	**Ambient energy harvesting sensors [20, 155] [156]**
Cost	Low	Low	Moderate	High
Complexity	Low	Moderate	Low	Low
Bandwidth required	∼KHz	∼MHz	∼KHz	∼KHz
Anti-collision	Yes	Yes	Yes	Yes
Dense deployment	Yes	Yes	Yes	Yes
Accuracy	Moderate	Moderate	high	High
Range (m)	7.9	3–5	1–2	6

sandwiched between the copper layers of our PCB and takes time to dissipate the heat entrapped in it.

The accuracy of our proposed wireless sensor is much dependent on the inherent sensitivity of the reader. This is because the information is in the phase change of the backscattered signal. This signal is detected and demodulated at the reader. Therefore, it is important that the reader has a stable clock and is capable of detecting the phase with good accuracy. In our case, the overall accuracy of the temperature sensor, as shown in Fig. 4.13, was found within +/-2°C, which is acceptable for smart home applications. This error can further be reduced by simply averaging the received values.

A comparison of the proposed wireless sensor with other wireless sensors is shown in Table 5.1. The proposed sensor is cost-effective with the circulator being the most expensive component. However, it should be noted that the ambient energy harvesting-based sensors cost the most as they require solar cells and a huge capacitor for their operation. The proposed sensor has fewer complexities in its design because any RF sensing element can be easily attached to the sensor port without affecting other circuitry. On the other hand, the complexities are moderate in antenna resonance-based sensors as the sensor must ensure proper impedance matching between the antenna and chip along with sensing parameters. The bandwidth requirements for the proposed sensor are in the range of KHz, which is typically what is required for digitally communicating the ID of the sensor. To be more specific, it requires 500 kHz bandwidth at any given time as it can operate in any single channel of the RFID UHF band. It may be argued that reading in multiple channels is required to remove the phase ambiguity; however, once the ambiguity is resolved, reading from single channel is adequate. In the case of antenna resonance-based sensor, wider bandwidth is required since the frequency must be swept across a band to determine the sensor's value. All of the compared sensors provide anti-collision and dense deployment, which is an integral a part of the RFID technology.

The proposed sensor demonstrates only moderate accuracy because it uses analog communication for sending the sensed values. On the other hand, the digitally integrated sensor provides high accuracy because of digital communication. The proposed sensor provides a good operating range of around 7.9 meters, which is in accordance with the value calculated theoretically and can be easily extended up to 19 meters by using a higher power reader. On the other hand, ambient energy harvesting sensors have been shown to operate up to 6 meters. Hence the proposed design can be considered a good candidate for smart home IoT applications.

5.4 Conclusion

In this chapter, a novel battery-less wireless sensor is proposed and discussed. The proposed design integrates an RFID chip with an antenna and a frequency selective sensing element using a circulator. Due to the reactive nature of the sensing elements, a phase delay is added to the backscattered signal. A SAW filter is used with the sensing element to limit sensory responding to a limited frequency band. This allows removing any phase delay that is added due to the distance between the sensor and the reading device. Designs for a flood sensing element and a temperature sensing element along with a folded monopole antenna are shown. Results show that the sensor may be placed at any distance of up to 7.9 meters from the reader to sense different parameters such as flood/moisture and temperature. It was also discussed how the proposed architecture provides a longer range compared to other sensors, without using any battery. These attributes make our proposed sensor ideal for different environments ranging from smart home, medical, or industry to monitor liquid levels, temperature, and moisture, without having to ever worry about replacing the batteries of the installed sensors.

Chapter 6

A Battery-Less Six-Port RFID-Based Wireless Sensor Architecture for IoT Applications

In this chapter, a novel architecture for battery-less wireless sensors is proposed and demonstrated. The proposed architecture uses a six-port structure to integrate a UHF RFID chip with a resistive sensing element to enable the reading of environmental conditions wirelessly, without using a battery at the sensor node. The six-port structure divides an incoming RFID interrogator signal into an in-phase and quadrature branch and implements signal mixing without the use of a lossy or an active mixer. The amplitude and phase of the mixed signal are dependent on the value of the attached sensing element. By reading the phase of this signal at the reader, the value of the element can be easily determined using a non-coherent IQ demodulator. The design can easily integrate any type of resistive sensing element for parameters such as temperature, humidity, and water level. A pin diode is used to control the amplitude and phase of the backscattered signal to demonstrate the performance. These values are successfully read at a distance of 2 m.

6.1 Introduction

Several wireless sensor designs based on battery-less, or passive, RFID technology have been presented in the past [43, 51–53, 127–130, 132, 133, 136, 137, 139, 147, 157]. Moreover, the design presented in the previous chapters requires a bulky circulator that increases the cost of the sensor node. In addition, the design only allows the use of reactive sensing elements. To the best of the authors' knowledge, there is no RFID-phase-modulating sensor design that works without a circulator and allows the use of resistive sensing elements.

In this chapter, a novel wireless sensor design that addresses the aforementioned challenges is proposed. The proposed design consists of a six-port direct conversion network, an RFID chip, a UHF resistive sensing element network, and two antennas. These components are arranged such that the reader signal entering the six-port is first divided into two signals, namely in-phase and quadrature signals. The in-phase signal is fed to an RFID chip to harvest energy, while the quadrature signal is fed to the resistive sensing element network. When the RFID chip responds, the backscattered signal is combined with the signal that is being reflected from the sensing element due to the mismatch, which is based on the physical parameter being sensed. The phase of this combined signal is directly influenced by the state of the sensing element. Moreover, this signal is a combination of a digitally modulated signal, which is an RFID chip signal, and an analog modulated signal, which is the variations in phase due to the sensing element state. Through this phase variation, any changes in the sensing element value are easily determined at the reader through an IQ demodulator.

The goals addressed in this chapter are three-fold:

- propose a wireless sensor architecture that works without requiring any battery at the node;
- allow the integration of resistive sensing-elements;
- use the phase delay of the backscattered signal to determine the sensed value passively.

The remainder of this chapter is organized as follows. In Section 7.1, a thorough discussion of the proposed design is carried out, while Section 7.2 discusses the results. Finally, the chapter is concluded in Section 7.3.

6.2 System Design

The proposed system is designed by integrating an RFID chip and a sensing element using a six-port structure. First, the fundamental operating principles of a six-port structure will be discussed. Following that, its integration with the senor and RFID chip will be discussed.

6.2.1 System Model

A six-port structure operates on the principle of additive mixing of phase-shifted versions of an input RF signal. To achieve this behavior, three 90° hybrid couplers are attached along with a power splitter/combiner. A 90° hybrid coupler has four ports: an input port, a through-port, a coupled port, and an isolated port. A signal at the input port is sent to the through and the coupled ports. The signal provided to the coupled port is in quadrature phase with respect to that at the through port. Any signals reflected at the two ports are combined and delivered to the isolated port. A block diagram of the full system is shown in Fig. 7.1. The RF input signal ($v_{IN}(t)$) received at port 1 is split into an I and a Q using a 90° hybrid coupler, C_1. Both the in-phase and the quadrature signals are fed into separate 90° hybrid couplers, C_2 and C_3, respectively. This eventually provides the signals at port numbers 3, 4, 5, and 6, which could be backscattered based on the reflection coefficients of the RFID (Γ_{RFID}) [145] and sensing element (Γ_{sensor}). The in-phase and quadrature components of the backscattered signal, Γ_I, and Γ_Q, respectively, are mixed in the splitter/combiner (S_1) in a way to achieve a signal with all the required information, as will be explained in detail in what follows.

Consider an incoming RF signal incident on the antenna connected to port 1. The signal can be mathematically represented as,

$$v_{IN}(t) = V_{IN}\ cos\ \omega_{IN} t. \tag{6.1}$$

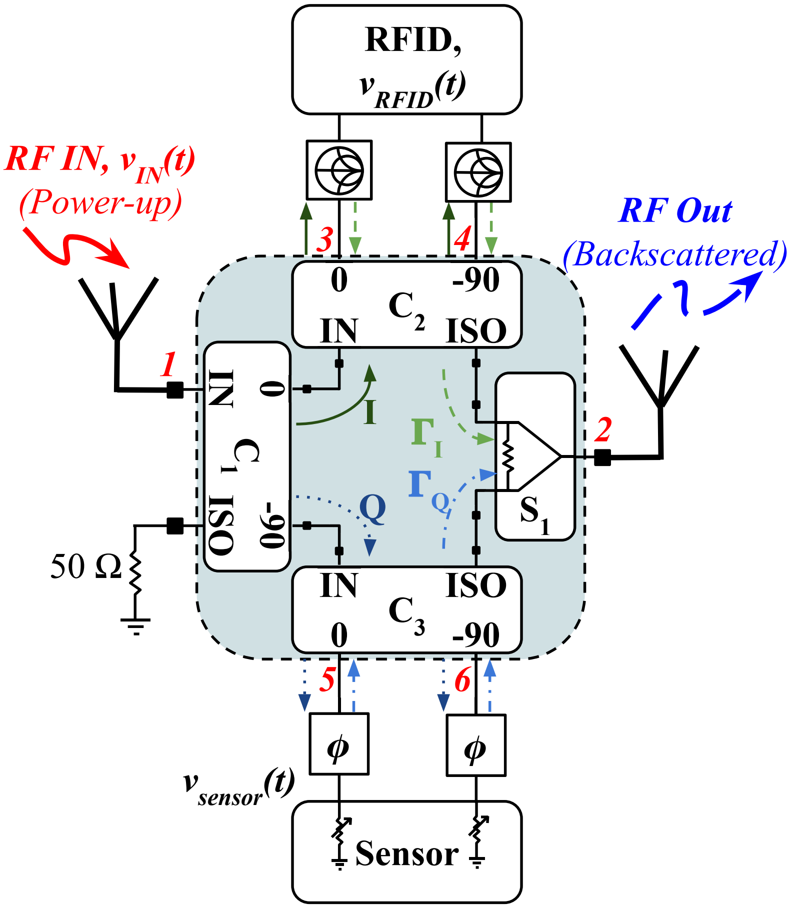

Figure 6.1: Block diagram of the proposed battery-less six-port wireless sensor.

The signals at the output ports of C_1 will be,

$$v_I(t) = \frac{1}{\sqrt{2}} V_{IN}\ cos(\omega_{IN} t + \phi), \tag{6.2}$$

$$v_Q(t) = \frac{1}{\sqrt{2}} V_{IN}\ sin(\omega_{IN} t + \phi), \tag{6.3}$$

where ϕ is any phase delay of the system, equally incurred by both the signals and therefore may be ignored.

The signals at port 3 and 4, which are generated from the in-phase component, are fed to an RFID chip. Normally, an RFID chip is not inherently matched to 50 Ω. Therefore, a matching network is required to enable maximum power transfer from the coupler C_2 of the six-port network to the RFID chip. For the matched case, the signal received by the RFID chip can be represented as,

$$v_{RFID}(t) = \frac{T_m}{\sqrt{2}} V_{IN}\ cos(\omega_{IN} t + \phi_m + \phi), \tag{6.4}$$

where T_m and ϕ_m are the transmission coefficient and phase delay of the matching network, respectively. For a well-designed matching network, T_m may be ignored.

When the RFID chip is harvesting energy, it acts as a matched circuit and thus all the power is delivered to it. At this moment, the reflections from the RFID chip are minimum and can be approximated to 0 ($\Gamma_{RFID,m} = 0$) and as a result, $v_{\Gamma_I}(t) = 0$. Here, $\Gamma_{RFID,m}$, and $v_{\Gamma_I}(t)$ are the reflection coefficient of the RFID chip and signal received at the ISO port of C_2, respectively, when the RFID chip is harvesting the energy.

On the other hand, when the RFID chip is unmatched and reflecting the power for communication with a coefficient of $\Gamma_{RFID,u}$, port 3 and 4 get shorted out and the power is reflected and combined at the ISO port of the coupler C_2. The signal at the ISO port is represented as,

$$v_{\Gamma_I}(t) = \frac{\Gamma_{RFID,u}}{\sqrt{2}} V_{IN}\ cos(\omega_{IN} t + 2\phi_m + \phi). \tag{6.5}$$

On the other hand, the signals at ports 5 and 6, which are generated in C_3 using the quadrature component of the incoming signal v_{in}, are fed to a resistive sensing element. This signal at port 5 can be represented as,

$$v_{sensor}(t) = \frac{1}{2} V_{IN}\ sin(\omega_{IN} t + \phi_{sensor} + \phi), \tag{6.6}$$

where ϕ_{sensor} is the delay of the sensing element and the transmission line. To ensure that the quadrature component undergoes a similar phase delay to its in-phase counterpart at the RFID chip, ϕ_{sensor} is made equal to ϕ_m (delay of the matching network of the RFID chip) at the operating frequency. This is achieved by varying the length of the transmission line attached to the sensing element.

Identical sensing elements are attached at ports 5 and 6. To utilize the full range of modulation, a resistive sensing element varying from a short circuit

(0 Ω) to an open circuit can be used. However, in practice, a sensing element with its variable resistance in the range of 50 Ω +/- 50 Ω, which is the circuit's characteristic impedance, is sufficient for operation. With the change in the physical parameter being sensed, the resistance of the sensor is changed, and then the magnitude of signals reflected from ports 5 and 6 varies. As the signal at port 6 is a 90° delayed version of the signal at port 5, the signals reflected by the sensing element are combined at the ISO port of the coupler, C_3. This reflected signal is written as,

$$v_{\Gamma_Q}(t) = \frac{\Gamma_{sensor}}{\sqrt{2}} V_{IN}\ sin(\omega_{IN}t + 2\phi_{sensor} + \phi), \tag{6.7}$$

where Γ_{sensor} depends on the resistance of the sensing element. It should be noted that the resistance is variable and depends on the value being sensed by the sensing element.

To ensure that the signals available at the ISO ports of each coupler, C_2, and C_3, are quadrature, along with matching ϕ_{sensor} and ϕ_m, it is important that the reactance of the sensing element should be very low and/or should not vary with its resistance while sensing; otherwise, the signal at the ISO ports of C_3 will have variations in phase and it will no longer be in phase quadrature with respect to the ISO port of C_2. Moreover, any imbalance in the phases caused due to variations in the sensing element's reactance will introduce errors in the signal demodulated at the reader. Therefore, capacitive sensing elements may not be used with this sensor architecture, and only resistive sensing elements should be used.

Finally, the reflected in-phase (Γ_I) signal and the quadrature signal (Γ_Q) are combined using the splitter/combiner, S_1. The output signal is expressed as,

$$v_{out}(t) = v_{\Gamma_I}(t) + v_{\Gamma_Q}(t), \tag{6.8}$$

$$\begin{split} v_{out}(t) = \frac{\Gamma_{RFID,u}}{\sqrt{2}} V_{IN}\ cos(\omega_{IN}t + 2\phi_m + \phi) \\ + \frac{\Gamma_{sensor}}{\sqrt{2}} V_{IN}\ sin(\omega_{IN}t + 2\phi_{sensor} + \phi). \end{split} \tag{6.9}$$

For the case when $\phi_m = \phi_{sensor}$, they both can be attributed as the system delay and can be incorporated into ϕ. Hence, the signal at the output, after passing through S_1, is expressed as,

$$v_{out}(t) = \frac{AV_{IN}}{2} \, cos(\omega_{IN} t - \phi_{out} + \phi). \tag{6.10}$$

Where,

$$A = \sqrt{\Gamma^2_{RFID,u} + {\Gamma_{sensor}}^2}, \tag{6.11}$$

$$\phi_{out} = tan^{-1}\left[\frac{\Gamma_{sensor}}{\Gamma_{RFID,u}}\right], \tag{6.12}$$

are the amplitude and the phase of the output signal, respectively. These results are obtained by using the scattering matrix of the Wilkinson power divider and applying a trigonometric identity to (7.10). Moreover, this is the final backscattered signal sent to the reading device.

It can be seen that the amplitude and the phase of the backscattered signal depend on the signal reflected by the sensing element, which is directly related to the sensing element's resistance. As a result, changes in the environment produce a change in the sensing element resistance, which in turn causes a detectable change in the phase and amplitude of the backscattered signal.

6.2.2 Physical Realization of the Components

Six-port

To realize a six-port structure, three couplers along with one splitter/combiner are required. Here, three hybrid 3 dB quadrature couplers, X3C09P1-03S, and a Wilkinson power divider, PD0810J5050S2HF by Anaren were used. These are small-sized components that support the North American UHF RFID frequency band of 902 to 928 MHz. All these components were integrated on a 0.81 mm RO4003C substrate with a relative permittivity of 3.38 and a loss tangent of 0.0027.

A layout of the designed circuit is shown in Fig. 7.3. A simple network of transmission lines was used along with the footprints provided in the data sheets of the components to connect them to the six-port network. To avoid

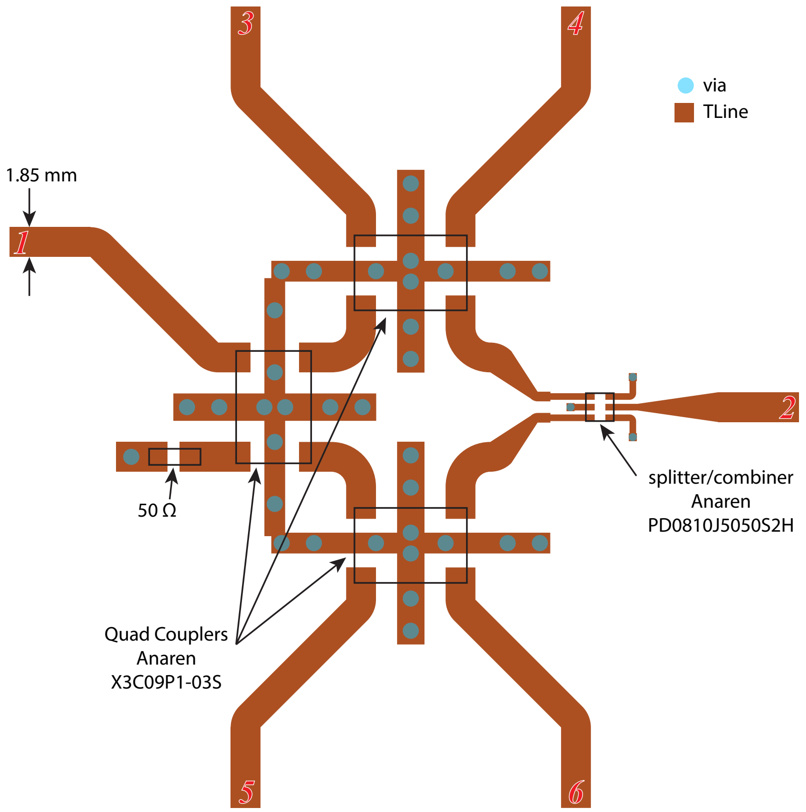

Figure 6.2: Circuit layout of the six-port structure used in the proposed system.

any phase imbalance, the lengths of transmission lines connecting ports 3 to 6 were kept identical.

RFID chip

The chips used in an RFID-based wireless sensor design greatly influence the range of the sensor node. In this work, a Higgs-4 by Alien technology was used. The minimum wake-up power of this RFID chip is -18.5 dBm while the input impedance is $Z_{in} = 18 - j181\ \Omega$. To integrate this RFID chip with the six-port structure, its impedance must be transformed to 50Ω. For this purpose, two single-section open-circuited series stubs were used at both ports. This matching network connects the two ports of the RFID to the six-port structure. The layout and frequency response of the matching network are shown in Figs. 7.4 and 7.5, respectively.

To measure the frequency response of the matching network, a balun was

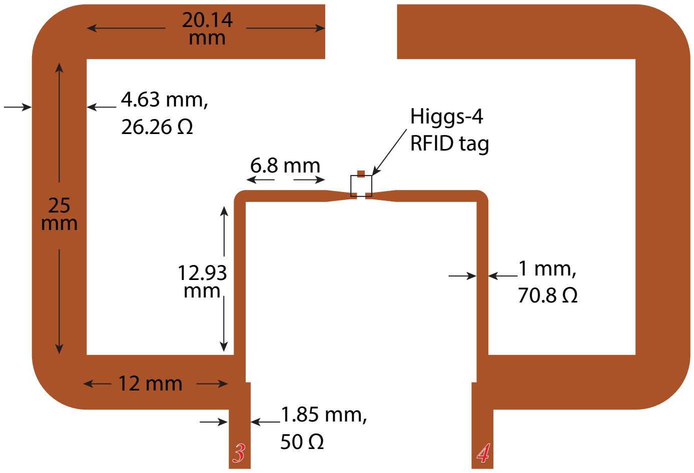

Figure 6.3: Circuit layout of the matching network used to connect the RFID chip with the system.

connected at port 3 and port 4. Therefore, in this specific instance of Fig. 7.5, the input port of the balun, which was used to feed the matching network, corresponds to port 1 while the complex impedance of the RFID chip corresponds to port 2. As the complex impedance of the IC models its internal energy harvesting circuitry, port 2 is hypothetical and it is practically not possible to measure the signal transmitted to it. Hence S_{21} was mathematically estimated using the reflections at the input of the feeding balun.

Resistive sensing element

Although resistive sensing elements for physical parameters are widely available in the market, the currently available options exhibit very poor response and sensitivity at UHF. Therefore, to test the architecture, a pin diode, SMP-1307 by Skyworks Solutions Inc., which operates in the UHF band, was used. As a pin diode, its resistance could be easily changed from low to high by simply varying its biasing voltage. This helps in performing an in-depth analysis of the system.

Another important factor that requires attention is the adjustment of the length of the transmission lines connecting the sensing elements with the six-port structure. The length of these lines should introduce a delay that is

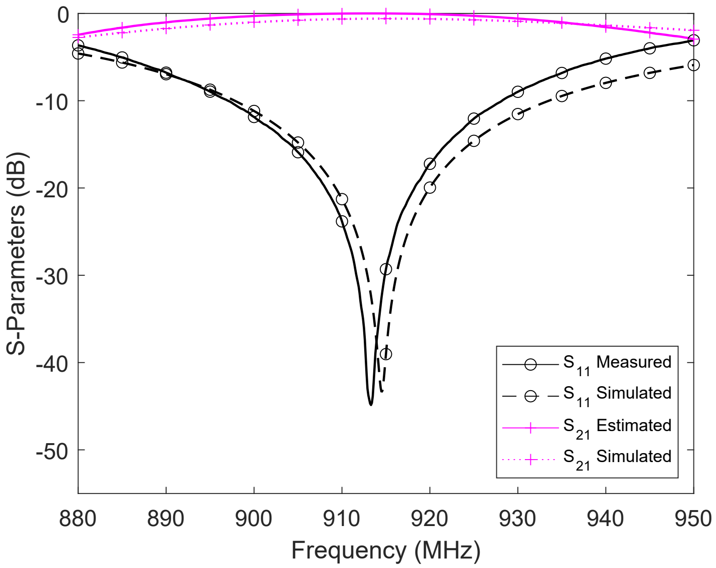

Figure 6.4: Frequency response of the matching network used to connect RFID chip. Port 1 and port 2 correspond to the inputs of the test balun and RFID chip, respectively.

identical to what is being added by the RFID chip's matching network. The lengths should be adjusted until I and Q signals are achieved simultaneously at the ISO ports of the coupler. As an RFID chip backscatters for a very short time interval, simulations may be set up to compare the I and Q signals and determine the delay required in the transmission lines.

A circuit layout designed to connect the pin diode with the six-port structure, along with its biasing circuit, is shown in Fig. 7.6. These lengths were optimized to ensure IQ phases at the splitter/combiner for the specific RFID chip's matching network shown in Fig. 7.4.

The magnitude and phase of the signals reflected at the input port of the pin diode circuit (S55/S66) are shown in Fig. 7.7. The simulated results were obtained by using the model of the pin diode in ADS 2020. Initially, when the voltage is below 400 mV, the diode acts as an open circuit, and thus the reflected signal is high in magnitude. At around 500 mV the diode starts to conduct, thus the magnitude of the reflected signal starts to decrease. As the voltage increases, the conduction of the pin diode increases and the resistance drops. At around 700 mV, the diode resistance is approximately 50 Ω and

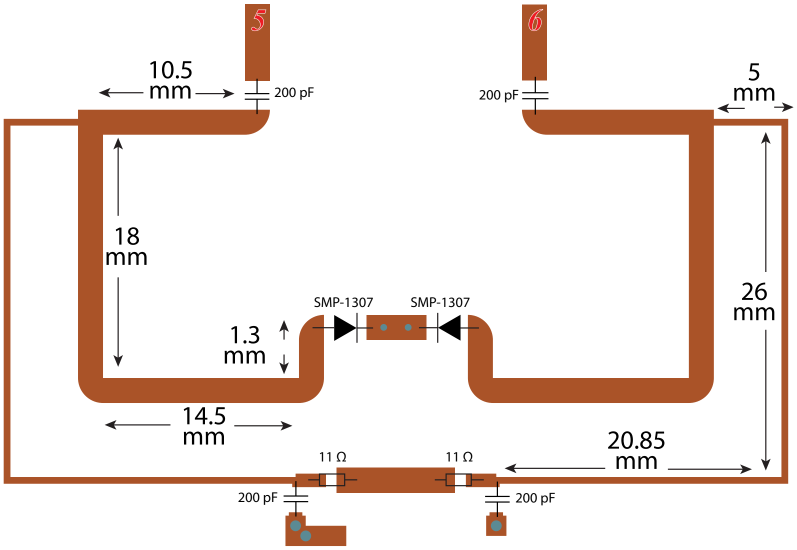

Figure 6.5: Layout of the designed circuit for the variable resistor/pin diode.

thus the reflected signal is minimum. Beyond this voltage, an expected phase reversal can be seen. Moreover, the resistance tends to drop beyond this voltage and due to the mismatch, the magnitude of the reflected signal starts to increase once again.

It can be seen from the graphs that mostly the resistance changes while the reactance change is minimal since the reflected phase is constant. This is important because if the reactance also changes, the phase of the signal reflected from the quadrature branch will vary with the variation in the sensing element. As a result, the reflected signal will no longer be in quadrature relative to the signal being backscattered by the RFID chip. It may be useful to mention here that the phase reversal observed around 750 mV in Fig. 7.7 does not invalidate quadrature requirements as this change is ∼180°, which still adheres to 90° difference between the in-phase and the quadrature signals. The only difference is that if the phase difference below 750 mV is lagging by 90°, it will lead by 90° after this value.

In practice, the measured phase change was less than 180°, as also observed in Fig. 7.7. This error generally results in crosstalk between the demodulated I and Q components. However, in the proposed sensor, the in-phase component remains fixed, as it is the reflection coefficient of the RFID chip in the

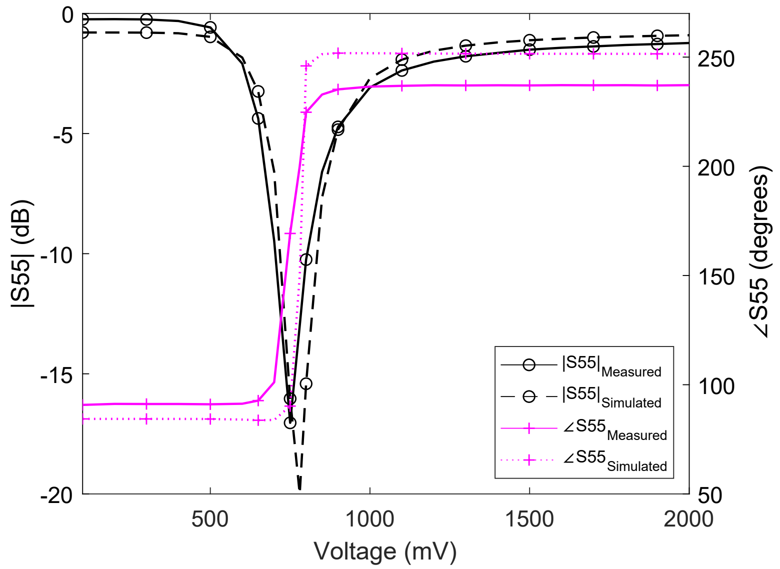

Figure 6.6: S55/S66 of the pin diode for varying voltage levels at 915 MHz.

unmatched position. Therefore, any change in the backscattered signal will still only be due to the sensing element. However, due to the crosstalk, the dynamic range of the phase due to the quadrature component will be reduced, which eventually affects the sensitivity of the sensor.

6.2.3 Components Integration

Finally, all the aforementioned components were integrated by connecting the RFID chip, the resistive sensing element, and the antennas to the appropriate ports of the six-port structure, as shown in Fig. 7.8. Antennas used in the design were linearly polarized meandered monopoles. Using different polarizations would help keep the incoming signal and the backscattered signals separate. Otherwise, the signals would enter from both the ports and intermix with unpredictable phases. This would complicate the operation of the system and results might become unpredictable. Therefore, vertical polarization was reserved for the power-up signal at port 1, whereas horizontal polarization was used for the backscattered signal at port 2.

It should be noted that since the RFID chip receives the signals that are 90° apart instead of 180°, the voltage developed inside its internal circuitry is

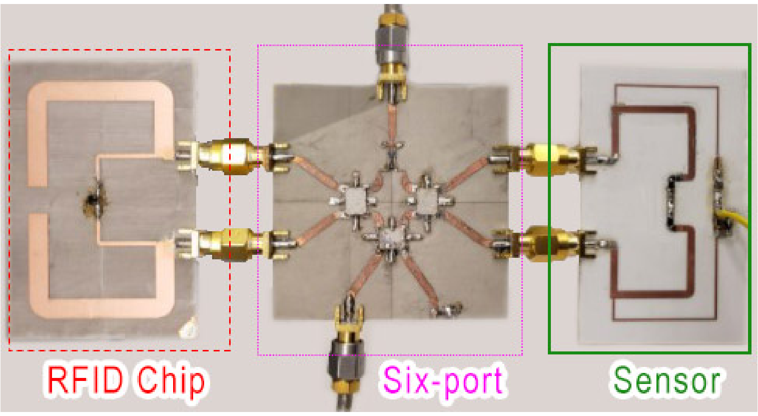

Figure 6.7: Fabricated design of the six-port RFID-based wireless sensor.

not maximum and thus the optimum results may not be achieved. In terms of performance, this will reduce the range of the RFID chip. An additional 90° delay may be added to the current design, however, this will stop the backscattered signal from combining at the ISO port of C_2.

Using simulations, the length of the transmission line connecting the pin diode was optimized to ensure the signal received at the ISO ports of coupler C_2 and coupler C_3 are 90° out of phase. Once this optimization was performed, a parametric study of the pin diode's resistance was conducted to observe its effect on the signal received by the RFID chip. It could be seen in Fig. 7.9 that for the optimized dimensions, shown in Fig. 7.6, the signal received by the RFID tag is not drastically affected by the variations in the resistive sensing element, which is being controlled by the voltage across the pin diode (Fig. 7.7). The variations observed are attributed to the imperfect isolation between the ports of the couplers used in the design. Theoretically, this results in a reduction of only 2.72 cm in the read range, which can be neglected.

6.2.4 Reader

To power up the RFID chip and read the signal backscattered from the wireless sensor, an RFID reader is required. However, to be able to read the phase of the backscattered signal, the reader should use an IQ demodulator. Therefore, in this work, AS3993 Fermi by AMS AG was used to carry out the experiments. This RFID reader provides an output power of 22 dBm [143]. The reader uses

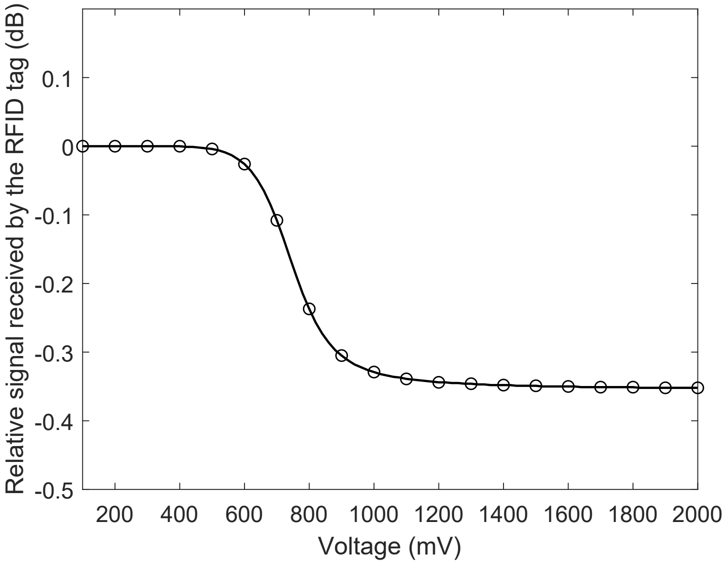

Figure 6.8: Effect of pin diode resistance variation on the signal received by the RFID chip at 915 MHz.

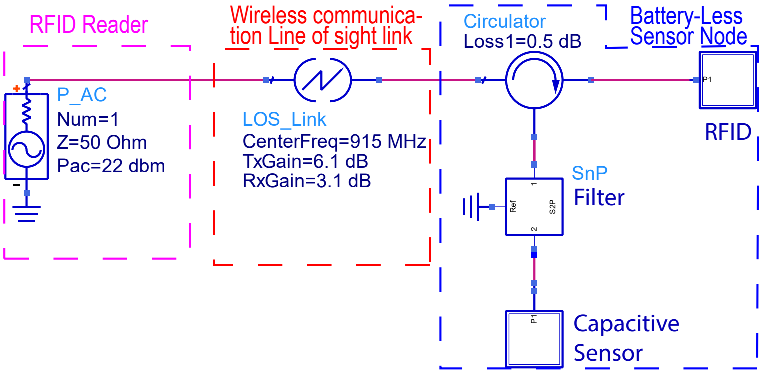

Figure 6.9: ADS schematic of the battery-less wireless sensor design.

an IQ mixer to demodulate the backscattered signal.

To separate the incoming and outgoing signals at the reader, a circulator was attached to the output of the reader. Instead of using a circularly polarized antenna, two separate antennas were used. This is to ensure that the sensor node receives most of the power at port 1 and backscatters only from port 2 to avoid any signal mixing inside of it that may otherwise occur if both ports start to receive and backscatter the RFID power-up signal simultaneously.

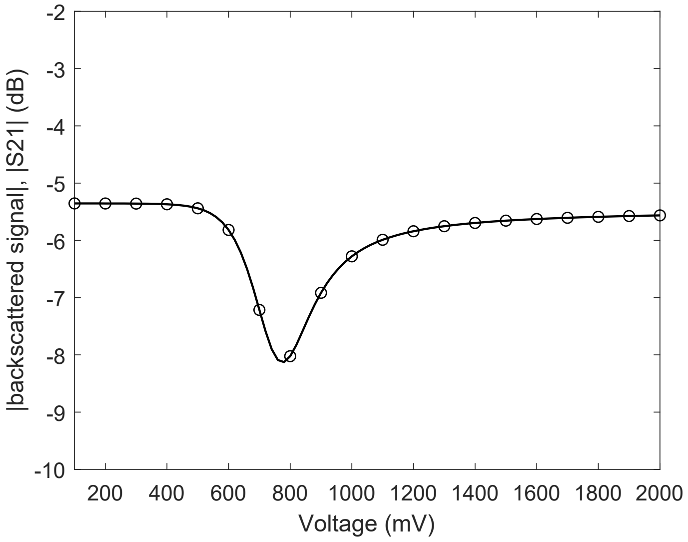

Figure 6.10: Change in the magnitude of the backscattered signal with respect to voltage across the pin diode at 915 MHz.

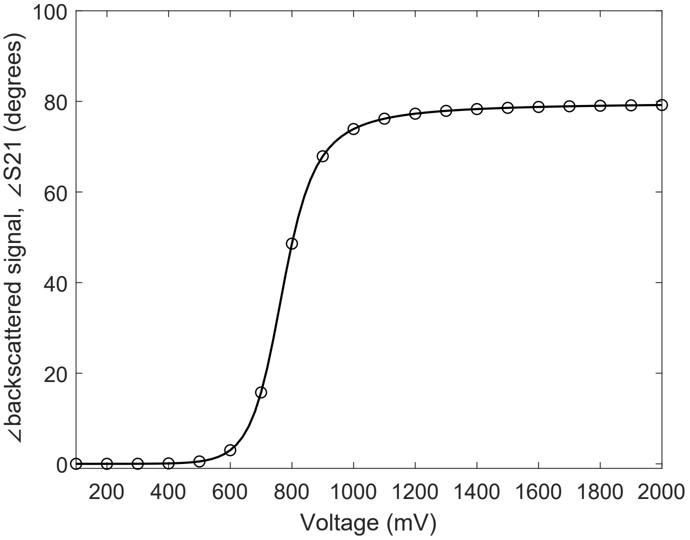

Figure 6.11: Change in the phase of the backscattered signal with respect to voltage across the pin diode at 915 MHz.

6.3 Results

Initially, simulations were used to analyze the operation and performance of the proposed architecture. The model was implemented in ADS 2020, as shown in Fig. 7.10. In this setup, models of all the components including the hybrid coupler, splitter/combiner, the RFID chip, and the pin diode, were used. The

Figure 6.12: battery-less wireless RFID sensor with pin diode attached at the sensing element port.

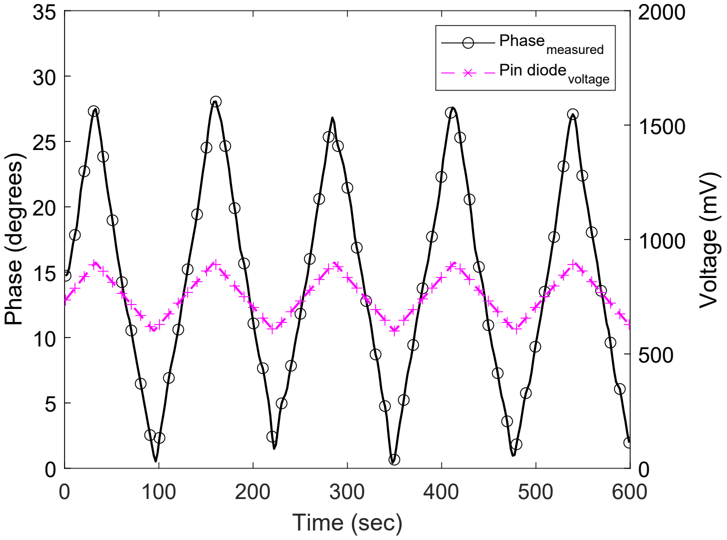

Figure 6.13: Measured phase change at the receiver as the voltage across the pin diode is changed with time at 915 MHz.

simulation was set up to measure the difference of magnitude and phase between the input and the output port. The simulations were performed for the whole North American RFID frequency band, i.e., 902 MHz to 928 MHz. Since the selected components maintain the quadrature-phase requirement of the proposed architecture across the whole RFID frequency band, similar results were observed at other frequencies. Therefore, results at only the center frequency of 915 MHz are shown here.

It can be seen in Fig. 7.11 how the magnitude of the reflected signal varies due to the variation in the resistance of the pin diode. The variation in the magnitude of the backscattered signal due to the changes in resistance of the pin diode corroborates the expression given in (7.11). From 100 mV to 400 mV, the mismatch between the sensor's resistance and the transmission line is high, resulting in higher reflection that increases the magnitude of the backscattered signal. From 400 mV to ∼1000 mV, the mismatch reduces and the magnitude of the backscattered signal also reduces. For example, at 750 mV where the reflections through the sensor are minimum, $\Gamma_{sensor} = 0$. From (7.11) it can be deduced that the output signal voltage should be smaller by a factor of $\sqrt{2}$. This corresponds to a 3 dB reduction, which is also observed in Fig. 7.11. In addition to this variation, a 3 dB loss in the signal was observed, which is attributed to the IQ conversion loss. This loss is inevitable in a simple six-port structure and it is in also accordance with the expression given in (7.11). Finally, some additional losses of ∼2.2 dB were observed and are attributed to imperfect IQ phase difference and miscellaneous component losses.

A change in the phase of the backscattered signal was also observed. This phase change with respect to the voltage across the pin diode is shown in Fig. 7.12. It can be seen that the phase is almost constant below 400 mV. This is because the pin diode is in an open-circuit state. After 400 mV, its resistance starts to drop, therefore, the phase delay of the backscattered signal starts to increase. This increase continues until the voltage reaches around 1000 mV, which corresponds to nearly zero resistance. Beyond this point, the change in the resistance of the pin diode is insignificant. Therefore, the change in the phase of the backscattered signal drops, and hence its mostly useful between 400 mV and 1000 mV. Moreover, the phase of the backscattered signal in the sensitive region of 400 mV to 1000 mV, unlike the amplitude is unambiguous and therefore preferred over the amplitude in the final determination of the sensed value.

The dynamic range of the phase was measured to be 79.2° as opposed to 90°, which was theoretically derived in (7.13). The reason for this reduction in the measured dynamic range is attributed to the parasitic capacitance of the pin diode, which introduces crosstalk between the I and the Q component of the system.

Finally, the performance of the proposed architecture was tested in a real-world scenario. The designed wireless sensor was placed at a distance of 1.5 m from the reader, as shown in Fig. 7.13. The voltage across the pin diode was varied in a triangular fashion between 600 mV to 800 mV. The phase of the backscattered signal was recorded at the reader with an averaging factor of 64 readings and is shown in Fig. 6.13. A clear one-to-one relationship was observed in the recorded results. Moreover, accuracy was found to be within +/- 11 mV.

With the change in the resistance of a sensing element, this architecture allows to vary the phase of the backscattered signal of an RFID chip. Since the amplitude of the signal backscattered by an RFID does not change significantly, the phase variation of the backscattered signal is mostly attributed to the sensing element and thus can be easily determined at the reader. Hence, resistive sensing elements can be easily used in the proposed architecture, without the need for any additional circuitry.

It should be noted here that the ID of the RFID chip is sent to the reader as a digitally modulated signal, whereas the sensor information is sent in analog form through phase modulation. RFID readers are generally equipped with an IQ demodulator and can therefore easily capture the ID and provide the amplitude and phase as a byproduct of the demodulated signal. The provided phase is used to measure the sensed value at the six-port RFID-based wireless sensor.

A comparison of the proposed wireless sensor architecture with other state-of-the-art RFID-based wireless sensors is shown in Table 6.1. Although the proposed architecture does not outperform other sensors in terms of range, it is a very low-cost and low-complexity design that allows the use of resistive sensing elements. These sensing elements were not supported by any previously proposed battery-less wireless sensors. The reduction in the wireless range is because the incident power is split into two and the tag receives only one-half of the input power. Hence, the minimum power required is higher in this case or conversely, the read range is lower. However, it should be reiterated that the proposed architecture's use of simple quad couplers and a splitter/combiner as opposed to a circulator in [147, 157] affords a significant

Table 6.1: Comparison of the proposed six-port wireless sensor with other passive wireless sensors.

Parameter	**This work**	**RFID three-port [147, 157]**	**RFID chip based [51–53, 132, 133]**
Battery	No	No	No
Cost	Low	High	Medium
Complexity	Low	Low	Medium
Range (m)	2	7	3–5
Sensing element	Resistive	Capacitive	N.A.
Bandwidth required	∼kHz	∼kHz	∼MHz

cost reduction. Moreover, it requires less bandwidth as it can operate in any single channel of the UHF RFID band, which is typically 500 kHz.

Future work will focus on improving the range of the proposed design and propose new UHF resistive sensing elements that could be used in daily-life IoT applications.

6.4 Conclusion

In this chapter, a novel battery-less wireless sensor is proposed that works without a battery. The proposed architecture integrates an RFID chip with a resistive sensing element and antenna using a six-port structure. An example design is shown, which operates at the UHF band. Based on the mismatch, the amplitude of the quadrature signal reflected by the resistive sensing element is varied. This signal is combined with the in-phase component, using the six-port structure. As a result, information is added to the phase of the backscattered signal by the RFID chip. The combined modulated signal contains the node ID in digital form and the sensed value in analog form. To verify the performance of the proposed architecture, a pin diode operating as a variable resistor was used in the experiments and found operational as predicted by the simulations.

Chapter 7

A Battery-Less Non-Hybrid Six-Port RFID-Based Wireless Sensor Architecture for IoT Applications

This chapter introduces a novel battery-less wireless sensor architecture, which is based on the principle of direct frequency conversion. The proposed architecture uses a non-hybrid six-port structure to integrate a UHF RFID chip with sensing elements to create a sensor node. The RFID chip provides a unique identification to the sensor node and the sensing element enables the reading of environmental conditions. The non-hybrid six-port structure unequally divides an incoming RFID interrogator signal into an in-phase and quadrature branch. Using the novel unequal distribution in a six-port allows higher power being directed to the RFID chip to ensure a longer read range. The I and Q signals reflected by the RFID chip and the sensing element, respectively, are mixed without the use of a lossy or an active mixer. The mixed signal's amplitude and phase are directly dependent on the values of the attached sensing element. To read the value of the sensing element wirelessly at a reader, an IQ demodulator is used, which determines the phase of the backscattered signal. As a result, various sensed parameters such as light intensity, voltage, or force may be read wirelessly without requiring a battery at the node. To demonstrate the performance, a pin diode is used as a sensing element to read voltages wirelessly at a distance of up to 2.45 m.

In the previous chapter, a six-port based on a battery-less wireless sensor was presented, which was extremely cost-effective [158]. However, the presented design had limited read range due to the way the power is distributed in that architecture.

In this chapter, a novel wireless sensor design is proposed, which modifies a conventional six-port structure to address the aforementioned challenges. The proposed design uses a non-hybrid six-port direct conversion network, an RFID chip, a UHF voltage sensing element network, and two antennas. The higher power in-phase signal of the non-hybrid structure is fed to an RFID chip to harvest energy, while the lower power quadrature signal is fed to the resistance-based voltage sensing element. The higher power signal, when reflected from the RFID, is passed through an attenuator to make it comparable to the lower power quadrature signal that is reflected from the sensing element to ensure that maximum range is achieved without compromising the sensitivity of the sensor. These two quadrature signals are combined and transmitted back to the reader. The phase of the final output is directly dependent on the signal amplitude reflected by the sensing element. The non-hybrid technique improves the maximum read range along with higher sensitivity of the wireless sensor than the previously proposed six-port wireless sensors [97, 158].

The goals addressed in this chapter are four-fold:

- propose a wireless sensor architecture that operates without the need for any battery at the node;
- allow the integration of resistive sensing-elements;
- use variation in the phase delay of the backscattered RFID signal to determine the sensed parameter in a passive manner;
- improved read range and sensitivity performance compared to conventional six-port based wireless sensor;

The remainder of this chapter is organized as follows. In Section 7.1, a detailed analysis of the proposed design is provided. Section 7.2 discusses the results before concluding the chapter in Section 7.3.

7.1 System Design

The proposed wireless sensor is designed using a non-hybrid six-port structure that passively integrates an RFID chip with sensing elements. A block diagram is shown in Fig. 7.1. In the following subsections, the operating principles of the proposed wireless sensor will be discussed along with its physical realization.

7.1.1 System Model

At the core of this wireless sensor lies a non-hybrid six-port architecture, which is formed by modifying a simple six-port structure. A basic six-port structure operates on the principle of additive mixing of in-phase and quadrature components of an input RF signal. This behavior is achieved by attaching three 90° hybrid couplers along with a power splitter/combiner. On the other hand, in the non-hybrid six-port, unequal splitting and combining techniques can be used to gain certain benefits. In our case, it provides more power to the RFID chip while sacrificing the backscattered power, which doesn't impact the performance.

To elaborate this further, an input RF signal ($v_{IN}(t)$) received at port 1 is unequally split into an I and a Q using a 90° non-hybrid coupler, C_1. This coupler has a coupling factor β. The in-phase and the quadrature signals from the coupler are delivered into two 90° hybrid couplers, C_2 and C_3, respectively. As a result, signals at port 3, 4, 5, and 6 are produced. Due to unequal split in C_1, signal strength at port 3 and 4 is higher than port 1 and 2. Thus RFID chip is connected to this port to achieve a longer read range. The resistive sensing element, on the other hand, is attached to port 5 and 6. The signals are backscattered based on the reflection coefficients of the RFID (Γ_{RFID}) in the reflection mode and the sensing element (Γ_{sensor}) [145]. The in-phase and quadrature components of the backscattered signal, Γ_I, and Γ_Q, respectively, are mixed in the splitter/combiner (S_1) to generate an IQ modulated signal. To ensure that the sensitivity of the sensor is not compromised due to an unequal split in C_1, an attenuator is added to the in-phase path to cause the

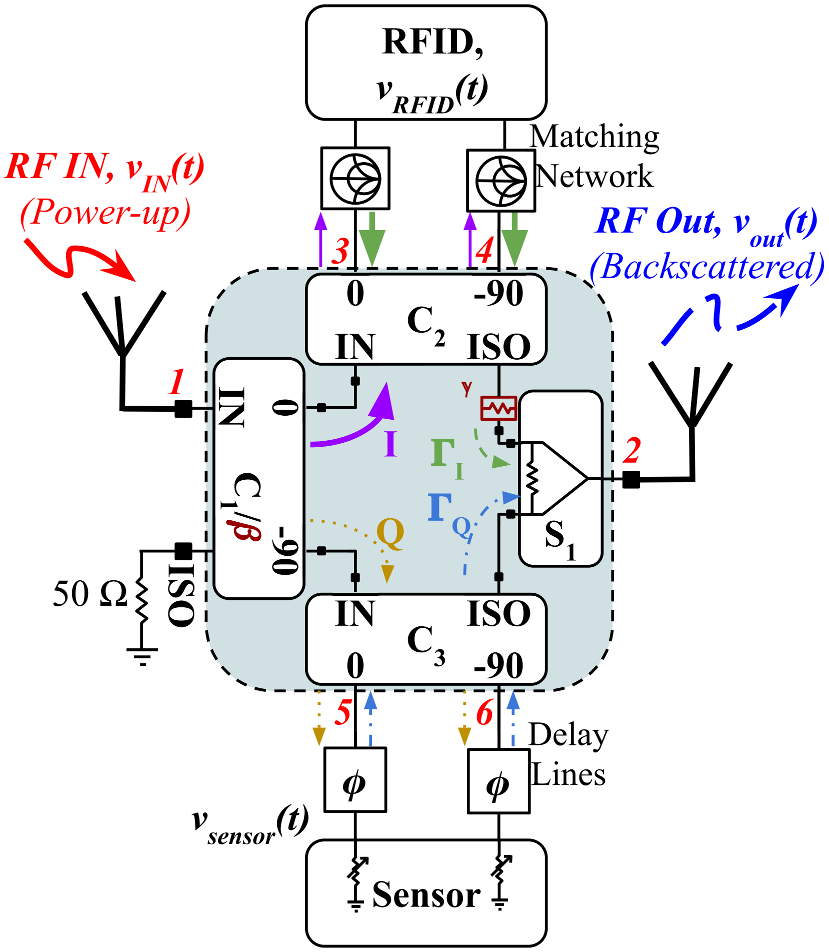

Figure 7.1: Block diagram of the proposed battery-less six-port wireless sensor.

signal amplitudes of both branches to be comparable to each other.

To understand this further, an incident RF signal is considered to be received at port 1. This signal can be mathematically represented as,

$$v_{IN}(t) = V_{IN}\ cos\ \omega_{IN} t. \tag{7.1}$$

The signals at the output ports of C_1 having a coupling factor of β will be,

$$v_I(t) = \alpha V_{IN}\ cos(\omega_{IN} t), \tag{7.2}$$

where, $\alpha^2 = 1 - \beta^2$.

$$v_Q(t) = \beta V_{IN}\ sin(\omega_{IN} t). \tag{7.3}$$

For any $\beta < 1/\sqrt{2}$, signal strength received at ports 3 and 4 will be higher than that at ports 5 and 6. Hence, the in-phase component received at ports 3 and 4 may be fed to an RFID chip. Usually, an RFID chip may not be inherently matched to 50 Ω. Therefore, a matching network must be incorporated between the RFID chip and the six-port structure. The signal received by the RFID chip can be represented as,

$$v_{RFID}(t) = T_m \alpha V_{IN}\ cos(\omega_{IN} t + \phi_m), \tag{7.4}$$

where ϕ_m and T_m are the phase delay and transmission coefficient of the matching network, respectively. For an optimally matched network, T_m may approximated as 1.

During the harvesting mode, the RFID chip acts as a matched circuit and thus all the in-phase power of the six-port structure is absorbed in it. Therefore, the reflection coefficient for this specific duration is approximated to 0 ($\Gamma_{RFID,m} = 0$) and consequently, $v_{\Gamma_I}(t) = 0$. Here, $\Gamma_{RFID,m}$, and $v_{\Gamma_I}(t)$ are the reflection coefficient of the RFID during the matched state and the corresponding signal received at the ISO port of C_2, respectively.

When the RFID backscatters for communication, ports 3 and 4 are internally connected, and the incident power at these ports is reflected due to the mismatch and combined at the ISO port of the coupler C_2. This signal can be represented as,

$$v_{\Gamma_I}(t) = \alpha \Gamma_{RFID,u} V_{IN}\ cos(\omega_{IN} t + 2\phi_m), \tag{7.5}$$

where, $\Gamma_{RFID,u}$ represents the reflection coefficient of the RFID chip when it is internally unmatched.

On the other hand, the quadrature signal, arriving at ports 5 and 6, is fed to a resistive sensing element. The signals at port 5 and 6 can be represented as,

$$v_{sensor}(t) = \frac{\beta}{\sqrt{2}} V_{IN}\ sin(\omega_{IN} t + \phi_{sensor} + \phi), \tag{7.6}$$

and

$$v_{sensor}(t) = \frac{\beta}{\sqrt{2}} V_{IN}\ sin(\omega_{IN} t + \phi_{sensor} + \phi + \frac{\pi}{2}), \tag{7.7}$$

respectively. Where ϕ_{sensor} is the delay of the transmission line and the sensing element. The length of the transmission line is controlled to ensure that the quadrature component undergoes a similar phase delay to its in-phase counterpart.

Two identical resistive sensing elements are attached at ports 5 and 6. To achieve maximum dynamic sensing range, a sensing element with resistance varying from a short circuit (0 Ω) to an open circuit may be used. However, in practice, resistance in the range of 50 Ω +/- 50 Ω, which is the transmission line's characteristic impedance, is sufficient for operation. The mismatch between the sensing element and transmission line will determine the magnitude of reflection at ports 5 and 6.

The signals reflected by the sensing element are combined at the ISO port of the coupler, C_3 and are expressed as,

$$v_{\Gamma_Q}(t) = \beta\Gamma_{sensor}V_{IN}\ sin(\omega_{IN}t + 2\phi_{sensor} + \phi), \tag{7.8}$$

where $\Gamma_{sensor} = (Z_{sensor} - Z_c)/(Z_{sensor} + Z_c)$. Here, the impedance of the sensor, Z_{sensor}, depends on the physical parameter being sensed by the sensing element.

Finally, the in-phase (Γ_I) signal and the quadrature signal (Γ_Q) are combined using the splitter/combiner, S_1. The output signal is expressed as,

$$v_{out}(t) = v_{\Gamma_I}(t) + v_{\Gamma_Q}(t), \tag{7.9}$$

$$\begin{aligned} v_{out}(t) = \alpha\gamma\Gamma_{RFID,u}V_{IN}\ cos(\omega_{IN}t + 2\phi_m + \phi) \\ + \beta\Gamma_{sensor}V_{IN}\ sin(\omega_{IN}t + 2\phi_{sensor} + \phi). \end{aligned} \tag{7.10}$$

For the case when $\phi_m \approx \phi_{sensor}$, the combined signal may be simplified as,

$$v_{out}(t) = \frac{AV_{in}}{\sqrt{2}}\ cos(\omega_{IN}t - \phi_{out} + \phi), \tag{7.11}$$

where,

$$A = \sqrt{\alpha^2\gamma^2\Gamma_{RFID,u}^2 + \beta^2{\Gamma_{sensor}}^2}, \tag{7.12}$$

$$\phi_{out} = tan^{-1}\left[\frac{\beta\Gamma_{sensor}}{\alpha\gamma\Gamma_{RFID,u}}\right], \tag{7.13}$$

are the amplitude and the phase of the output signal, respectively. Moreover, this is also the backscattered signal received at the reading device. Here,

$\phi_m \approx \phi_{sensor}$ ensures the signal entering the splitter/combiner remains in the quadrature phase.

Considering $\Gamma_{RFID,u}$ as a constant, it is evident from the 7.11, 7.12, and 7.13 that the amplitude and the phase of the backscattered signal depends on the value being sensed by the sensing element.

To ensure that the sensing element's signal remains in quadrature with respect to the RFID signal when combined in the splitter/combiner, it is necessary to use a sensing element for which the reactance does not vary with changes in the physical parameter being sensed. Any imbalance in the phases will introduce errors in the signal and must be characterized beforehand.

Moreover, to make sure that the sensitivity of the sensor is not compromised due to the imbalance of magnitude created in the non-hybrid coupler C_1, the in-phase signal at the ISO port of C_2 is attenuated by a factor of γ before it is combined with the quadrature signal in the splitter/combiner, S_1. This interesting feature allows another degree of freedom in the non-hybrid six-port design. An attenuation factor higher than the coupling factor helps improve the sensitivity of the sensor. This is because the signal from the Q branch, which is connected to the sensing element, gets dominated by the signal from the I branch.

7.1.2 Physical Realization of the Components

non-hybrid Six-port

To realize a non-hybrid six-port structure, an unequal coupler, two hybrid couplers, an attenuator, and a splitter/combiner are required. In the presented design example, the coupling factor β and attenuation factor γ were numerically optimized to achieve maximum distance while ensuring that the signal strength of the backscattered signal does not fall below the reader sensitivity. Generally, readers with sensitivity level or around -75 dBm are easily available in the market. Moreover, RFID chips with a minimum required power of -18 dBm are also available. Using Fig. 7.2, a 6.8 dB branch line coupler was selected and used in the design. While the attenuator was found to be

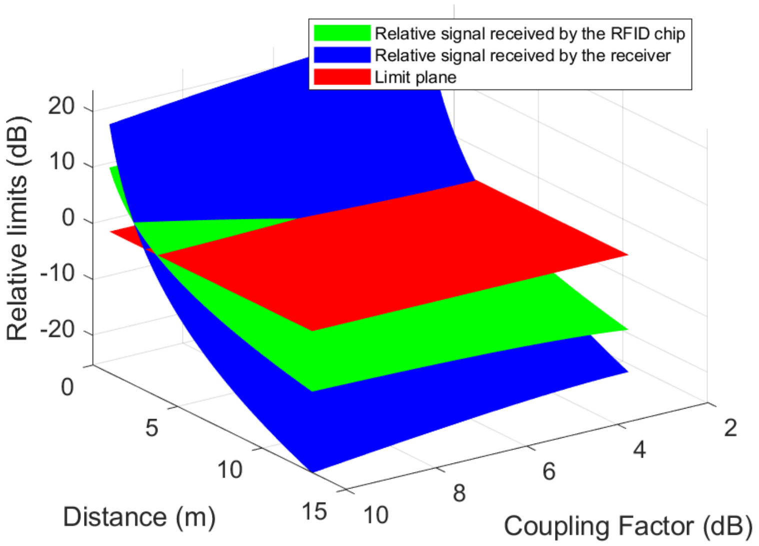

Figure 7.2: Determining optimal coupling factor.

12 dB. To connect the sensing element and RFID chip, 3 dB quadrature couplers, X3C09P1-03S, and a Wilkinson power divider, PD0810J5050S2HF by Anaren, were used. SMD components supporting the North American UHF RFID frequency band of 902 to 928 MHz were used to miniaturize the overall design. The substrate used was a 32 mil RO4003C with a relative permittivity of 3.38 and a loss tangent of 0.0027. A layout of the designed circuit is shown in Fig. 7.3.

RFID chip

For physical realization, a Higgs-4 RFID chip by Alien Technology was used. This RFID chip offers a minimum wake-up power of -18.5 dBm with an input impedance of $Z_{in} = 18 - j181\ \Omega$. Since the couplers used in the realization of the six-port structure provide 50 Ω input impedance at each port, the impedance of the RFID chip is transformed to achieve maximum power transfer between both the components. Two single-section series stubs were used to perform the impedance transformation. The matching network connects the RFID chip on one side and the non-hybrid six-port structure on the other. The layout and frequency response of the matching network are shown in Figs. 7.4 and 7.5, respectively.

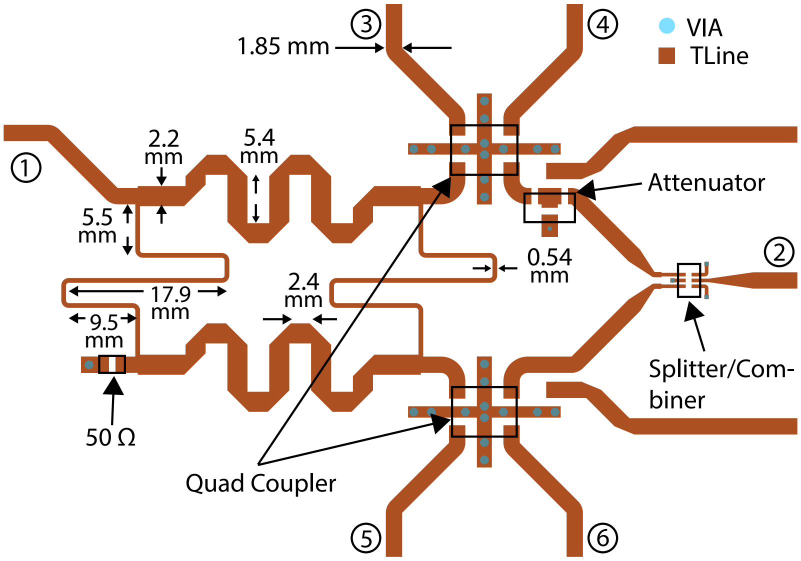

Figure 7.3: Circuit layout of the six-port structure used in the proposed system.

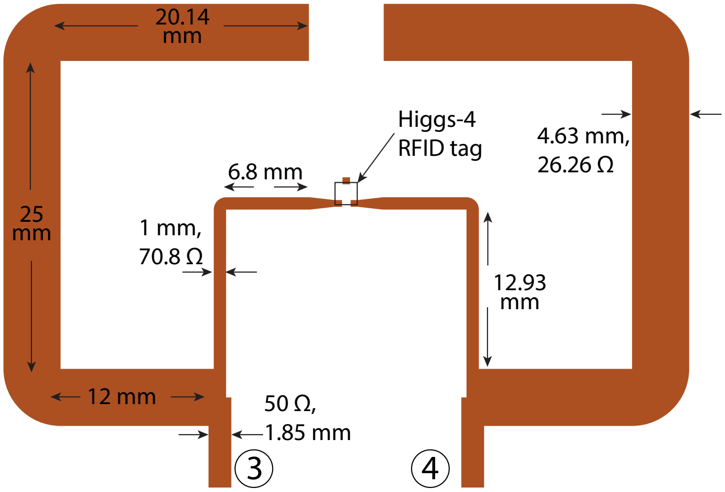

Figure 7.4: Circuit layout of the matching network used to connect RFID chip with the system.

Voltage Sensor

Sensing elements used in the proposed architecture must only vary the magnitude of the reflected signal. Therefore, to avoid any change in the phase of the signal being reflected by the sensing element, only resistive elements, operating at the frequency of interest, may be used. Several resistive sensing elements are available in the market, however, they exhibit poor response and sensitivity at UHF. Therefore, to demonstrate the proposed architecture, a pin diode,

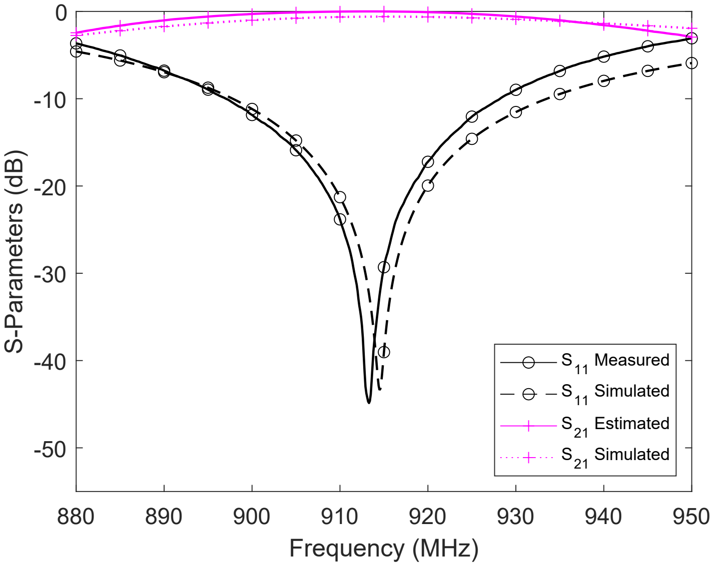

Figure 7.5: Frequency response of the matching network used to connect RFID chip.

SMP-1307 by Skyworks Solutions Inc., was used as a voltage sensing element. Its resistance changes from low ($\sim 0\ \Omega$) to high ($> 100\Omega$) by simply varying its biasing voltage. This creates a mismatch between the 50 Ω impedance of the non-hybrid six-port and the sensing element to vary reflections in the quadrature branch.

To make sure that the delay in the quadrature signal entering the sensing element remains equal to the RFID chip matching network and the attenuator, a piece of transmission line is added before the sensing element. The length is adjusted until I and Q signals are achieved simultaneously at the input of the splitter/combiner. Simulations were performed to determine the required electrical length. A circuit layout of the voltage sensing element is shown in Fig. 7.6.

The magnitude and phase of the pin diode (S55/S66) were simulated and measured using a VNA. The simulated results were obtained using the model of the pin diode in ADS 2020. The results are shown in Fig. 7.7. For voltages below 400 mV, the diode provides high resistance. Therefore, the reflection coefficient is high. Around 500 mV the diode resistance starts decreasing and the reflection coefficient drops. At ∼700 mV, the diode resistance is $\sim 50\ \Omega$

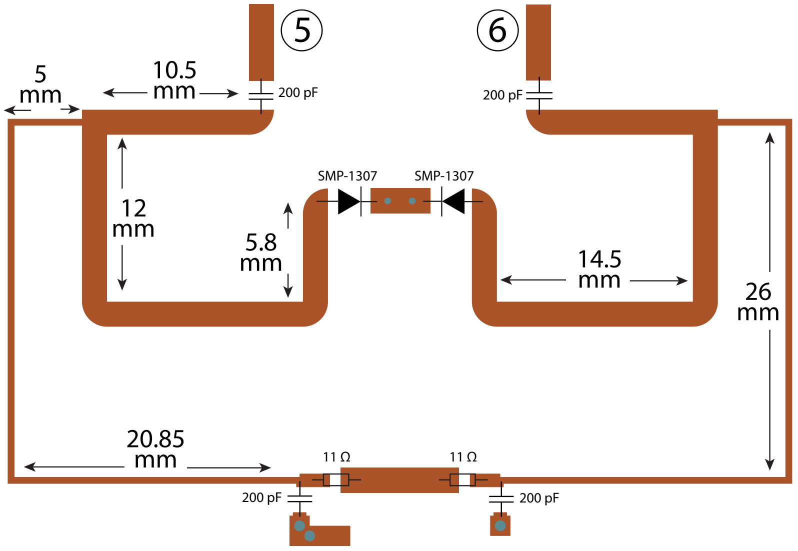

Figure 7.6: Layout of the designed circuit for the variable resistor/pin diode.

and thus the reflection coefficient is minimum. With further increase in the voltage, the resistance drops below 50 Ω and an increase in the impedance mismatch results in a higher reflection coefficient.

It can also be observed in the measurements that the sensing element is mostly resistive. This is determined by the fact the phase of the reflected signal remains constant while the voltage is varied. If this is not the case, the signal at the sensor branch will lose its quadrature requirement with variations in the voltage being sensed. It should be noted here that the phase reversal observed at ∼750 mV in Fig. 7.7 is because the phase below this voltage is lagging by 90°, while it leads by 90° above this voltage.

7.1.3 Components Integration

Once all the individual components are designed, a final integrated sensor is made by connecting the RFID chip, the voltage sensing element, and the antennas to the designated ports of the non-hybrid six-port structure. The final integrated version is shown in Fig. 7.8. To avoid entering signals from both the input and the output ports, linearly polarized meandered monopole antennas were used. Vertical polarization was used to power up the sensor by connecting it to port 1, whereas, horizontal polarization was reserved to

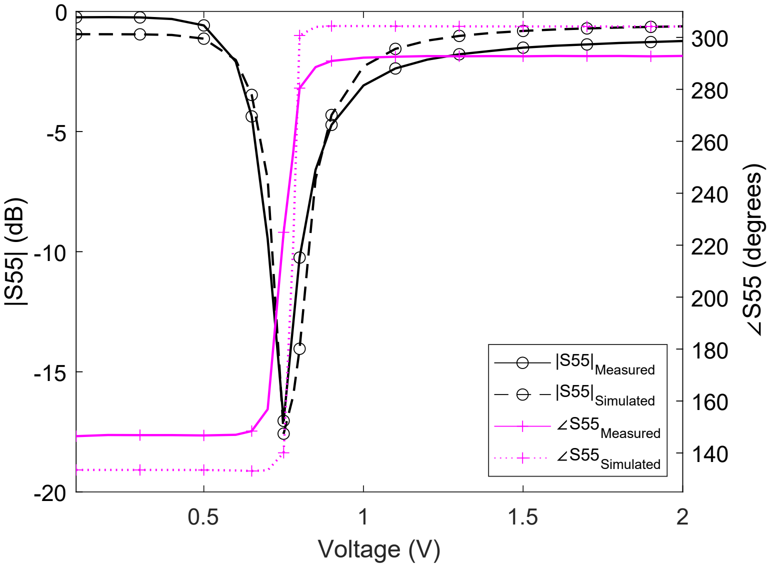

Figure 7.7: S55/S66 of the pin diode for varying voltage levels at 915 MHz.

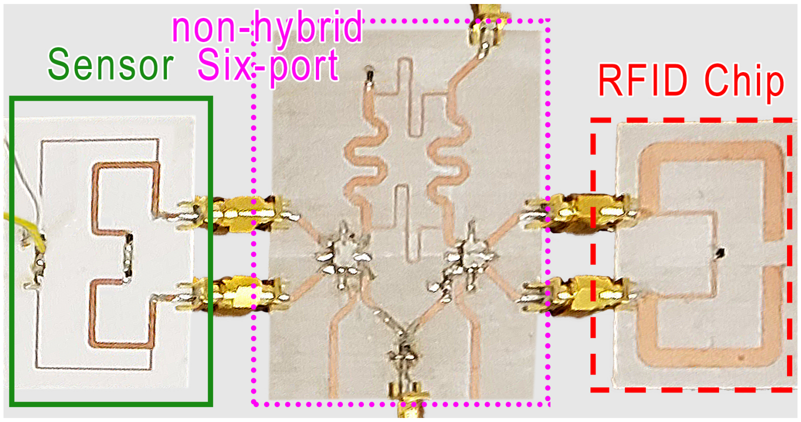

Figure 7.8: Fabricated design of the six-port RFID-based wireless sensor.

radiate the backscattered IQ signal arriving at port 2 of the sensor.

To observe the impact of variations in the voltage sensing element on the signal received by the RFID chip, a parametric study of the pin diode's resistance was conducted. It is evident in Fig. 7.9 that for the dimensions provided in Fig. 7.6, the signal received by the RFID tag is minimally affected. This shows good isolation between the in-phase and the quadrature branch of the non-hybrid six-port structure.

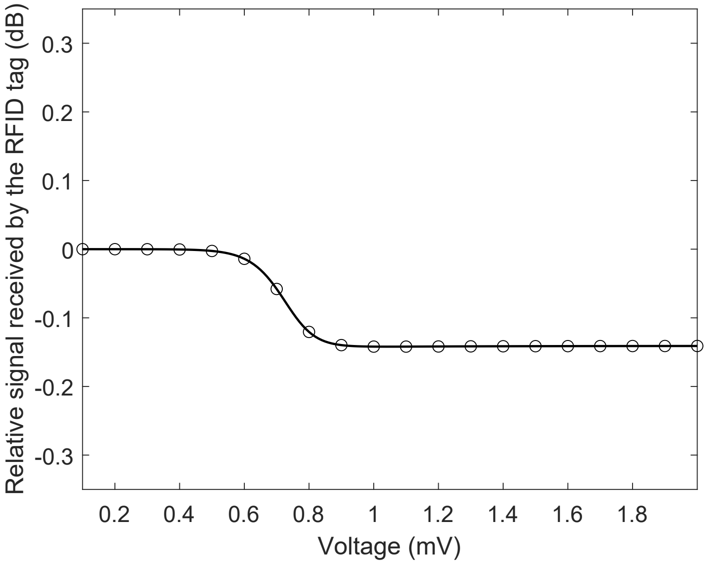

Figure 7.9: Effect of pin diode resistance variation on the signal received by the RFID chip at 915 MHz.

7.1.4 Reader

To be able to read the ID of the RFID chip and phase change due to the sensing element, it is necessary to use an RFID reader that reads the phase as well. In this work, the AS3993 Fermi by AMS was used as it uses an IQ demodulator to read the phase of the backscattered signal. The maximum transmit power of this reader is 22 dBm [143], while the sensitivity of the receiver is ∼-80 dBm.

Similar to the sensor, two linearly polarized antennas were used to isolate the power-up signal from the backscattered signal. The antennas were connected to the reader using a circulator to allow both antennas to be connected at the same port.

7.2 Results

To predict the performance of the sensor, simulations were performed in ADS 2020, as shown in Fig. 7.10. Where available, accurate models were used. Otherwise, measured data was employed in the simulations. The simulations performed for the whole North American RFID frequency band i.e., 902 MHz

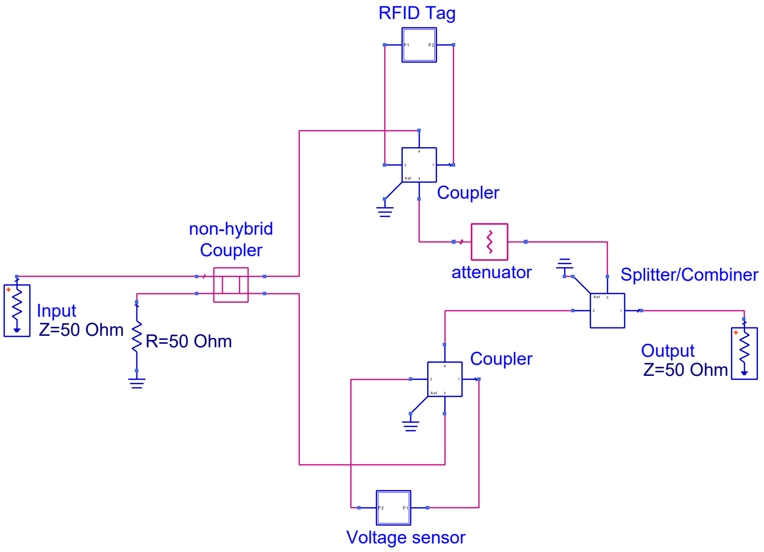

Figure 7.10: ADS schematic of the battery-less wireless sensor design.

to 928 MHz helped in quantifying the overall variations in the magnitude and phase of the backscattered signal. The results, hereafter, are analyzed at the center frequency of 915 MHz.

To observe the effect of the voltage sensing element on the backscattered signal, the voltage was swept across the terminals of the pin diode, and the magnitude of S21 was determined at 915 MHz, as shown in Fig. 7.11. A baseline loss of ~10 dB was observed, which is attributed to IQ conversion loss and attenuator loss in the in-phase branch. This loss is inevitable in the proposed non-hybrid six-port structure and is easily compensated for by using a low-noise amplifier (LNA) at the reader. Loss for a particular coupler C1 and attenuator can be determined using (7.12).

In addition to the magnitude, changes in the phase of the backscattered signal with respect to varying pin diode voltage were also observed. The results are shown in Fig. 7.12. In the regions where the sensing element acts as a highly reflective load (below 400 mV and above 1000 mV), the phase remains constant. Between 400 mV to 1000 mV, the mismatch between the sensing element's impedance and the transmission line varies rapidly. Initially, from 400 mV to 700 mV the resistance drops from high to 50 Ω. As a result, the phase delay of the backscattered signal increases. As the voltage is increased

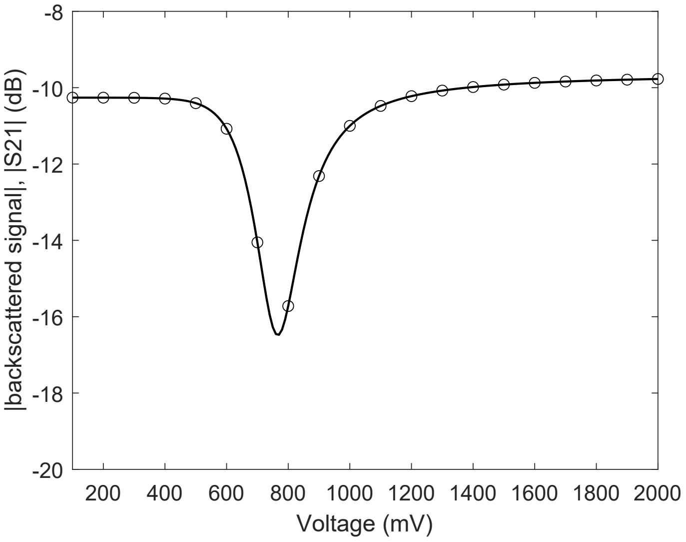

Figure 7.11: Change in the magnitude of the backscattered signal with respect to voltage across pin diode at 915 MHz.

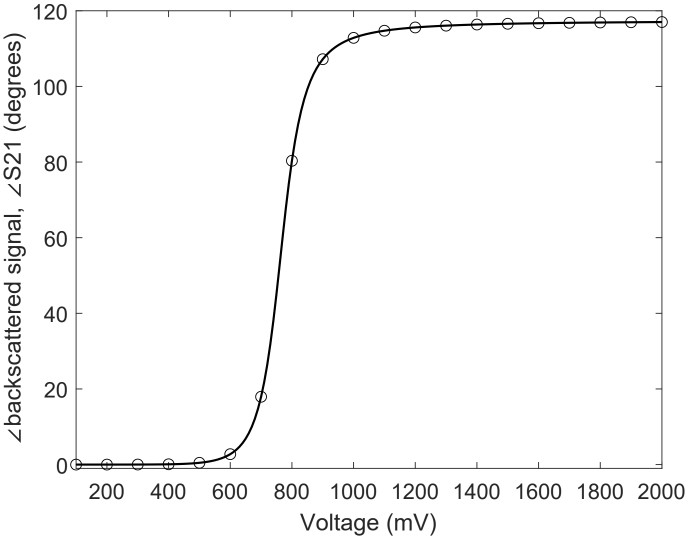

Figure 7.12: Change in the phase of the backscattered signal with respect to voltage across the pin diode.

from 700 mV to 1000 mV, the resistance drops from 50 Ω to almost short circuit. The corresponding phase delay continues to increase and hence it is most sensitive in this region of 400 mV to 1000 mV.

Although the magnitude also changes in the sensitive region, it introduces ambiguity as it shows similar values for two different voltages, whereas,

Figure 7.13: Test setup for the proposed non-hybrid six-port RFID-based battery-less wireless with pin diode attached at the sensing element port.

the phase remains unambiguous in the whole sensitive region of 400 mV to 1000 mV. Therefore, using the phase of the backscattered is more meaningful than using its magnitude.

The proposed architecture with sensing element and RFID was finally tested in a real-world scenario at 915 MHz. The proposed sensor node was placed at a distance of 2.4 m from the reader, as shown in Fig. 7.13. A triangular shaped time-varying voltage was applied across the voltage sensor. The voltage was varied from 600 mV to 800 mV. The corresponding phase of the backscattered signal was measured using the RFID reader and the results are shown in Fig. 7.14. The accuracy was found to be within +/- 20 mV.

The proposed non-hybrid six-port-based wireless sensor architecture is compared with other state-of-the-art RFID-based wireless sensor technologies in Table 7.1. Although the range of the proposed architecture is not the highest, it provides an intermediate range at a very low cost.

Future work may focus on proposing appropriate UHF resistive sensing elements that could be used with the proposed architecture.

7.3 Conclusion

A novel architecture of a battery-less wireless sensor is proposed and analyzed in this chapter. The proposed architecture uses a non-hybrid six-port structure to integrate an RFID chip with a sensing element. The non-hybrid feature

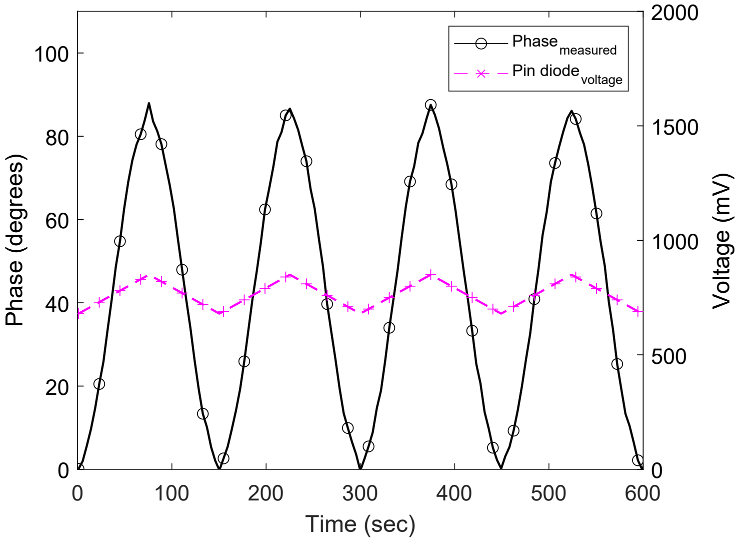

Figure 7.14: Measured phase change at the reader at 915 MHz along with the triangular voltage applied across the pin diode.

Table 7.1: Performance comparison of the proposed non-hybrid six-port wireless sensor system with other wireless sensors.

Parameter	**This work**	**Three-port [147, 157]**	**Chip-based [51–53, 132, 133]**
Cost	Low	High	Medium
Bandwidth required	∼KHz	∼KHz	∼MHz
Sensing element	Resistive	Capacitive	N.A.
Range (m)	2.45	7	3–5

improves ranges and sensitivity of the proposed wireless sensor. The performance was verified using a batteryless voltage sensor. The non-hybrid input coupler directs a major portion of the incident signal towards the RFID chip connected to the in-phase branch. The signal backscattered by the RFID chip is attenuated to achieve optimal sensor sensitivity and reader sensitivity. The attenuated signal is combined with the quadrature signal which is reflected based on the mismatch between the sensing element and the transmission line characteristic impedance. Any change in this amplitude directly affects the phase of the combined signal transmitted by the sensor. The final backscattered signal includes the node ID in digital form and the sensed parameter in analog form. A voltage sensor operating at a distance of 2.45 m is shown as a proof of concept.

Chapter 8

Conclusion

8.1 Concluding Remarks

This thesis proposes 4 novel RFID-based wireless sensors and provides an in-depth review of similar sensors proposed in the past. Moreover, a detailed discussion of components of an RFID sensor, including the antenna, rectifier, digital circuit, and sensing element was provided. Various topologies that use the components in different ways were investigated. It was observed how the utilization of the limited power and arrangements of the components can affect the read range of a battery-less RFID-based wireless sensor.

Detailed designs of the proposed architectures were discussed and analyzed. The first proposed architecture integrates an RFID chip with an antenna and a frequency selective sensing element using a circulator. Due to the reactive nature of the sensing elements, a phase delay is added to the backscattered signal. In the second design, a compact antenna is introduced to reduce the size of the proposed design. Moreover a SAW filter is introduced with the sensing element to limit sensory responding to a limited frequency band. This allows removing any phase delay through signal processing that is added due to the distance between the sensor and the reading device. Detailed analysis and in-depth models are provided for the proposed architectures and sensing elements. Designs for a flood sensor and a temperature sensor along with a folded monopole antenna are shown. Results show that the sensor may be placed at any distance of up to 7.9 meters from the reader to sense different parameters such as flood/moisture and temperature. It was also discussed how the proposed architecture provides a longer range compared to other sensors, without using any battery. These attributes make our proposed sensor ideal for different environments ranging from smart home, medical, or industry to monitoring liquid levels, temperature, and moisture, without having to ever worry about replacing the batteries of the installed sensors. It was also observed that the phase accuracy was reduced below and above 20 and 70 degrees because of the reader that was used in the study.

To reduce the cost and remove the bulky circulator, six-port RFID-based wireless sensor designs are proposed. The proposed design integrates an RFID chip, sensing elements, and a separate receiving and transmitting antenna using a six-port structure. The six-port structure distributes the incoming signals equally and sends them to the RFID chip and the sensor. The backscattered signal is combined as an IQ modulation and transmitted back to the reader. It was shown how this architecture supports resistive sensing elements. To improve the performance of the structure, a novel non-hybrid six-port RFID-based wireless sensor was also proposed. This architecture utilizes margins between the power signal and the reader sensitivity by unequally distributing the power and sending a higher portion to the RFID chip, while the signal reflected by the chip is attenuated to ensure that the sensitivity of the sensing element is not compromised. A voltage sensor operating at a distance of 2.45 m was demonstrated. The proposed architectures show promising results and will help push boundaries limiting battery-less wireless sensors. A comparative evaluation of all the proposed sensors is carried out in table 8.1.

8.2 Future Directions

Although a vast amount of research has already been carried out on battery-less RFID-based wireless sensors, it is clear that a great deal of potential remains for future discoveries. Among the several sensor parameters discussed in this review (e.g. read range, accuracy, cost, and size), it is evident that improvement in sensor read range is still of prime interest to the community. By looking at the aforementioned topologies, we can deduce that a combina-

Table 8.1: Performance comparison of all the proposed passive wireless sensors.

Parameter	**Three Port (Ch. 4)**	**Three Port with filter (Ch. 5)**	**six-port (Ch. 6)**	**Non-hybrid six-port (Ch. 7)**
Cost	Moderate	Moderate	Low	Low
Complexity	Low	Moderate	Low	Moderate
Bandwidth required	∼KHz	∼KHz	∼KHz	∼KHz
Anti-collision	Yes	Yes	Yes	Yes
Dense deployment	Yes	Yes	Yes	Yes
Accuracy	Moderate	Moderate	Moderate	Moderate
Range (m)	7	7.9	2	2.45
Mobility	No	Yes	No	No

tion of chip-based multi-port and ambient energy harvesting can yield a much higher range — theoretically, up to 50 m.

We have also seen that the size and cost of the multi-port topology are not optimal, but may be significantly improved through the use of highly miniaturized antennas employing novel matching techniques to enable compact, long-range RFID-based battery-less wireless sensors [64, 65].

If accuracy is a concern, digitally integrated sensor topologies with ambient energy harvesting show a great deal of promise. To increase the read range, ambient PV and RF energy may be combined. Moreover, the fabrication of the rectifier circuitry must be engineered to achieve better results. This involves using detailed models of the fabrication process that produce more accurate results and higher consistencies between different batches.

In addition, multiple sensors may be combined by using diplexers. This will allow access to each sensor at a given frequency.

Lastly, we have observed that there is a scarcity of sensor components operating in the low GHz range. Research that seeks high-frequency sensing component design is also needed. This will allow RFID-based battery-less sensors to be used in many new applications, readying them for deployment in the future Internet-of-Things.

Bibliography

[1] Martin Wollschlaeger, Thilo Sauter, and Juergen Jasperneite. “The future of industrial communication: Automation networks in the era of the internet of things and industry 4.0”. In: *IEEE industrial electronics magazine* 11.1 (2017), pp. 17–27.

[2] Emiliano Sisinni et al. “Industrial internet of things: Challenges, opportunities, and directions”. In: *IEEE Transactions on Industrial Informatics* 14.11 (2018), pp. 4724–4734.

[3] Kevin Mc Gee, Prince Anandarajah, and David Collins. “Current Progress towards the Integration of Thermocouple and Chipless RFID Technologies and the Sensing of a Dynamic Stimulus”. In: *Micromachines* 11.11 (2020), p. 1019.

[4] C. M. Roberts. “Radio frequency identification (RFID)”. In: *Computers and Security* 25.1 (2006), pp. 18–26. ISSN: 01674048. DOI: `10.1016/j.cose.2005.12.003`.

[5] Jeremy Landt. “The history of RFID”. In: *IEEE Potentials* 24.4 (2005), pp. 8–11. ISSN: 02786648. DOI: `10.1109/MP.2005.1549751`.

[6] V Daniel Hunt, Albert Puglia, and Mike Puglia. *RFID: a guide to radio frequency identification.* John Wiley & Sons, 2007.

[7] R. Want. “Enabling ubiquitous sensing with RFID”. In: *Computer* 37.4 (2004), pp. 84–86. DOI: `10.1109/MC.2004.1297315`.

[8] Benjamin S. Cook et al. “RFID-based sensors for zero-power autonomous wireless sensor networks”. In: *IEEE Sensors Journal* 14.8 (2014), pp. 2419–2431. ISSN: 1530437X. DOI: `10.1109/JSEN.2013.2297436`.

[9] Li Yang, Amin Rida, and Manos M Tentzeris. “Design and development of radio frequency identification (RFID) and RFID-enabled sensors on flexible low cost substrates”. In: *Synthesis Lectures on RF/Microwaves* 1.1 (2009), pp. 1–89.

[10] Saba Akbari. “Energy harvesting for wireless sensor networks review”. In: *2014 Federated Conference on Computer Science and Information Systems, FedCSIS 2014* 2 (2014), pp. 987–992. ISSN: 2300-5963. DOI: `10.15439/2014F85`.

[11] Tushar S Muratkar, Ankit Bhurane, and Ashwin Kothari. “Battery-less internet of things–A survey”. In: *Computer Networks* 180 (2020), p. 107385.

[12] Sangkil Kim et al. “No battery required: Perpetual RFID-enabled wireless sensors for cognitive intelligence applications”. In: *IEEE Microwave magazine* 14.5 (2013), pp. 66–77.

[13] Mariusz Wkeglarski and Piotr Jankowski-Mihulowicz. “Factors affecting the synthesis of autonomous sensors with RFID interface”. In: *Sensors* 19.20 (2019), p. 4392.

[14] Jun Zhang et al. “A review of passive RFID tag antenna-based sensors and systems for structural health monitoring applications”. In: *Sensors* 17.2 (2017), p. 265.

[15] G Marrocco and F Amato. “Self-sensing passive RFID: From theory to tag design and experimentation”. In: *2009 European Microwave Conference (EuMC)*. IEEE. 2009, pp. 001–004.

[16] Raquib Md Ferdous, Ahmed Wasif Reza, and Muhammad Faisal Siddiqui. “Renewable energy harvesting for wireless sensors using passive RFID tag technology: A review”. In: *Renewable and Sustainable Energy Reviews* 58 (2016), pp. 1114–1128.

[17] Shubin Ma et al. “A Batteryless Semi-Passive RFID Sensor Platform”. In: *2019 IEEE International Conference on RFID Technology and Applications (RFID-TA)*. IEEE. 2019, pp. 171–173.

[18] Amin Rida, Li Yang, and Manos M Tentzeris. *RFID-enabled sensor design and applications*. Artech House, 2010.

[19] Massimo Merenda, Corrado Felini, and Francesco G Della Corte. “Battery-less smart RFID tag with sensor capabilities”. In: *2012 IEEE International Conference on RFID-Technologies and Applications (RFID-TA)*. IEEE. 2012, pp. 160–164.

[20] Sai Nithin R Kantareddy et al. “Long range battery-less PV-powered RFID tag sensors”. In: *IEEE Internet of Things Journal* 6.4 (2019), pp. 6989–6996.

[21] Jian Zhang et al. “Standards for passive UHF RFID”. In: *GetMobile: Mobile Computing and Communications* 23.3 (2020), pp. 10–15.

[22] Xiaohua Yi et al. “Passive wireless smart-skin sensor using RFID-based folded patch antennas”. In: *International Journal of Smart and Nano Materials* 2.1 (2011), pp. 22–38. ISSN: 1947542X. DOI: `10.1080/19475411.2010.545450`.

[23] Karn Opasjumruskit et al. “Self-powered wireless temperature sensors exploit RFID technology”. In: *IEEE Pervasive Computing* 5.1 (2006), pp. 54–61. ISSN: 15361268. DOI: `10.1109/MPRV.2006.15`.

[24] S. Kim et al. “No Battery Required: Perpetual RFID-Enabled Wireless Sensors for Cognitive Intelligence Applications”. In: *IEEE Microwave Magazine* 14.5 (2013), pp. 66–77. DOI: `10.1109/MMM.2013.2259398`.

[25] Alexander Vaz et al. “Full passive UHF tag with a temperature sensor suitable for human body temperature monitoring”. In: *IEEE Transactions on Circuits and Systems II: Express Briefs* 57.2 (2010), pp. 95–99.

[26] Asanga Wickramasinghe and Damith C Ranasinghe. “Ambulatory monitoring using passive computational RFID sensors”. In: *IEEE Sensors Journal* 15.10 (2015), pp. 5859–5869.

[27] Sabina Manzari et al. “Development of an UHF RFID chemical sensor array for battery-less ambient sensing”. In: *IEEE Sensors Journal* 14.10 (2014), pp. 3616–3623.

[28] MC Caccami et al. “Design and experimentation of a batteryless on-skin RFID graphene-oxide sensor for the monitoring and discrimination of breath anomalies”. In: *IEEE Sensors Journal* 18.21 (2018), pp. 8893–8901.

[29] Alírio J Soares Boaventura and Nuno Borges Carvalho. “A batteryless RFID remote control system”. In: *IEEE transactions on microwave theory and techniques* 61.7 (2013), pp. 2727–2736.

[30] Nemai Chandra Karmakar. *Handbook of smart antennas for RFID systems.* John Wiley & Sons, 2011.

[31] Trang T Thai et al. “Design of a highly sensitive wireless passive RF strain transducer”. In: *2011 IEEE MTT-S International Microwave Symposium.* IEEE. 2011, pp. 1–4.

[32] Benjamin Stassen Cook, Atif Shamim, and MM Tentzeris. “Passive low-cost inkjet-printed smart skin sensor for structural health monitoring”. In: *IET Microwaves, Antennas & Propagation* 6.14 (2012), pp. 1536–1541.

[33] Hervé Aubert et al. “Wireless sensing and identification of passive electromagnetic sensors based on millimetre-wave FMCW RADAR”. In: *2012 Ieee International Conference on Rfid-Technologies and Applications (Rfid-Ta).* IEEE. 2012, pp. 398–403.

[34] Rushi Vyas et al. “Inkjet printed, self powered, wireless sensors for environmental, gas, and authentication-based sensing”. In: *IEEE Sensors Journal* 11.12 (2011), pp. 3139–3152.

[35] Radislav A Potyrailo et al. “Battery-free radio frequency identification (RFID) sensors for food quality and safety”. In: *Journal of agricultural and food chemistry* 60.35 (2012), pp. 8535–8543.

[36] C Zhang, JQ Huang, and QA Huang. “A passive wireless graphene oxide based humidity sensor and associated portable telemetry unit”. In: *2013 Transducers & Eurosensors XXVII: The 17th International Conference on Solid-State Sensors, Actuators and Microsystems (TRANSDUCERS & EUROSENSORS XXVII)*. IEEE. 2013, pp. 278–281.

[37] Mohammad Mahdi Honari et al. “An RFID sensor for early expiry detection of packaged foods”. In: *2018 18th International Symposium on Antenna Technology and Applied Electromagnetics (ANTEM)*. IEEE. 2018, pp. 1–2.

[38] Hossein Saghlatoon et al. “Sensor antenna transmitter system for material detection in wireless-sensor-node applications”. In: *IEEE Sensors Journal* 18.21 (2018), pp. 8812–8819.

[39] Hossein Saghlatoon, Rashid Mirzavand, and Pedram Mousavi. “Fixed-frequency low-loss dielectric material sensing transmitter”. In: *IEEE Transactions on Industrial Electronics* 68.4 (2020), pp. 3517–3526.

[40] Nabil Khalid et al. “A Three-Port Zero-Power RFID Sensor Architecture for IoT Applications”. In: *IEEE Access* 8 (2020), pp. 66888–66897.

[41] N. Khalid et al. “Three-Port Zero-Power RFID Flood Sensor for IoT Applications”. In: *2020 IEEE Wireless Power Transfer Conference (WPTC)*. 2020, pp. 61–64. DOI: `10.1109/WPTC48563.2020.9295554`.

[42] N. Khalid et al. “A Three-Port Zero-Power RFID Wireless Sensor for IoT Applications”. In: *2020 IEEE International Symposium on Antennas and Propagation and North American Radio Science Meeting (AP-S CNC/USNC-URSI)*. 2020, pp. 1–2.

[43] José Fernández-Salmerón et al. “Passive UHF RFID tag with multiple sensing capabilities”. In: *Sensors* 15.10 (2015), pp. 26769–26782.

[44] Kerem Kapucu and Catherine Dehollain. “A passive UHF RFID system with a low-power capacitive sensor interface”. In: *2014 IEEE RFID Technology and Applications Conference (RFID-TA)*. IEEE. 2014, pp. 301–305.

[45] Ren Usami et al. “Photovoltaic-assisted self-Vth-cancellation CMOS rectifier for synergistic RF energy harvesting”. In: *IEICE Electronics Express* 17.13 (2020), pp. 1–6. ISSN: 13492543. DOI: `10.1587/ELEX.17.20200186`.

[46] Rushi J Vyas et al. “E-WEHP: A batteryless embedded sensor-platform wirelessly powered from ambient digital-TV signals”. In: *IEEE Transactions on microwave theory and techniques* 61.6 (2013), pp. 2491–2505.

[47] Alanson Sample and Joshua R Smith. “Experimental results with two wireless power transfer systems”. In: *2009 IEEE Radio and Wireless Symposium*. IEEE. 2009, pp. 16–18.

[48] Arseny Dolgov, Regan Zane, and Zoya Popovic. “Power management system for online low power RF energy harvesting optimization”. In: *IEEE Transactions on Circuits and Systems I: Regular Papers* 57.7 (2010), pp. 1802–1811.

[49] *Passive RFID technology*. farsense. URL: `http://www.farsens.com/en/2013/10/18/basic-guide-developing-rfid-sensor-solutions/`.

[50] *UHF RFID Tag (Set of 5)*. sparkfun. URL: `https://www.sparkfun.com/products/14147`.

[51] B. S. Cook, J. R. Cooper, and M. M. Tentzeris. “An Inkjet-Printed Microfluidic RFID-Enabled Platform for Wireless Lab-on-Chip Applications”. In: *IEEE Transactions on Microwave Theory and Techniques* 61.12 (2013), pp. 4714–4723. ISSN: 0018-9480. DOI: `10.1109/TMTT.2013.2287478`.

[52] S. Kim et al. “Low-cost Inkjet-Printed Fully Passive RFID Tags Using Metamaterial-Inspired Antennas for Capacitive Sensing Applications”. In: *IEEE MTT-S International Microwave Symposium Digest (MTT)*. 2013, pp. 1–4. DOI: `10.1109/MWSYM.2013.6697644`.

[53] Xiaochen Chen, Leena Ukkonen, and Toni Björninen. “Passive E-Textile UHF RFID-Based Wireless Strain Sensors With Integrated References”. In: *IEEE Sensors Journal* 16.22 (2016), pp. 7835–7836. ISSN: 1530-437X. DOI: `10.1109/JSEN.2016.2608659`.

[54] Mariusz Wkeglarski et al. “Designing Antennas for RFID Sensors in Monitoring Parameters of Photovoltaic Panels”. In: *Micromachines* 11.4 (2020), p. 420.

[55] Zhi Ning Chen and Xianming Qing. “Antennas for RFID applications”. In: *Final Program and Book of Abstracts - iWAT 2010: 2010 International Workshop on Antenna Technology: Small Antennas, Innovative Structures and Materials* (2010), pp. 13–16. DOI: `10.1109/IWAT.2010.5464865`.

[56] G. Marrocco, A. Fonte, and F. Bardati. “Evolutionary design of miniaturized meander-line antennas for RFID applications”. In: *IEEE Antennas and Propagation Society International Symposium (IEEE Cat. No.02CH37313)*. Vol. 2. 2002, 362–365 vol.2. DOI: `10.1109/APS.2002.1016099`.

[57] G. Marrocco. “Gain-optimized self-resonant meander line antennas for RFID applications”. In: *IEEE Antennas and Wireless Propagation Letters* 2 (2003), pp. 302–305. DOI: `10.1109/LAWP.2003.822198`.

[58] T. Çiftçi, B. Karaosmanoğlu, and Ergül. “Low-cost inkjet antennas for RFID applications”. In: *IOP Conference Series: Materials Science and Engineering* 120.1 (2016). ISSN: 1757899X. DOI: `10.1088/1757-899X/120/1/012005`.

[59] G. Marrocco. "The art of UHF RFID antenna design: impedance-matching and size-reduction techniques". In: *IEEE Antennas and Propagation Magazine* 50.1 (2008), pp. 66–79. DOI: `10.1109/MAP.2008.4494504`.

[60] Milan Švanda and Milan Polívka. "Horizontal five-arm folded dipole over metal screening plane for UHF RFID of dielectric objects". In: *Microwave and Optical Technology Letters* 52.10 (2010), pp. 2291–2294.

[61] Carol L Baumbauer et al. "Printed, flexible, compact UHF-RFID sensor tags enabled by hybrid electronics". In: *Scientific reports* 10.1 (2020), pp. 1–12.

[62] Horng-Dean Chen and Yu-Hung Tsao. "Low-profile meandered patch antennas for RFID tags mountable on metallic objects". In: *IEEE Antennas and Wireless Propagation Letters* 9 (2010), pp. 118–121.

[63] Simone Genovesi and Agostino Monorchio. "Low-profile three-arm folded dipole antenna for UHF band RFID tags mountable on metallic objects". In: *IEEE Antennas and Wireless Propagation Letters* 9 (2010), pp. 1225–1228.

[64] Sanghamitro Das et al. "A strongly miniaturized and inherently matched folded dipole antenna for narrowband applications". In: *arXiv* 68.5 (2019), pp. 3377–3386.

[65] Sanghamitro Das et al. "A Highly Miniaturized and Inherently Conjugately Matched Folded Dipole-Based RFID Tag Antenna". In: *IEEE Access* 7 (2019), pp. 101658–101664. ISSN: 2169-3536. DOI: `10.1109/access.2019.2930956`.

[66] Smail Tedjini, Tan Phu Vuong, and Vincent Beroulle. "Antennas for RFID tags". In: *ACM International Conference Proceeding Series* 121.october (2005), pp. 19–22. DOI: `10.1145/1107548.1107557`.

[67] Jing Lun Jheng et al. "Circularly polarized RFID tag for metal surface mount". In: *Asia-Pacific Microwave Conference Proceedings, APMC* (2012), pp. 1037–1039. DOI: `10.1109/APMC.2012.6421817`.

[68] Hamed Rahmani and Aydin Babakhani. "A dual-mode RF power harvesting system with an on-chip coil in 180-nm SOI CMOS for millimeter-sized biomedical implants". In: *IEEE Transactions on Microwave Theory and Techniques* 67.1 (2018), pp. 414–428.

[69] Ulkuhan Guler, Yaoyao Jia, and Maysam Ghovanloo. "A reconfigurable passive RF-to-DC converter for wireless IoT applications". In: *IEEE Transactions on Circuits and Systems II: Express Briefs* 66.11 (2019), pp. 1800–1804.

[70] C. Ma, C. Zhang, and Z. Wang. “A Low-Power AC/DC Rectifier for Passive UHF RFID Transponders”. In: *2007 International Symposium on Microwave, Antenna, Propagation and EMC Technologies for Wireless Communications*. 2007, pp. 309–314. DOI: `10.1109/MAPE.2007.4393608`.

[71] Sleebi K. Divakaran, Deepti Das Krishna, and Nasimuddin. “RF energy harvesting systems: An overview and design issues”. In: *International Journal of RF and Microwave Computer-Aided Engineering* 29.1 (2019), pp. 1–15.

[72] Changming Ma, Chun Zhang, and Zhihua Wang. “A low-power AC/DC rectifier for passive UHF RFID transponders”. In: *2007 International Symposium on Microwave, Antenna, Propagation and EMC Technologies for Wireless Communications*. IEEE. 2007, pp. 309–314.

[73] Maysam Ghovanloo and Suresh Atluri. “An integrated full-wave CMOS rectifier with built-in back telemetry for RFID and implantable biomedical applications”. In: *IEEE Transactions on Circuits and Systems I: Regular Papers* 55.10 (2008), pp. 3328–3334.

[74] Yasin Mohd, MK Khaw, MBI Reaz, et al. “Radio frequency identification: Evolution of transponder circuit design”. In: *Microwave journal* 49.6 (2006), p. 56.

[75] Y. Teh et al. “Development of CMOS UHF RFID modulator and demodulator using DTMOST techniques”. In: *2009 IEEE 8th International Conference on ASIC*. 2009, pp. 561–564. DOI: `10.1109/ASICON.2009.5351347`.

[76] Ma Changming, Zhang Chun, and Wang Zhihua. “A low-power AC/DC rectifier for passive UHF RFID transponders”. In: *IEEE 2007 International Symposium on Microwave, Antenna, Propagation and EMC Technologies for Wireless Communications, MAPE* (2007), pp. 309–314. DOI: `10.1109/MAPE.2007.4393608`.

[77] Maysam Ghovanloo and Suresh Atluri. “An integrated full-wave CMOS rectifier with built-in back telemetry for RFID and implantable biomedical applications”. In: *IEEE Transactions on Circuits and Systems I: Regular Papers* 55.10 (2008), pp. 3328–3334. ISSN: 10577122. DOI: `10.1109/TCSI.2008.924877`.

[78] Alireza Sharif Bakhtiar, M. Sadegh Jalali, and Shahriar Mirabbasi. “A high-efficiency CMOS rectifier for low-power RFID tags”. In: *RFID 2010: International IEEE Conference on RFID* (2010), pp. 83–88. DOI: `10.1109/RFID.2010.5467271`.

[79] Soumyajit Mandal and Rahul Sarpeshkar. “Low-power CMOS rectifier design for RFID applications”. In: *IEEE Transactions on Circuits and Systems I: Regular Papers* 54.6 (2007), pp. 1177–1188. ISSN: 10577122. DOI: `10.1109/TCSI.2007.895229`.

[80] Ahmed Ashry, Khaled Sharaf, and Magdi Ibrahim. "A simple and accurate model for RFID rectifier". In: *IEEE Systems Journal* 2.4 (2008), pp. 520–524. ISSN: 19328184. DOI: `10.1109/JSYST.2008.2009206`.

[81] Yuan Yao et al. "A fully integrated 900-MHz passive RFID transponder front end with novel zero-threshold RF-DC rectifier". In: *IEEE Transactions on Industrial Electronics* 56.7 (2009), pp. 2317–2325. ISSN: 02780046. DOI: `10.1109/TIE.2008.2010180`.

[82] Shu Yi Wong and Chunhong Chen. "Power efficient multi-stage CMOS rectifier design for UHF RFID tags". In: *Integration, the VLSI Journal* 44.3 (2011), pp. 242–255. ISSN: 01679260. DOI: `10.1016/j.vlsi.2011.03.005`. URL: `http://dx.doi.org/10.1016/j.vlsi.2011.03.005`.

[83] Paul T. Theilmann et al. "Near zero turn-on voltage high-efficiency UHF RFID rectifier in silicon-on-sapphire CMOS". In: *Digest of Papers - IEEE Radio Frequency Integrated Circuits Symposium* (2010), pp. 105–108.

[84] Huichu Liu et al. "Tunnel FET-based ultra-low power, high-sensitivity UHF RFID rectifier". In: *International Symposium on Low Power Electronics and Design (ISLPED)*. IEEE. 2013, pp. 157–162.

[85] Y. K. Teh et al. "The design of batteryless, TIRIS/spl reg/-compliant RFID transponder IC employing TSMC 0.18/spl mu/m process". In: *2004 IEEE International Conference on Semiconductor Electronics*. 2004, 5 pp.–. DOI: `10.1109/SMELEC.2004.1620938`.

[86] Leandro Grasso et al. "Codesign of differential-drive CMOS rectifier and inductively coupled antenna for RF harvesting". In: *IEEE Transactions on Microwave Theory and Techniques* 68.1 (2020), pp. 364–375. ISSN: 15579670. DOI: `10.1109/TMTT.2019.2936560`.

[87] Kai-Meng Mui, Mei-Kum Khaw, and Faisal Mohd-Yasin. "Power Management IC for a Dual-Input-Triple-Output Energy Harvester". In: *Micromachines* 11.10 (2020), p. 937.

[88] Xiao Lu et al. "Wireless networks with rf energy harvesting: A contemporary survey". In: *IEEE Communications Surveys and Tutorials* 17.2 (2015), pp. 757–789. ISSN: 1553877X. DOI: `10.1109/COMST.2014.2368999`. arXiv: `1406.6470`.

[89] Ulkuhan Guler and Maysam Ghovanloo. "Power Management in Wireless Power-Sipping Devices: A Survey". In: *IEEE Circuits and Systems Magazine* 17.4 (2017), pp. 64–82. ISSN: 1531636X. DOI: `10.1109/MCAS.2017.2757090`.

[90] Y. Teh and P. K. T. Mok. "Design of Transformer-Based Boost Converter for High Internal Resistance Energy Harvesting Sources With 21 mV Self-Startup Voltage and 74% Power Efficiency". In: *IEEE Journal of Solid-State Circuits* 49.11 (2014), pp. 2694–2704. DOI: `10.1109/JSSC.2014.2354645`.

[91] Y. Teh et al. “Design and Analysis of UHF Micropower CMOS DTMOST Rectifiers”. In: *IEEE Transactions on Circuits and Systems II: Express Briefs* 56.2 (2009), pp. 122–126. DOI: `10.1109/TCSII.2008.2010190`.

[92] Taoran Le et al. “Inkjet-printed graphene-based wireless gas sensor modules”. In: *Proceedings - Electronic Components and Technology Conference* (2012), pp. 1003–1008. ISSN: 05695503. DOI: `10.1109/ECTC.2012.6248958`.

[93] Taoran Le et al. “A novel graphene-based inkjet-printed WISP-enabled wireless gas sensor”. In: *European Microwave Week 2012: "Space for Microwaves", EuMW 2012, Conference Proceedings - 42nd European Microwave Conference, EuMC 2012* (2012), pp. 412–415. DOI: `10.23919/eumc.2012.6459158`.

[94] YT Chen and HL Kao. “Humidity sensors made on polyvinyl-alcohol film coated SAW devices”. In: *Electronics Letters* 42.16 (2006), p. 1.

[95] Alexandru Oprea et al. “Capacitive Humidity Sensors on Flexible RFID Labels”. In: *TRANSDUCERS 2007-2007 International Solid-State Sensors, Actuators and Microsystems Conference.* IEEE. 2007, pp. 2039–2042.

[96] Rashid Mirzavand, Mohammad Mahdi Honari, and Pedram Mousavi. “High-resolution dielectric sensor based on injection-locked oscillators”. In: *IEEE Sensors Journal* 18.1 (2017), pp. 141–148.

[97] Rashid Mirzavand and Pedram Mousavi. “A zero-power sensor using multi-port direct-conversion sensing”. In: *IEEE Sensors Journal* 18.22 (2018), pp. 9243–9250.

[98] Burcu Ertuğ. “The Fabrication of Porous Barium Titanate Ceramics via Pore-Forming Agents (PFAs) for Thermistor and Sensor Applications”. In: *Powder Metallurgy* 4.1 (2012), pp. 73–98.

[99] Alexandru Oprea et al. “Capacitive humidity sensors on flexible RFID labels”. In: *Sensors and Actuators B: Chemical* 132.2 (2008), pp. 404–410.

[100] J Courbat et al. “Inkjet printing on paper for the realization of humidity and temperature sensors”. In: *2011 16th International Solid-State Sensors, Actuators and Microsystems Conference.* IEEE. 2011, pp. 1356–1359.

[101] Cong Zhang et al. “Passive wireless integrated humidity sensor based on dual-layer spiral inductors”. In: *Electronics letters* 50.18 (2014), pp. 1287–1289.

[102] Emran Md Amin et al. “Development of a low cost printable chipless RFID humidity sensor”. In: *IEEE sensors Journal* 14.1 (2013), pp. 140–149.

[103] JGD Hester and MM Tentzeris. "Inkjet-printed Van-Atta reflectarray sensors: A new paradigm for long-range chipless low cost ubiquitous Smart Skin sensors of the Internet of Things". In: *2016 IEEE MTT-S International Microwave Symposium (IMS)*. IEEE. 2016, pp. 1–4.

[104] Hui Yang et al. "Stable and fast-response capacitive humidity sensors based on a ZnO nanopowder/PVP-RGO multilayer". In: *Sensors* 17.10 (2017), p. 2415.

[105] Rashid Mirzavand et al. "An unpowered sensor node for real-time water quality assessment (humic acid detection)". In: *Electronics* 7.10 (2018), p. 231.

[106] F Mohd-Yasin, MK Khaw, and MBI Reaz. "Radio frequency identification: Evolution of reader and antenna circuit design". In: *Microwave Journal* 49.5 (2007), pp. 89–95.

[107] Pradeep Basappa Khannur et al. "A universal uhf rfid reader ic in 0.18-μm cmos technology". In: *IEEE Journal of solid-state circuits* 43.5 (2008), pp. 1146–1155.

[108] Scott Chiu et al. "A 900 MHz UHF RFID Reader Transceiver IC". In: *IEEE Journal of Solid-State Circuits* 42.12 (2007), pp. 2822–2833.

[109] W Jiang, T Hong, and SX Gong. "Research on the scattering characteristics and the RCS reduction of circularly polarized microstrip antenna". In: *International Journal of Antennas and Propagation* 2013 (2013).

[110] Sudhir Shrestha et al. "A method to measure radar cross section parameters of antennas". In: *IEEE transactions on antennas and propagation* 56.11 (2008), pp. 3494–3500.

[111] Eugene F Knott, John F Schaeffer, and Michael T Tulley. *Radar cross section*. SciTech Publishing, 2004.

[112] JA McEntee. "A technique for measuring the scattering aperture and absorption aperture of an antenna". In: *Antenna Laboratory, Ohio State University, Columbus, OH, Rep* 612-14 (1957).

[113] H. Saghlatoon et al. "Substrate integrated waveguide groove sensor antenna for permittivity measurements". In: *12th European Conference on Antennas and Propagation (EuCAP 2018)*. 2018, pp. 1–3. DOI: `10.1049/cp.2018.0648`.

[114] Mohammad Mahdi Honari et al. "A two-port microstrip sensor antenna for permittivity and loss tangent measurements". In: *2019 13th European Conference on Antennas and Propagation (EuCAP)*. IEEE. 2019, pp. 1–4.

[115] Hossein Saghlatoon et al. “Sensor antenna for dielectric constant measurement of materials in contact with the structure”. In: *2019 13th European Conference on Antennas and Propagation (EuCAP)*. IEEE. 2019, pp. 1–3.

[116] Mahdi Behdani et al. “High-Resolution Dielectric Constant Measurement Using a Sensor Antenna With an Allocated Link for Data Transmission”. In: *IEEE Sensors Journal* 20.24 (2020), pp. 14827–14835.

[117] Xiaohua Yi et al. “Passive frequency doubling antenna sensor for wireless strain sensing”. In: *Smart Materials, Adaptive Structures and Intelligent Systems*. Vol. 45097. American Society of Mechanical Engineers. 2012, pp. 625–632.

[118] Chunhee Cho et al. “Passive wireless frequency doubling antenna sensor for strain and crack sensing”. In: *IEEE Sensors Journal* 16.14 (2016), pp. 5725–5733.

[119] Guorong Song et al. “Application of frequency doubling in micro-strip patch antenna for wireless strain detection”. In: *Sensors and Actuators A: Physical* (2020), p. 112403.

[120] Rashid Mirzavand, Mohammad Mahdi Honari, and Pedram Mousavi. “N-ZERO direct conversion wireless sensor based on six-port structures”. In: *2017 IEEE MTT-S International Microwave Symposium (IMS)*. IEEE. 2017, pp. 1225–1227.

[121] Rashid Mirzavand, Mohammad Mahdi Honari, and Pedram Mousavi. “Direct-conversion sensor for wireless sensing networks”. In: *IEEE Transactions on Industrial Electronics* 64.12 (2017), pp. 9675–9682.

[122] Xianjun Huang et al. “Graphene oxide dielectric permittivity at GHz and its applications for wireless humidity sensing”. In: *Scientific reports* 8.1 (2018), pp. 1–7.

[123] Hans Danneels, Kristof Coddens, and Georges Gielen. “A fully-digital, 0.3 V, 270 nW capacitive sensor interface without external references”. In: *2011 Proceedings of the ESSCIRC (ESSCIRC)*. IEEE. 2011, pp. 287–290.

[124] Shuang-Ming Yu, Peng Feng, and Nan-Jian Wu. “Passive and Semi-Passive Wireless Temperature and Humidity Sensors Based on EPC Generation-2 UHF Protocol”. In: *IEEE Sensors Journal* 15.4 (2014), pp. 2403–2411.

[125] O. B. Akan et al. “Internet of Hybrid Energy Harvesting Things”. In: *IEEE Internet Things J.* 5.2 (2018), pp. 736–746. DOI: `10.1109/JIOT.2017.2742663`.

[126] Benjamin S Cook et al. “RFID-based Sensors for Zero-Power Autonomous Wireless Sensor Networks”. In: *IEEE Sensors Journal* 14.8 (2014), pp. 2419–2431.

[127] T. T. Thai et al. "Design of a Highly Sensitive Wireless Passive RF Strain Transducer". In: *IEEE MTT-S International Microwave Symposium.* 2011, pp. 1–1. DOI: `10.1109/MWSYM.2011.5973265`.

[128] H. Aubert et al. "Wireless Sensing and Identification of Passive Electromagnetic Sensors Based on Millimetre-Wave FMCW RADAR". In: *IEEE International Conference on RFID-Technologies and Applications (RFID-TA).* 2012, pp. 398–403. DOI: `10.1109/RFID-TA.2012.6404554`.

[129] B. S. Cook, A. Shamim, and M. M. Tentzeris. "Passive Low-Cost Inkjet-Printed Smart Skin Sensor for Structural Health Monitoring". In: *IET Microwaves, Antennas Propagation* 6.14 (2012), pp. 1536–1541. ISSN: 1751-8725. DOI: `10.1049/iet-map.2012.0188`.

[130] X. Yi et al. "Wireless Strain and Crack Sensing Using a Folded Patch Antenna". In: *6th European Conference on Antennas and Propagation (EUCAP).* 2012, pp. 1678–1681. DOI: `10.1109/EuCAP.2012.6206690`.

[131] S. Bouaziz et al. "Novel Microfluidic Structures for Wireless Passive Temperature Telemetry Medical Systems Using Radar Interrogation Techniques in Ka-Band". In: *IEEE Antennas and Wireless Propagation Letters* 11 (2012), pp. 1706–1709. ISSN: 1536-1225. DOI: `10.1109/LAWP.2013.2242272`.

[132] Han He et al. "Clothing-Integrated Passive RFID Strain Sensor Platform for Body Movement-Based Controlling". In: *2019 IEEE International Conference on RFID Technology and Applications (RFID-TA).* IEEE. 2019, pp. 236–239.

[133] Xiaochen Chen et al. "Textile-Based Batteryless Moisture Sensor". In: *IEEE Antennas and Wireless Propagation Letters* (2019).

[134] Ajith Adhur Kutty et al. "A Novel Carbon Nanotube Loaded Passive UHF RFID Sensor Tag with Built-in Reference for Wireless Gas Sensing". In: *IEEE MTT-S International Microwave Symposium.* IEEE. 2016, pp. 1–4.

[135] L. Yang et al. "A Novel Conformal RFID-Enabled Module Utilizing Inkjet-Printed Antennas and Carbon Nanotubes for Gas-Detection Applications". In: *IEEE Antennas and Wireless Propagation Letters* 8 (2009), pp. 653–656. ISSN: 1536-1225. DOI: `10.1109/LAWP.2009.2024104`.

[136] R. Vyas et al. "Inkjet Printed, Self Powered, Wireless Sensors for Environmental, Gas, and Authentication-Based Sensing". In: *IEEE Sensors Journal* 11.12 (2011), pp. 3139–3152. ISSN: 1530-437X. DOI: `10.1109/JSEN.2011.2166996`.

[137] *SL900A EPC Class 3 Sensory Tag Chip - For Automatic Data Logging Datasheet Addendum.* AMS. URL: `https://ams.com/sl900a\#tab/documents(accessedon21January2021)`.

[138] José Fernández Salmerón et al. "Design and Development of Sensing RFID Tags on Flexible Foil Compatible with EPC Gen 2". In: *IEEE Sensors Journal* 14.12 (2014), pp. 4361–4371.

[139] Aniello Falco et al. "Fully Printed Flexible Single-Chip RFID Tag with Light Detection Capabilities". In: *Sensors* 17.3 (2017), p. 534.

[140] David M Pozar. "Microwave engineering". In: *Wiley* (2012).

[141] *Specification Sheet: SKYFR-001400: 925–960 MHz Single Junction Robust Lead Circulator*. Accessed: Jul 26, 2020. SKYWORKS. URL: `https://www.skyworksinc.com/-/media/SkyWorks/Documents/Products/2401-2500/SKYFR_001400_2.pdf`.

[142] *Higgs4 SOT Datasheet Addendum*. Accessed: Jul 26, 2020. Alien. URL: `https://www.alientechnology.com/products/ic/higgs-4/`.

[143] *Application Note: UHF RFID Fermi Reader HW-Description*. Accessed: Jul 26, 2020. AMS. URL: `https://www.digikey.com/reference-designs/en/wireless-communication/rfid/160`.

[144] *BB135 - UHF variable capacitance diode product specification*. Accessed: Jul 26, 2020. NXP. URL: `https://www.nxp.com/docs/en/data-sheet/BB135.pdf?`.

[145] J. D. Griffin and G. D. Durgin. "Complete Link Budgets for Backscatter-Radio and RFID Systems". In: *IEEE Antennas and Propagation Magazine* 51.2 (2009), pp. 11–25. ISSN: 1558-4143. DOI: `10.1109/MAP.2009.5162013`.

[146] Simon Haykin. *Communication systems*. John Wiley, 2001.

[147] N. Khalid et al. "A Three-Port Zero-Power RFID Sensor Architecture for IoT Applications". In: *IEEE Access* 8 (2020), pp. 66888–66897.

[148] Somnath Mukherjee and Ashis Khan. *Radio frequency identification system with improved accuracy and detection efficiency in presence of clutter*. US Patent App. 12/482,410. 2009.

[149] S. W. Y. Mung and W. S. Chan. "Active Three-Way Circulator Using Transistor Feedback Network". In: *IEEE Microwave and Wireless Components Letters* 27.5 (2017), pp. 476–478.

[150] Christopher Bowick. *RF circuit design*. Elsevier, 2011.

[151] Zhenxin Hu et al. "Low-Profile Top-Hat Monopole Yagi Antenna for End-Fire Radiation". In: *IEEE Transactions on Antennas and Propagation* 63.7 (2015), pp. 2851–2857.

[152] S. Das et al. "A Highly Miniaturized and Inherently Conjugately Matched Folded Dipole-Based RFID Tag Antenna". In: *IEEE Access* 7 (2019), pp. 101658–101664.

[153] KV Seshagiri Rao, Pavel V Nikitin, and Sander F Lam. “Antenna design for UHF RFID tags: A review and a practical application”. In: *IEEE Transactions on antennas and propagation* 53.12 (2005), pp. 3870–3876.

[154] *Technical Data Sheet for CM23-1.9*. Accessed: Jul 26, 2020. Marlow. URL: `https://cdn2.hubspot.net/hubfs/547732/Data_Sheets/CM23-1.9.pdf`.

[155] Sai Nithin R Kantareddy et al. “Perovskite PV-powered RFID: Enabling low-cost self-powered IoT sensors”. In: *IEEE Sensors Journal* 20.1 (2019), pp. 471–478.

[156] Jan Slapšak et al. “Wireless system for in situ monitoring of moisture ingress in PV modules”. In: *IEEE Journal of Photovoltaics* 9.5 (2019), pp. 1316–1323.

[157] Nabil Khalid et al. “A Battery-Less RFID Sensor Architecture with Distance Ambiguity Resolution for Smart Home IoT Applications”. In: *IEEE Internet of Things Journal* (2021), pp. 1–1. DOI: `10.1109/JIOT.2021.3095136`.

[158] Nabil Khalid, Ashwin K. Iyer, and Rashid Mirzavand. “A Battery-Less Six-Port RFID-Based Wireless Sensor Architecture for IoT Applications”. In: *IEEE Internet of Things Journal* (2022), pp. 1–1. DOI: `10.1109/JIOT.2022.3161261`.